



universität
wien

DISSERTATION / DOCTORAL THESIS

Titel der Dissertation / Title of the Doctoral Thesis

“Impact of caloric restriction on the gastrointestinal
tract and the role of taurine and bile acids”

verfasst von / submitted by

András Gregor, BSc MSc

angestrebter akademischer Grad / in partial fulfilment of the requirements for the
degree of

Doktor der Naturwissenschaften (Dr.rer.nat.)

Wien, 2022 / Vienna 2022

Studienkennzahl lt. Studienblatt /
degree programme code as it appears on
the student record sheet:

UA 796 610 474

Studienrichtung lt. Studienblatt /
degree programme as it appears on
the student record sheet:

Ernährungswissenschaften

Betreut von / Supervisor:

Univ.-Prof. Dr. Jürgen König

Mitbetreut von / Co-Supervisor:

Dr. Kalina Duszka

Table of Contents

I.	ABSTRACT	- 4 -
II.	ZUSAMMENFASSUNG	- 6 -
III.	ABBREVIATIONS	- 8 -
1.	INTRODUCTION	- 9 -
1.1.	CALORIC RESTRICTION	- 9 -
1.2.	FIBRE	- 11 -
1.3.	GUT MICROBIOTA	- 11 -
1.4.	BILE ACIDS	- 12 -
1.5.	TAURINE	- 14 -
1.6.	GLUTATHIONE	- 15 -
2.	AIMS OF THE THESIS	- 17 -
2.1.	ORIGINAL ARTICLE 1: CAGE BEDDING MODIFIES METABOLIC AND GUT MICROBIOTA PROFILES IN MOUSE STUDIES APPLYING DIETARY RESTRICTION	- 17 -
2.2.	ORIGINAL ARTICLE 2: CALORIC RESTRICTION INCREASES LEVELS OF TAURINE IN THE INTESTINE AND STIMULATES TAURINE UPTAKE BY CONJUGATION TO GLUTATHIONE	- 17 -
2.3.	ORIGINAL ARTICLE 3: MICROBIOTA CONTRIBUTES TO THE REGULATION OF INTESTINAL GLUTATHIONE AND TAURINE LEVELS IN RESPONSE TO CALORIC RESTRICTION	- 18 -
3.	MATERIALS AND METHODS	- 19 -
3.1.	STUDY DESIGN: ORIGINAL ARTICLE 1: CAGE BEDDING MODIFIES METABOLIC AND GUT MICROBIOTA PROFILES IN MOUSE STUDIES APPLYING DIETARY RESTRICTION	- 19 -
3.1.1	<i>Experimental groups</i>	- 19 -
3.1.2	<i>Experimental procedure</i>	- 19 -
3.1.3	<i>Metabolomics</i>	- 20 -
3.2.	STUDY DESIGN: ORIGINAL ARTICLE 2: CALORIC RESTRICTION INCREASES LEVELS OF TAURINE IN THE INTESTINE AND STIMULATES TAURINE UPTAKE BY CONJUGATION TO GLUTATHIONE	- 22 -
3.2.1	<i>Experimental groups</i>	- 22 -
3.2.2	<i>Experimental Procedure</i>	- 22 -
3.2.3	<i>Intestinal sacs assay</i>	- 23 -

3.3.	STUDY DESIGN: ORIGINAL ARTICLE 3: MICROBIOTA CONTRIBUTES TO THE REGULATION OF INTESTINAL GLUTATHIONE AND TAURINE LEVELS IN RESPONSE TO CALORIC RESTRICTION	- 23 -
3.3.1	<i>Experimental groups</i>	- 23 -
3.3.2	<i>Experimental Procedure</i>	- 24 -
3.3.3	<i>Tissue lysate assay</i>	- 24 -
3.4.	SHARED METHODS IN THE ORIGINAL ARTICLES	- 25 -
3.4.1	<i>Animals</i>	- 25 -
3.4.2	<i>Sequencing and metataxonomic analysis</i>	- 25 -
3.4.3	<i>Gene expression</i>	- 27 -
3.4.4	<i>GSH, taurine, and taurine conjugates analysis</i>	- 27 -
3.4.5	<i>Identification of taurine and GSH conjugates</i>	- 28 -
3.4.6	<i>Bile acid analysis</i>	- 29 -
3.4.7	<i>Protein concentration and activity assays</i>	- 30 -
3.4.8	<i>Electron spin resonance</i>	- 30 -
3.4.9	<i>Statistics</i>	- 31 -
4.	SUMMARY OF FINDINGS AND DISCUSSION	- 33 -
4.1.	ORIGINAL ARTICLE 1: CAGE BEDDING MODIFIES METABOLIC AND GUT MICROBIOTA PROFILES IN MOUSE STUDIES APPLYING DIETARY RESTRICTION	- 33 -
4.2.	ORIGINAL ARTICLE 2: CALORIC RESTRICTION INCREASES LEVELS OF TAURINE IN THE INTESTINE AND STIMULATES TAURINE UPTAKE BY CONJUGATION TO GLUTATHIONE	- 34 -
4.3.	ORIGINAL ARTICLE 3: MICROBIAL CONTRIBUTION TO THE CALORIC RESTRICTION-TRIGGERED REGULATION OF THE INTESTINAL LEVELS OF GLUTATHIONE TRANSFERASES, TAURINE, AND BILE ACIDS	- 36 -
5.	CONCLUSIONS	- 38 -
6.	REFERENCES	- 42 -
7.	FURTHER PUBLICATIONS AND CONFERENCE PROCEEDINGS	- 50 -
7.1.	PUBLICATIONS	- 50 -
7.2.	ORAL/POSTER PRESENTATIONS	- 51 -
ORIGINAL ARTICLE 1		
ORIGINAL ARTICLE 2		
ORIGINAL ARTICLE 3		

I. ABSTRACT

Background

Caloric restriction (CR) lowers the incidence of multiple diseases, promotes longevity, and is one of the primary intervention tools applied for weight loss.

Objectives

The presented project aimed to investigate potential mechanisms required for the beneficial effects of CR in the gastrointestinal tract and the involvement of taurine, bile acids, and the gut microbiota in response to CR.

Methods

Mice were submitted to CR, over-night fasting, antibiotics treatment, and fecal transplant. For housing CR mice, wood, cellulose, and corncob beddings were used. Hunger level, bedding consumption, and feces production were evaluated. Metabolites, fatty acids, bile acids, GSH, taurine, and taurine conjugates were analysed using LC-MS. Cecum was sequenced to assess bacterial abundance. Antioxidative capacity was measured in the intestine epithelium using ESR. In connection with the glutathione system, gene expression, protein concentrations, and activity were measured. The expression of genes responsible for taurine and bile acid synthesis and transport were analysed. Taurine transport capacity was assessed by *ex vivo* intestinal sacs assay.

Results

CR applied to mice resulted in increased consumption of cage bedding which affected multiple physiological parameters as well as cecum microbiota and metabolome. CR increased taurine and bile acid (BA) production in the liver, export of BAs from the liver into the

gastrointestinal tract, and deconjugation of taurine-conjugated BAs. Subsequently, it promoted the creation of various taurine conjugates as well as their reabsorption into the bloodstream. Glutathione (GSH), next to CR, was identified as a promoter of intestinal taurine absorption. Depleting gut microbiota by applying antibiotics reduced the CR-driven conjugation of GSH and taurine, modified the composition of the BA pool; however, BA synthesis, transport, and taurine production remained unchanged. Reintroducing microbiota from CR mice to antibiotic-treated mice by fecal transplantation increased the conjugative capacity of GSH transferases and the occurrence of GSH-taurine and other taurine conjugates.

Conclusion

Our results show that CR significantly increases the consumption of cage bedding-derived fibre by mice. Therefore, future CR experiments involving rodents should provide information on the bedding used and should consider the effects of increased fibre consumption. Furthermore, a novel connection has been established between taurine, BAs, GSH, and the microbiota, which could be an important mediator of CR-related health benefits.

Keywords

Caloric restriction, fibre, GSH, taurine, bile acid, intestine.

II. ZUSAMMENFASSUNG

Hintergrund

Kalorienrestriktion (CR) senkt das Auftreten zahlreicher Krankheiten, fördert die Langlebigkeit und ist eines der wichtigsten Mittel zur Gewichtsreduktion.

Ziele

Ziel des Projekts war es, mögliche Mechanismen zu untersuchen, die für die positiven Auswirkungen von CR im Magen-Darm-Trakt verantwortlich sind. Dazu wurde die Rolle von Taurin, Gallensäuren und der Darmmikrobiota erforscht.

Methoden

CR Mäuse wurden über Nacht gefastet, mit Antibiotika behandelt und Fäkaltransplantation wurde durchgeführt. Für die Unterbringung der CR Mäuse wurden Holz-, Zellulose- und Maiskolbeneinstreu verwendet. Der Hunger, der Verbrauch von Einstreu und die Kotproduktion wurden erfasst. Metaboliten, Fettsäuren, Gallensäuren, GSH, Taurin und Taurin-Konjugate wurden mittels LC-MS analysiert. Der Zäkuminhalt wurde sequenziert. Die antioxidative Kapazität wurde mittels ESR gemessen. Im Zusammenhang mit dem Glutathionsystem wurden die Genexpression, die Proteinkonzentrationen und Aktivität gemessen. Die Expression von Genen, die für die Synthese und den Transport von Taurin und Gallensäuren verantwortlich sind, wurde analysiert. Die Taurin-Transportkapazität wurde mit Ex-vivo-Darmsäcken bewertet.

Ergebnisse

Die CR führte bei Mäusen zu einem erhöhten Konsum von Käfigeinstreu, was sich auf mehrere physiologische Parameter sowie auf die Mikrobiota und das Metabolom des Blinddarms auswirkte. CR

steigerte die Produktion von Taurin und Gallensäuren in der Leber, den Export von Gallensäure aus der Leber in den Gastrointestinaltrakt und die Dekonjugation von Taurin-konjugierten Gallensäuren. Zusätzlich förderte es die Bildung verschiedener Taurinkonjugate sowie deren Rückresorption in den Blutkreislauf. Neben CR förderte auch Glutathion (GSH) die intestinalen Taurinabsorption. Die Verringerung der Darmmikrobiota durch den Einsatz von Antibiotika verringerte die CR-gesteuerte Konjugation von GSH und Taurin und veränderte die Zusammensetzung des Gallensäuren-Pools und die Gallensäuren-Synthese. Der Transport und die Taurinproduktion veränderten sich jedoch nicht. Die Wiedereinführung der Mikrobiota von CR-Mäusen in antibiotisch behandelte Mäuse durch fäkale Transplantation erhöhte die Konjugationskapazität der GSH-Transferasen und das Auftreten von GSH-Taurin und anderen Taurin-Konjugaten.

Schlussfolgerung

Unsere Ergebnisse zeigen, dass sich die Ballaststoffaufnahme von Mäusen durch CR, aufgrund von erhöhtem Konsum des Käfigeinstreus erhöhte. Daher sollten künftige CR-Nageterversuche Informationen über den verwendeten Einstreu liefern und die Auswirkungen der erhöhten Ballaststoffaufnahme berücksichtigen. Darüber hinaus wurde eine neue Verbindung zwischen Taurin, Gallensäuren, GSH und der Mikrobiota hergestellt, die die gesundheitsfördernden Eigenschaften von CR erklären könnte.

Schlagwörter

Kalorienrestriktion, Ballaststoffe, GSH, Taurin, Gallensäure, Darm.

III. ABBREVIATIONS

Ad lib	<i>Ad libitum</i>
AT	Antibiotics Treated
BA	Bile Acid
BSEP	Bile Salt Export Pump
BSH	Bile Salt Hydrolase
C	Cellulose bedding
CC	Corncob bedding
CID	Collision-Induced Dissociation
CR	Caloric Restriction
CRM	Caloric Restriction Mimetics
DMEM	Dulbecco's Modified Eagle Medium
DNA	Deoxyribonucleic Acid
DPP	Dipeptidyl Peptidase
ESR	Electron Spin Resonance
FT	Fecal Transplant
FXR	Farnesoid X Receptor
GC-MS	Gas Chromatography-Mass Spectrometry
GIT	Gastro-Intestinal Tract
GPx	Glutathione Peroxidase
GR	Glutathione Reductase
GSH	Reduced Glutathione
GSSG	Oxidized Glutathione
GST	Glutathione S Transferase
HPLC	High-Pressure Liquid Chromatography
IBAT	Ileal Bile Acid Transporter

LC-MS	Liquid Chromatography-Mass Spectrometry
mRNA	messenger Ribonucleic Acid
MSI	Metabolomics Standards Initiative
MSTFA	N-methyl-N-trimethylsilyltrifluoroacetamid
Nrf2	Nuclear factor erythroid 2-Related Factor 2
NTCP	Sodium-dep. taurocholate co-transporting peptide
OGTT	Oral Glucose Tolerance Test
ON	Over Night fasting
OTU	Operational Taxonomic Unit
PBS	Phosphate-Buffered Saline
PCR	Polymerase Chain Reaction
PLS	Partial Least Square
TauT	Taurine Transporter
TGR5	Takeda G-protein coupled Receptor 5
W	Wooden bedding
WAT	White Adipose Tissue

1. Introduction

1.1. Caloric Restriction

Caloric restriction (CR) is a diet aiming to reduce the daily energy intake below the average consumption without malnutrition. CR is one of the primary intervention tools applied for weight management and health maintenance showing outstanding health benefits. Studies show that CR delays the onset of age-related decline, attenuates immune

senescence and sarcopenia, prevents atrophy of the brain grey matter, and neurodegenerative diseases, diminishes the rate of age-specific mortality, and lowers the incidence of diseases such as cancer, diabetes, atherosclerosis, and cardiovascular diseases [1-5]. Consequently, it has been repeatedly shown that CR extends the lifespan of multiple species, including yeast, fruit fly, rodents, and monkeys [6, 7]. Depending on the age at CR initiation, human studies suggest a life span increase of 1-5 years [8]; however, these studies were carried out on healthy test subjects between 20 and 65 years old, thus the benefits could vary for elderly and diseased. CR is known to modify gut microbiota composition [9, 10], which may in turn affect a number of pathologies like obesity, inflammatory bowel disease, or colorectal cancer [11]. Furthermore, CR decreases cardiometabolic risk factors, such as blood pressure, triglycerides, and cholesterol [12] and levels of circulating tumor necrosis factor- α [8].

At the end of the 20th century, interest arose for CR mimetics (CRM) that could mimic the biochemical and functional effects of CR without the need to reduce food intake significantly. Several pathways were identified that CRMs could target, such as the stimulation of autophagy by deacetylation of cellular proteins [13], disruption of cellular glucose metabolism [14], activation of sirtuins [15, 16], and AMPK [17, 18], and inhibition of mTOR [19]. So far discovered CRMs are HCA, resveratrol, spermidine, and aspirin, while there are a number of potential CRM candidates like quercetin, CAPE, curcumin, EGCG, and metformin [20]. Specifically, the gastrointestinal tract was not a focal point of the CR research so far. Thus, elucidating molecular pathways, changes in microbiota, and effects of different macronutrients in the intestine could benefit fundamental and CRM research, as well as the treatment of gastrointestinal diseases.

1.2. Fibre

Dietary fibre includes all carbohydrates that have a degree of polymerization of three or more monomeric units and are neither hydrolyzed by endogenous enzymes nor absorbed in the small intestine [21]. Ingested fiber is fermented by gut bacteria and it constitutes a substrate for the formation of various metabolites [22, 23] and shapes bacteria composition [22, 24, 25]. Fibre affects nutrient digestion and absorption, improves glycaemic and lipaemic responses, regulates plasma cholesterol by limiting bile salt resorption, influencing gut transit and microbiota composition, growth, and metabolism [26].

Epidemiological cohort studies showed that dietary fibre reduces the risk of cardiovascular disease, stroke, colorectal cancer, rectal cancer, and diabetes and reduces all-cause mortality [27]. Intervention studies shed some light on the clinical use of fibre, especially in the context of the gastrointestinal tract and inflammation [28-30]. These results were convincing enough for several associations to formulate recommendations for treating gastrointestinal disorders such as irritable bowel syndrome, inflammatory bowel disease, diverticular disease, and constipation [26]. Despite that, in the case of the therapeutic application, the data is conflicting on the type, source, dose of the fibre, and duration of the treatment [26], and thus the recommendations are often unspecific or controversial.

1.3. Gut microbiota

Gut microbiota research is crucial for this project and it is affected by both CR and fibre. The number of microorganisms inhabiting the human digestive tract is around 10^{13-14} , which is equal to approximately the number of body cells in a human body [31].

Moreover, the collective genome of the intestinal microbiota harbors 100 times more genes than the human genome [32]. A major part of the gut microbial community consists of bacteria with 500-1000 different species [33], with the most populous phyla constituting more than 90% of gut microbiota being Firmicutes and Bacteroidetes [32]. Once gut microbiota is established early in life, it remains relatively stable even for decades throughout adulthood [34]. This stable core consists of the most abundant phyla such as Bacteroidetes, Firmicutes, Proteobacteria, and Actinobacteria. However, minor changes in the microbiota, especially in lower-abundance bacterial taxa, may occur depending on multiple factors, including diet, age, body weight, humidity, environmental conditions, health status, and pregnancy [35-38]. Microbiota contribute to the formation of the intestinal architecture, protect against colonization by opportunistic pathogens, metabolize residual dietary components, and supply essential nutrients [39]. Microbiota ferments fibre to its key bacterial metabolites, short-chain fatty acids [40], while bile acids secreted by the host are metabolized to secondary bile acids by gut bacteria. Due to these functions, the microbiota has an immense impact on the well-being of the host, including metabolism, immune function, and physiology; therefore, a healthy microbiota is important for host's overall health [41].

1.4. Bile acids

Bile acids are synthesized from cholesterol in the liver by a complex network of enzymes. After being produced by activation of the key enzyme of the main synthesis pathway Cyp7a1, approximately 98% of BAs are amidated either with glycine or taurine. Conjugation reduces hydrophobicity and provides protection against toxicity. In the case of

rodents, 95% of BAs are taurine conjugated [42], while in humans, the glycine to taurine conjugation ratio is about three to one [43]. After conjugation, primary BAs are transported via the bile salt export protein (BSEP) across the canalicular membrane from the hepatocytes to the bile and are stored in the gall bladder. Following intake of food, the duodenum secretes cholecystokinin to stimulate gallbladder contraction and the release of BAs into the small intestine. Once reaching the intestine, BAs travel along the GI tract to solubilize monoacylglycerols and fatty acids and aid the digestion and absorption of lipids and fat-soluble vitamins. As the last steps of the enterohepatic circulation, in the ileum, 95% of BAs are reabsorbed via the ileal BA transporter (IBAT) and conveyed back to the liver through the portal vein where they are taken up by the sodium-dependent taurocholate co-transporting peptide (NTCP) [44, 45].

The main components of the BA pool are the primary BAs cholic acid, chenodeoxycholic acid, and their conjugated variants. Their purpose exceeds the aid in digestion, as they have functional roles in the global mammalian system and undergo extensive enterohepatic recycling and gut microbial modification. In the intestine, BAs regulate bacterial overgrowth and proliferation, whereas bacterial enzymes modify primary BAs and produce the secondary BAs through deconjugation by bile salt hydrolase (BSH) and their subsequent dehydrogenation, dihydroxylation, and sulfation. The secondary BAs deoxycholic acid and lithocholic acid undergo further modifications, such as epimerisation, sulphation, glucuronidation, and conjugation with N-acetylglucosamine in the liver, kidney, and gut resulting in the tertiary BAs tauroursodeoxycholic acid, ursodeoxycholic acid, and sulpholithocholic acid [46]. Taurine and glycine are metabolized to CO_2 and NH_3 in the gut, which can be used by certain bacteria as energy sources [47]. BAs have many fundamental roles, such as signaling through the farnesoid

X receptor (FXR) and the G protein-coupled membrane receptor 5 (TGR5). Through these receptors, a signaling cascade is activated, and gene expression is stimulated, regulating the metabolism of BAs, lipids, and carbohydrates and energy expenditure as well as inflammation, predominantly in enterohepatic organs [48, 49].

1.5. Taurine

Taurine is a sulfur-containing amino acid present in high concentrations in red algae [50], seaweed [51], and in the animal kingdom except for protozoa [52]. In mammals, taurine can be found abundantly in bile, intestine, heart, skeletal muscle, brain, neural tissue, liver, kidney, retina, and leukocytes [53]. Synthesis of taurine occurs mainly in the liver and kidney through the cysteine sulfinic acid pathway. To a lesser extent, taurine is produced by the cysteamine dioxygenase (ADO), which converts the coenzyme A-derived cysteamine to the taurine precursor hypotaurine [54]. After synthesis, taurine is delivered to the target tissues by the circulation [52]. The capacity for endogenous synthesis and turnover rate varies in different animal species, and aging in mammals is accompanied by a reduced ability of taurine synthesis [55]. Taurine uptake from the diet is limited by the saturability of transporters in the intestine [56], while the excess of taurine within the body is eliminated through urine [55]. Taurine is involved in many actions connected with the prevention and protection of various organ dysfunctions and is therefore known as a polyfunctional molecule [57]. Crucial roles of taurine are assigned to developmental, cytoprotective, and survival attributes [58], hence the high concentration in colostrum. One of the most established biological actions of taurine is its conjugation with primary bile acids (BAs) to promote their water solubility in bile and decrease their membrane

permeability, thus, leading to efficient facilitation of the absorption of lipids and lipid-soluble vitamins and reduced cytotoxicity [45, 59]. Furthermore, its role in the optical and immune systems, osmotic regulation, reproduction, stabilization of membranes, cardiac muscle regulation, and inflammation [60, 61] make it one of the most essential substances in the body. Taurine protects against various diseases and disorders in different organ systems such as the integumentary [62], cardiovascular [63, 64], respiratory [65], muscular [66], circulatory [67], nervous [57, 68], and endocrine systems [69]. Due to its pharmacological potential, taurine and its derivatives have been clinically studied in the context of several disorders such as metabolic or inflammatory diseases [70].

1.6. Glutathione

Glutathione is a non-enzymatic antioxidant tripeptide (cysteine, glycine, and glutamic acid) found in animals, plants, fungi, and some bacteria and archaea. The two existing states of glutathione are reduced (GSH) and oxidized (GSSG) forms. GSH de novo synthesis is catalyzed by glutamate-cysteine ligase (GCL) and glutathione synthetase (GS) in the cytosol. GSH is the dominant form in most cells, whereas GSSG occurs more often in the endoplasmic reticulum (ER) [71]. To restore free GSH from GSSG, the enzyme glutathione reductase (GR) uses NADPH to cleave GSSG and produces two molecules of GSH [72].

In its reduced form, the exposed sulfhydryl group (-SH) of the cysteinyl moiety is a reducing agent and a nucleophile that reacts with toxins directly or through glutathione S-transferases (GST). GSTs are a family of enzymes catalyzing the conjugation of glutathione to electrophilic substrates, producing more water-soluble compounds for elimination

through urine and bile [73]. Additionally, GSH acts as a co-substrate of glutathione peroxidases (GPx), a group of enzymes responsible for the reduction of H_2O_2 and other oxides to their respective alcohols and oxygen. Eight different isoforms (GPx1-8) have been identified [74]. GR, GST, and GPx form the glutathione system, which is especially present in the gastrointestinal tract [75]. Age [76], sex [77], food [78], alcohol [79], drug intake [80], and bile acid homeostasis [81] can influence cellular glutathione concentration.

2. Aims of the Thesis

This project aimed to untangle the effects of CR in the gastrointestinal tract and to identify underlying mechanisms contributing to the CR phenotype.

2.1. Original Article 1: Cage bedding modifies metabolic and gut microbiota profiles in mouse studies applying dietary restriction

The aims of the study were:

- to investigate the consequences of CR on mice body parameters, metabolic organs, and outcome of metabolic assays;
- to assay the amount of cage bedding consumed by mice and the ability of mice to extract energy from different types of bedding;
- to verify the impact of mice cage bedding on gut microbiota, fibre fermentation in the cecum, and the phenotype shaped by CR.

2.2. Original Article 2: Caloric restriction increases levels of taurine in the intestine and stimulates taurine uptake by conjugation to glutathione

The aims of the study were:

- to assess the mechanisms behind the increased concentration of taurine conjugated bile acids in the intestinal content of mice;
- to identify transportation pathways of taurine in the intestine of mice;

- to investigate the involvement of GSH in the optimization of the uptake of taurine and bile acids.

2.3. Original Article 3: Microbiota contributes to the regulation of intestinal glutathione and taurine levels in response to caloric restriction

The aims of the study were:

- to analyze the role of the microbiota in bile acid deconjugation as well as GSH and taurine conjugation;
- to identify changes in microbiota composition that can be linked to taurine and bile acid levels and synthesis;
- to assess if microbiota takes part in the regulation of oxidative stress during caloric restriction.

3. Materials and Methods

3.1. Study design: Original Article 1: Cage bedding modifies metabolic and gut microbiota profiles in mouse studies applying dietary restriction

3.1.1 Experimental groups

- W: *ad libitum* fed mice housed on wooden bedding
- C: *ad libitum* fed mice housed on cellulose bedding
- CC: *ad libitum* fed mice housed on corncob bedding
- CR-W: calorie restricted mice housed on wooden bedding
- CR-C: calorie restricted mice housed on cellulose bedding
- CR-CC: calorie restricted mice housed on corncob bedding
- ON-W: overnight fasted mice housed on wooden bedding
- ON-C: overnight fasted mice housed on cellulose bedding
- ON-CC: overnight fasted mice housed on corncob bedding
- ON-E: overnight fasted mice housed in empty cages
- ON-G: overnight fasted mice housed on metal grids

3.1.2 Experimental procedure

Ten weeks old C57BL/6NRj mice were housed for seven days in cages containing a mix of wooden, cellulose, and corncob beddings. Following the habituation period, mice were placed in single cages with one of the chosen beddings and were assigned to one of the experimental groups. The control groups were kept *ad libitum*. CR mice were submitted to two weeks of CR; which reduced their calorie intake to 75% of their average daily consumption. To assess bedding

consumption and feces production, cage beddings were collected daily for three days, then dried and separated from the feces. CR mice's body weight was monitored daily. The hunger level of CR mice was estimated by measuring the time it took them to initiate the daily portion of the meal delivered at 5 PM. Fresh fecal samples were collected on days 12 and 13 of CR and from *ad libitum*-fed mice. Feces were snap-frozen in liquid nitrogen and stored at -80 °C. Additionally to the three beddings, two subgroups of ON (overnight) group were kept without bedding or on metal grids to prevent bedding consumption and coprophagy. ON mice were fasted overnight for 16 hours with free access to water. The morning after the fast, mice were submitted an oral glucose tolerance test (OGTT). Mice received 3 mg intragastric bolus of glucose per gram body weight, and blood glucose levels were monitored over 2h. Afterward, the animals were given one week for recovery and the ON fasting procedure was repeated and followed by dissection. All mice were euthanized by isoflurane overdose, followed by blood withdrawal by cardiac puncture. Weight of the body, cecum, stomach, liver, and white adipose tissue (WAT) was measured. Samples of the liver, WAT, epithelium scrapings of the stomach and the intestine as well as cecum content and blood, were collected and stored at -80 °C. Blood was mixed with 10 µl/ml EDTA, 20 µl/ml aprotinin, and 10 µl/ml dipeptidyl peptidase (DPP) IV. Plasma was separated from the blood cells by centrifugation for 10 min at 3 600 x g 4 °C and was stored at -80 °C.

3.1.3 Metabolomics

Extraction and analysis of cecal metabolites were performed based on the method by Weckwerth et al. [82] with slight modifications. Frozen samples weighing around 30 mg were transferred into "Precellys lysis kit" homogenizing tubes with 1.4 mm ceramic beads and 800 µl ice-

cold MCW extraction buffer (methanol:chloroform:water = 2.5:1:0.5) was added. The samples were homogenized in a Precellys24 Tissue Homogenizer (Bertin Instruments) twice for 15 s at 5 000 rpm and were incubated on ice for 15 min. Next, samples were vortexed and centrifuged for 5 min at 10 500 rpm at 4 °C then the supernatant was transferred to a 2 ml Eppendorf tube. The extraction step was repeated by short vortexing the pellet with 400 µl ice-cold MCW followed by 15 min incubation on ice and centrifugation for 5 min at 10 500 rpm at 4 °C. The two supernatants were combined and to separate the chloroform phase from the water/methanol phase 400 µl H₂O was added. After vortexing and centrifuging the samples for another 5 min at 14 000 rpm at 4 °C, the upper polar phase was transferred to a new Eppendorf tube, and both fractions were dried in a speed vac using an optimized pressure gradient to prevent boiling retardation. The polar fraction was dissolved in 50 µl of methoxamine hydrochloride solution (20 mg/ml pyridine) and incubated at 30 °C for 90 min with continuous shaking. Then 80 µl of N-methyl-N-trimethylsilyltrifluoroacetamid (MSTFA) was added to derivatize polar functional groups at 37 °C for 30 min. The derivatized samples were stored at room temperature for 120 min before injection. Gas chromatography-mass spectrometry (GC-MS) analysis was performed using a Leco Pegasus BT-TOF (Leco Instrumente GmbH, Mönchengladbach, Germany) equipped with a PAL3 Autosampler (CTC Analytics AG, Zwingen, Switzerland). Chromatographic separation and data validation were conducted as published earlier with slight modifications [83, 84]. Derivatized extract (1 µl) was injected on an HP-5MS column (30 m × 0.25 mm × 0.25 µm) (Agilent Technologies) in split less mode. Mass spectral data acquisition was performed using the following instrument parameters. Electron impact ionization was conducted at 70 eV and 1 mA emission current. Ion source and transfer line temperature were set to 250 °C. Mass spectra were collected at an acquisition rate of 10 spectra/sec and a

mass range of 40–600 Th using a relative detector voltage with an offset of -100 V from the optimized detector voltage.

3.2. Study design: Original Article 2: Caloric restriction increases levels of taurine in the intestine and stimulates taurine uptake by conjugation to glutathione

3.2.1 Experimental groups

- Ad lib: *ad libitum* fed mice
- CR: caloric restricted mice

3.2.2 Experimental Procedure

Male C57BL/6NRJ mice aged 12 weeks were randomly divided into experimental groups of nine control *ad libitum* fed (ad lib) or CR mice. The groups did not differ significantly in body weight when starting the experimental procedures. Animal food intake was measured for one week before the intervention to determine the amount of chow diet to be given daily under the 14 days of CR.

Fresh fecal samples were collected on days 12 and 13 of CR and from *ad libitum*-fed mice. Feces were snap-frozen in liquid nitrogen and stored at -80 °C. All mice were euthanized by isoflurane overdose, followed by blood withdrawal by cardiac puncture. Weights of the body, cecum, stomach, liver, and white adipose tissue (WAT) were measured. Samples of the liver, WAT, epithelium scrapings of the stomach, duodenum, jejunum, ileum, colon as well as cecum content and blood were collected and stored at -80 °C. Blood was mixed with

10 µl/ml EDTA, 20 µl/ml aprotinin, and 10 µl/ml DPP IV. Plasma was separated from the blood cells by centrifugation for 10 min at 3 600 x g 4 °C and was stored at -80 °C.

3.2.3 Intestinal sacs assay

The freshly dissected small intestine was divided into five even parts. Part one is the proximal and part five is the distal small intestine. Part four was flushed with PBS and was loosely tied at the ends with a thread resulting in a 4 cm-long sac. Through an opening of the sac, a blunted needle was inserted and the intestine was filled with 200 µl of taurine (25 mg/ml) or taurine (25 mg/ml) and GSH (61.5 mg/ml) solutions. After this, the opening was closed tightly and the sac was transferred into a 50 ml falcon tube containing 10 ml of prewarmed Dulbecco's Modified Eagle Medium (DMEM) and incubated in a 37 °C water bath. Samples of 200 µl DMEM were collected three times over 1.5 h and stored at -20 °C until LCMS measurement.

3.3. Study design: Original Article 3: Microbiota contributes to the regulation of intestinal glutathione and taurine levels in response to caloric restriction

3.3.1 Experimental groups

- Ad lib: *ad libitum* fed mice
- CR: caloric restricted mice
- AT: *ad libitum* fed mice treated with antibiotics
- AT CR: caloric restricted mice treated with antibiotics
- FT: *ad libitum* fed mice treated with antibiotics and receiving fecal transplant from ad libitum fed mice

- FT CR: caloric restricted mice treated with antibiotics and receiving fecal transplant from caloric restricted mice

3.3.2 Experimental Procedure

Male C57BL/6NRJ mice aged 12 weeks were randomly divided into *ad lib*, CR, AT, AT CR, FT, and FT CR experimental groups. To deplete gut microflora, AT, AT CR, FT, and FT CR groups were gavaged with 200 μ l of an antibiotic cocktail (vancomycin 0.5 g/l, neomycin 1 g/l, ampicillin 1 g/l, metronidazole 1 g/l; all from Sigma-Aldrich, Vienna, Austria). The AT and AT-CR groups were gavaged three times within 14 days of the experimental procedure, and the FT group was gavaged twice: 5 and 3 days before microbiota transplant. After antibiotics treatment, the mice from the FT groups were gavaged with freshly extracted fecal microbiota from CR or *ad libitum* mice. The second gavage followed the first one after two days. To obtain inoculants, fresh feces were mixed with sterile PBS. The mixture was vortexed and centrifuged for 3 min at 1 000 \times g, and the isolated supernatant was immediately gavaged into FT or FT CR mice. FT and FT CR mice were dissected seven days after the first gavage.

Body and organ weight measurement, as well as sample collection, preparation, and storage, was executed as described in Original Article 2.

3.3.3 Tissue lysate assay

Freshly extracted tissue was lysed in 10x volume (w/v) of lysis buffer (150 mM NaCl, 1% IGEPAL, 50 mM Tris-HCL) by disrupting with a syringe and needle. Afterward, 5 μ l of the lysate was mixed with 10 μ l of 2 M GSH and 2 M taurine and filled up to 200 μ l with the lysis buffer.

The lysates were incubated at 37 °C and samples were collected after 10 and 20 min of incubation.

3.4. Shared methods in the original articles

3.4.1 Animals

Male C57BL/6NRj mice purchased from Janvier Inc. Labs (Le Genest, France) were kept under a 12h light/12h dark cycle and housed in standard SPF conditions using a Tecniplast IVC system (cage type 2L, blue line) with free water access. If not stated otherwise mice were fed a standard chow (V1535 R/M-H Extrudate; ssniff Spezialdiäten GmbH, Soest, Germany).

All animal experimentation protocols were approved by the Federal Ministry of Science, Research and Economy, Unit for Animal Experiments and Genetic Engineering in Austria (BMFWF-66.006/0017-WF/V/3b/2016). All experiments were performed in agreement with the Austrian Federal Act on Animal Welfare.

3.4.2 Sequencing and metataxonomic analysis

The samples for sequencing were processed according to the previously published protocol [85]. Cecum samples were homogenized in MagNA Pure Bacteria Lysis Buffer from the MagNA Pure LC DNA Isolation Kit III (Bacteria, Fungi) in MagNA Lyser green beads tubes at 6 500 rpm for three 30 s cycles in a MagNA Lyser Instrument (all from Roche, Mannheim, Germany). The homogenized samples were mixed with 25 µl lysozyme (100 mg/ml), incubated at 37 °C for 30 min, followed by adding 43.4 µl Proteinase K (20 mg/ml), and incubation at 65 °C overnight. Afterwards, the enzymes were heat-inactivated at 95 °C for

10 min and 250 µl lysed supernatant was used for DNA extracted on a MagNA Pure LC 2.0 following the instructions for the MagNA Pure LC DNA Isolation Kit III (Bacteria, Fungi) (Roche). PCR reactions were run in triplicates using a FastStart High Fidelity PCR system and contained 5 µl of total DNA, 1 × Fast Start High Fidelity Buffer, 1.25 U High Fidelity Enzyme, 200 µM dNTPs, 0.4 µM primers, and PCR-grade water in 25 µl reaction volume (all reagents from Roche, Mannheim, Germany). The following target primers were applied for the amplification of phylogenetic informative hypervariable regions V1-V2: 27F—AGAGTTTGATCCTGGCTCAG and 375R—CTGCTGCCTYCCGTA. The primers were used with Illumina adapters for indexing PCR reaction according to Illumina's 16S metagenomic sequencing library preparation guide. The PCR temperature cycles were as follows: initial denaturation at 95 °C for 3 min, 30 cycles of denaturation at 95 °C for 45 s, annealing of primers at 55 °C for 45 s and extension at 72 °C for 1 min, final extension step at 72 °C for 7 min and cooling to 4 °C. The PCR reaction triplicates were pooled and checked using 1% agarose gel and subsequent normalization of 20 µl PCR products was performed on a SequalPrep Normalization Plate (LifeTechnologies, Germany). Of the normalized PCR products, 15 µl was used as a template in a single 50 µl indexing PCR reaction for eight cycles; the temperature cycles conditions were as described above for the targeted PCR. For the final sequencing library, 5 µl of PCR products from each sample were pooled, and 30 µl of the library was purified using a 1% agarose gel and the QIAquick gel extraction kit (Qiagen, Germany). The obtained library was quantified with QuantiFluor ONE dsDNA Dye on Quantus Fluorometer (Promega, Germany), its quality was verified using an Agilent BioAnalyzer 2100 (Waldbronn, Germany), and the 6 pM library was sequenced on a MiSeq desktop sequencer (Illumina, Netherlands) containing 20% PhiX control DNA (Illumina) with v2 chemistry for 500 cycles. FastQ raw reads were used for subsequent data analysis.

Raw sequencing data in fastq format was imported into Galaxy web-based platform [86] and analyzed with the QIIME2 2018.4 microbiome analysis pipeline. After initial quality control data was preprocessed with DADA268 using default parameters and removing specific primer sequences. The resulting feature representative sequences were classified with the QIIME2 pre-fitted sklearn-based taxonomy classifier against SILVA 16S rRNA database version 132 at 99% identity [87]. The resulting feature abundance table, also known as OTUs table over all samples, including taxonomy information, was used for all subsequent analyses. For the phylogenetic methods, representative sequences were aligned with MAFFT de novo multiple sequence aligner [88] followed by the creation of a phylogenetic tree with FastTree [89].

3.4.3 Gene expression

RNA was isolated from intestinal scrapings using the RNeasy mini kit (Qiagen). Samples were thawed in lysis buffer, disrupted using a syringe and needle, and processed following the manufacturer's protocol. SuperScript® II Reverse Transcriptase (Invitrogen™, Life Technologies) was used for the reverse transcription step. Quantitative real-time PCR (qRT-PCR) reactions were carried out using the QuantStudio™ 6 Flex Real-Time PCR System (Applied Biosystems, Life Technologies) with the SYBR Green PCR Master Mix (Applied Biosystems, Life Technologies).

3.4.4 GSH, taurine, and taurine conjugates analysis

The quantification protocol was adapted from the method of Ito et al. [90] and Budinska et al. [91]. Frozen liver and intestinal mucosa samples were cut on dry ice to the size of 7-10 mg and homogenized. Liver samples were transferred into Precellys homogenizing tubes with

1.4 mm ceramic beads and nine times the volume of ethanol absolute at -20°C was added. Liver samples were homogenized in the Precellys®24 Tissue Homogenizer (Bertin Instruments) twice for 15 s at 5 000 rpm, vortexed for 30 s, and incubated at -20°C . Intestinal samples were transferred into 1.5 ml Eppendorf tubes and were disrupted in five thawing and freezing cycles. Next, nine times the volume of ethanol absolute -20°C was added, samples were vortexed for 30 s. After the homogenization, liver and intestinal samples were handled alike. Samples were incubated at -20°C for 24 h and centrifuged for 10 min at 18 000 g. The supernatants were transferred to new tubes, and, to remove the debris, the centrifugation step was repeated. The supernatants were transferred into HPLC vials in a thermostatic autosampler kept at 4°C . 60 μl of intestinal sacs samples were diluted with 600 μl ethanol, vortexed mixed, incubated for 20 min at -20°C , and centrifuged at 15 000 g for 15 min at 4°C . The supernatant was dried in a SpeedVac concentrator for 45 min at 60°C , then dissolved in 70 μl ethanol. Samples (10 μl) were analyzed by LC-MS in negative modus using an LCMS-8040 Liquid Chromatograph Mass Spectrometer (Shimadzu Corporation, Kyoto, Japan) with an Atlantis T3 3 μm column (2.1 \times 15 0mm, Waters, Milford, MA, USA). The column temperature was 40°C . The mobile phases consisted of 0.1% formic acid in water (eluent A) and 0.1% formic acid in acetonitrile (eluent B). The gradient was maintained at an initial 5% B for 2.5 min, to 20% B at 8 min, and was set back to 5% B at 9 min with a hold for one minute.

3.4.5 Identification of taurine and GSH conjugates

Standards of GSH and taurine (both from Sigma-Aldrich, St. Louis, MO, USA) were prepared in 70% ethanol. To induce the conjugation of taurine to GSH 150 mmol of each was weighted in the same 2 ml

Eppendorf tube, 70% ethanol was added, vortexed shortly, and incubated for 30 min at room temperature. Standards were separated with the column and HPLC gradient described above and were fragmented with an LC-MS system (LCMS-8040, Shimadzu, Korneuburg, Austria). The MS instrument was operated in multiple reaction mode (MRM) with the following settings: nebulizing gas flow 3 L/min, drying gas flow 12 L/min, desolvation line temperature 250 °C, and heat block temperature 350 °C. Argon was used as the collision-induced dissociation (CID) gas with a collision energy of 20eV. The fragmentation pattern was compared to METLIN's database. To identify GSH and taurine conjugates, samples were screened for precursor ions producing similar fragmentation patterns to GSH and taurine. The exact mass of the selected precursor ions was measured using an LC-ESI-TOF-system consisting of an Ultimate 3000 (Thermo Fischer Scientific, Waltham, Massachusetts, US) and a microTOF-Q II (Bruker Daltonics, Bremen, Germany) with an Atlantis T3 3 µm column (2.1×150 mm, Waters, Milford, MA, USA). The column temperature was 40 °C. The mobile phases consisted of 0.1% formic acid in water (eluent A) and 0.1% formic acid in acetonitrile (eluent B). The gradient was maintained at an initial 5% B for 2.5 min, to 20% B at 8 min, and was set back to 5% B at 9 min with a hold for one minute.

3.4.6 Bile acid analysis

Sample extraction and measurement of bile acids were carried out using a modified method by Rohn et al. [92]. Shortly, feces samples were weighted in Precellys homogenizing tubes with 1.4 mm ceramic beads, and nine times the volume of methanol absolute at -20 °C was added. Samples were homogenized in the Precellys 24 Tissue Homogenizer (Bertin Instruments, Montigny-le-Bretonneux, France) twice for 15 s at 5 000 rpm, vortexed for 30 s, and centrifuged for 10

min at 5 000 g at 4 °C. The supernatants were transferred to new 1.5 ml Eppendorf tubes, and, to remove the debris, the centrifugation step was repeated this time at 12 000 g. Supernatants were transferred into new Eppendorf tubes, and after the third centrifugation, supernatants were directly transferred into an HPLC vial. Samples (10 µl) were analyzed by LCMS in positive modus using an LCMS-8040 Liquid Chromatograph Mass Spectrometer (Shimadzu Corporation, Kyoto, Japan) with an Atlantis T3 3 µm column (2.1 × 150 mm, Waters, Milford, MA, USA). The column temperature was 30 °C. The mobile phase A consisted of water and eluent B was acetonitrile/methanol (3/1, v/v), both containing 0.1% formic acid and a concentration of 20 mM ammonium acetate. The gradient was maintained from an initial 30% B for 5 min, to 100% B at 25 min, which was kept constant for 20 min. Afterward, the composition was set back to the initial ratio of 30% B within 2 min, followed by 10 min of re-equilibration.

3.4.7 Protein concentration and activity assays

The levels of GSH and GSSG, as well as the activity of GST, GR, GPx (BioVision, CA, USA), and Nrf2 (Abcam, Cambridge, UK), were assessed using commercial assay kits according to the manufacturer's recommendations.

3.4.8 Electron spin resonance

Frozen samples were cut into 15 µg pieces and 144 µl of oxygen-free KHB, and 6 µl of oxygen-free 10 mM CMH solution were added. The samples were incubated for 60 min in a 37 °C shaking incubator and quickly spun down. 100 µl of the solution from each sample was transferred to a fresh tube and snap-frozen in liquid nitrogen until measuring. Electron spin resonance (ESR) measurements were

performed at 150 K in a capillary tube (100 μ l), which was placed into a high sensitivity resonator (Bruker ER 4122SHQE), using an X-band Bruker Eleksys-II E500 EPR spectrometer (Bruker Biospin GmbH) with a modulation frequency of 100 kHz and a microwave frequency of 9.4 GHz. Spectra were recorded every 20 s, averaging every ten consecutive spectra. The sweep width was 450 G, the sweep time 20 s, the modulation amplitude 5 G, the center field 3 400 G, the microwave power 20 mW, and the resolution 1 024 points. EPR spectra were simulated and the area under the curve was determined by double integration of the spectrum. A reference-free quantitation of the number of spins was performed, as described previously [93].

3.4.9 Statistics

OTUs table was reduced by removing all OTUs present in less than three samples per group. The obtained data gathered from GCMS and LC-MS were normalized according to the fresh weight, then annotated and classified based on the Metabolomics Standards Initiative (MSI). Data transformation, alignment, and integrative analysis, including correlation coefficient, partial least square (PLS) regression, one-way ANOVA, hierarchical clustering, and correlation network analysis were performed with the statistical software COVAIN [94] under MATLAB environment. The amount of each metabolite and bacteria OTUs were z-scored across all samples. The correlation network associating metabolites (classified as MSI 1 and 2) and bacteria OTUs was constructed by Pearson's correlation coefficients (cutoff value = 0.8). For network visualization, Girven-Newman algorithm [95] was applied and visualization was performed with Cytoscape v3.7.2.

Concerning other data sets, the experimental groups were compared by applying one-way ANOVA with Bonferroni posthoc corrections for

multiple testing using SPSS Statistics 26 (IBM Corp., Armonk, NY, USA). Where applicable, differences between two experimental groups were analyzed using Student's t-test with a statistical significance threshold set at $p < 0.05$. Each of the groups contained 8–10 biological replicates.

4. Summary of Findings and Discussion

4.1. Original Article 1: Cage bedding modifies metabolic and gut microbiota profiles in mouse studies applying dietary restriction

A growing problem of irreproducible results of metabolic research urged us to analyze potential critical factors contributing to disparities in rodent experiments. Therefore, we focused on the effects of consuming different kinds of beddings during CR and overnight (ON) fasting. The bedding consumption of CR mice was considerable; however, the amounts varied (22-55% of diet weight) between wood, cellulose, and corncob, suggesting differences in olfactory and gustatory properties, as well as in satiation. Changes in body weight loss, fat loss, cecum weight, stomach weight, and fecal output were strongly influenced by CR, while ON interventions resulted in less pronounced CR-like changes. Due to increased body weight loss, feces production, and poor fermentability, corncob was identified as the inferior energy provider compared to wood and cellulose. Mice from all ON groups had lighter stomachs and increased cecum weight compared to *ad libitum* and CR groups, indicating that a long-term food restriction triggers increased bedding or feces consumption. CR and ON groups showed increased plasma total and active ghrelin levels compared to *ad libitum* groups and CR groups showed a tendency towards increased total ghrelin levels compared to ON groups. However, bedding did not significantly influence the difference in ghrelin levels or how rapidly mice started consuming the daily feed portion; therefore, independently of the fibre composition, high fibre consumption cannot counterbalance hunger. We confirmed that a shift in the microbiome

occurs during CR regardless of the bedding type. However, compared to wood and cellulose, strong differences in cecal bacteria and metabolome were found in the group housed on corncob bedding which has the most distinct fibre profile compared to wood and cellulose beddings. Bedding consumption of CR mice correlated with fibre-dependent microbial changes; therefore, it is important to consider that the main trigger of microbiota composition changes in CR animal trials may not be the nutrient restriction but the bedding consumption. Interestingly, elevated bedding consumption lowered the levels of all short- to medium-chain fatty acids in cecum content, which might indicate poor fermentability of insoluble fibre or increased uptake efficiency due to CR. *Ad libitum*-fed control mice consumed negligible amounts of bedding and showed similar body, microbial, and metabolic bacterial composition.

In this article, we showed that restriction-related cage bedding intake modulates multiple physiological parameters.

4.2. Original Article 2: Caloric restriction increases levels of taurine in the intestine and stimulates taurine uptake by conjugation to glutathione

Our group research has previously discovered that CR leads to increased levels of taurine conjugated bile acids (BA) in the intestine [96]. Therefore, in this study, we tried to elucidate the effects of CR-triggered changes in the BA pool of mice. Liver levels of taurine and taurine conjugates were not influenced by the CR. However, mRNA expression of genes associated with BA synthesis, transport, and cysteine metabolism was upregulated, while taurine transporter (TauT) was not affected. This suggested increased taurine and BA production and that taurine is not exported from the liver as free taurine but as

bile conjugate. Taurine conjugated BAs are transported to the intestine. Accordingly, we found increased taurine and taurine conjugates levels in CR compared to *ad libitum* control in the mucosa along the small intestine. The differences were more pronounced in the distal part of the small intestine compared to the duodenum. Among the detected taurine conjugates, we identified a GSH-taurine conjugate. Similar to other taurine conjugates in the CR group, GSH-taurine levels increased in the small intestine, while free GSH levels decreased. Importantly, gene expressions connected with GSH synthesis were downregulated or remained unaffected in CR. Similarly, the antioxidant capacity and reactive oxygen species levels were not affected. However, the enzymatic activity of GR, that converts GSSG to GSH, was increased by CR. This could indicate a higher GSH demand that is driven by other function than antioxidative. Expression of GST genes increased in the epithelium of all parts of the GI tract from the stomach to the distal colon in the CR mice accompanied by an increased activity of GST as measured in jejunum. These changes lead to increased conjugation to taurine with GSH and were identified as the driver of the elevated GSH demand and intestinal levels. We hypothesized that GSH might aid taurine reabsorption. Therefore, we measured taurine transportation efficiency *ex vivo* in intestinal sacs. Results showed that increased transportation only occurred in CR intestinal sacs when a solution containing both taurine and GSH was infused.

In summary, in this article, we characterized a novel function of GSH regarding the CR-associated taurine abundance in the small intestine. Additionally, we elucidated the mechanisms leading to increased taurine synthesis in the liver and transport to the small intestine.

4.3. Original Article 3: Microbial contribution to the caloric restriction-triggered regulation of the intestinal levels of glutathione transferases, taurine, and bile acids

Following up on Original Article 2, we investigated whether the microbiota affects the levels of taurine, taurine conjugates, GSH, and BAs. To assess the role of the microbiota, mice were treated with a broad spectrum antibiotic cocktail and were submitted to *ad libitum* or CR diets. Antibiotics treatment (AT) diminished the CR-induced increase of GST mRNA expression and neutralized the increase of GST enzymatic activity. However, no differences were observed between the *ad libitum*-fed groups with or without antibiotics. Conjugation of taurine to GSH increased in jejunum epithelium in the CR group, and AT prevented the conjugation. Correspondingly, intestinal GSH level decrease was also mitigated in the CR group with antibiotics. Increased GSH-aurine levels correlated with decreased GSH levels in the intestine; however, GSSG remained unaffected. TauT was not affected by AT. Since AT did not show any effect, it was concluded that solely CR is the regulating factor on the expression of genes associated with BA synthesis and transport, as well as on cysteine metabolism. CR consistently increased BA levels in the plasma, small intestine, and liver and decreased BA levels in the feces. Compared to the CR group, a reverse trend was observed in the AT CR group. Furthermore, analysis of the small intestinal epithelium indicated an increase in BA deconjugation in the CR group and a decrease in the AT *ad libitum* and CR group. To further assess the role of the microbiota on taurine, taurine conjugates, GSH, taurine-GSH, and BAs levels, AT mice received microbiota from CR and *ad libitum* fed mice. CR transplant increased the occurrence of GSH-aurine in the jejunum, whereas no changes in the free taurine and taurine conjugates were observed. In

the ileum, GSH-aurine, aurine, and aurine conjugates levels were increased.

In this article, we demonstrated that modulation of the levels of GSH, aurine, and its conjugates and the expression, as well as activity of GSTs, are microbiota dependent. AT partially or completely negates the tested parameters affected by CR. Microbiota transplant reintroduces the CR phenotype to a certain extent. Therefore, the microbiota is crucial for the response to CR; however, it requires other CR-related triggers to mimic CR fully.

5. Conclusions

We found that outcomes of CR in mice might be influenced by the varying bedding-fibre consumption. The fibre intake during such interventions reaches up to 50% of the total weight of ingested food, which could lead to altered intestinal transit times, affected hunger perception, reduced bioavailability of certain nutrients by binding to fibre, and reshaped microbiota composition. Importantly, to a certain degree, indigestible fibre is broken down by microorganisms in the gastrointestinal tract, especially in the cecum and colon, where bacteria are most abundant. Such events lead to fibre type-dependent reshaping of the microbiota and consequently to an altered metabolite profile. Bedding-fibre intake can be determined by collecting and measuring the weight of the bedding mice were housed on. Measuring the weight of feces separated from the bedding gives an estimate of the fecal output, which correlates reversely with the microbial degradability of fibre [97]. Therefore, it could be assumed that CR mice with less feces production consumed more microbially degradable fibre and gained more calories from fibre derived short-chain fatty acids. However, measuring the weight of feces in the bedding does not deliver information on the degree of coprophagy. Thus, accurate measurement of feces production is not feasible and fibre fermentability or the amount of calories gained from the fibre cannot be concluded. Measuring the cecum weight while monitoring fibre consumption could give further information on the fermentability of the fibre. Restrictive diets could lead to increased bedding intake, which can be easily overlooked as the outcomes of a restriction are often attributed to the restriction alone. Neglecting the impact of unintentionally increased fibre intake might lead to flawed study conclusions. Therefore, we

propose that future metabolic experiments should report on the beddings used for housing mice. Furthermore, for enhanced comparability of interlaboratory experiments, the kind of bedding used should be similar.

Caloric restriction results in a complex interplay of a plethora of underlying factors. Some of the mechanisms could be influenced by a specific diet, supplement, or drug. Therefore, expanding the knowledge about the underlying mechanisms of CR might lead to the identification of critical factors needed to mimic caloric restriction. Specifically, in this project, we discovered a number of pathways connected to CR and taurine that could pave the way to identifying CR mimicking agents.

One of the intestinal responses to CR is the increased transport of taurine-conjugated BAs from the gall bladder to the intestinal lumen. Gene expression data indicates an increased taurine synthesis in the liver but not in the gastrointestinal tract. This could suggest an elevated taurine production and excretion from the liver into the intestinal tract. As the gene expression of TauT was not influenced in the liver, we hypothesised that taurine leaves the hepatocytes in the form of BA conjugates. After BAs are excreted to the duodenum and absorbed into the jejunum mucosa, the conjugated forms of BAs become less abundant and, at the same time, levels of taurine and non-BA related taurine conjugates increase. Supporting this, in the CR group, we found increased expression of genes related to BA synthesis and transport in the liver and an increased amount of unconjugated BAs in the blood. This shows that CR results in increased excretion of taurine conjugated BAs into the small intestine, where taurine is cleaved from the BAs, which leads to the formation of various types of taurine conjugates. *Ex vivo* analysis of taurine absorption from the intestine implied increased uptake of taurine-GSH conjugates in the CR group. Similarly, the plasma content of taurine-GSH, but not free

taurine, was increased in the CR group. Furthermore, feces content of free taurine is lower and plasma content is higher in the CR group indicating high efficiency of uptake in the gastrointestinal tract.

Demonstrated by us, taurine absorption assisted by GSH has never been described before; therefore, the molecular background is thus far unknown. Similarly, little is known about the increased taurine excretion and absorption through the enterohepatic circulation during CR. In addition, taurine upregulates immune and anti-microbial genes in the gastrointestinal tract [98-100], reduces superoxide anion formation, and takes a vital part in protein synthesis by binding to the tRNAs both of which are essential for normal mitochondrial functioning [101-103]. Consequently, as suggested before [104], taurine could be a prime CRM candidate.

REDOX processes are often associated with CR [105]; however, our results show that anti-oxidative capacity and levels of reactive oxygen species are not influenced in the gastrointestinal mucosa of CR mice. Additionally, MnSOD, Cat, and Trx levels indicated reduced oxidative stress in the CR group, which should result in increased GSH preservation. Surprisingly, we observed decreased GSH levels and concluded that the increased GSH demand came from the conjugative activity, a result which was supported by increased GST gene expression and activity. Therefore, we propose that due to increased GST activity, free GSH levels decrease, elevating GSSG/GSH ratio, which activates GR in an attempt to reestablish the basic state ratio.

A number of CR-related parameters are mediated by the microbiota, such as the effect on weight loss, levels of leptin and insulin, and metabolic factors such as fat browning, liver health, and glycemic control [106, 107]. After establishing that CR modulates the levels of GSH, taurine, taurine conjugates, and BAs, we investigated the role of

the microbiota, which is massively affected by CR. Firstly, antibiotic treatment partly neutralized or removed the features of the CR phenotype. The greatest effect was triggered in the distal part of the small intestine, which may be due to the higher bacterial abundance in that region. Secondly, fecal transplant from CR mice to *ad libitum*-fed mice partially reintroduced the phenotype. This data suggests a crucial role of the microbiota in response to CR. One of these roles is likely the hydrolysis of taurine-conjugated BAs upon increased BA excretion. Consequently, the intestinal content of free taurine and unconjugated BAs increase during CR. To regulate the levels of bioactive free taurine, taurine-GSH conjugate is formed. The occurrence of this conjugate enhances taurine absorption, especially in the ileum where the TauT gene expression is the highest. The preservation of taurine is crucial for the BA formation and secretion, thus plays a major role regulating cholesterol levels [108].

Interestingly, *ad libitum*-fed mice were not influenced by antibiotics treatment regarding the measured parameters. This result supports the hypothesis that CR-specific microbiota plays a major role in the up- and down-regulation of taurine, GSH, taurine-GSH, BAs, and taurine conjugates. In the liver, the gene expression and BA production were not influenced by the antibiotics treatment; therefore, the microbial changes seem to act specifically in the intestine. Fecal transplant further confirmed the observed effects of the microbiota.

In summary, we observed how CR changes the fibre intake of laboratory rodents and how this affects their microbiota. Furthermore, we described the CR enhanced enterohepatic circulation of taurine and bile acids and the factors responsible for the regulation of the free taurine levels.

6. References

1. Anderson, R.M., D. Shanmuganayagam, and R. Weindruch, *Caloric restriction and aging: studies in mice and monkeys*. Toxicologic pathology, 2009. **37**(1): p. 47-51.
2. Colman, R.J., et al., *Caloric restriction delays disease onset and mortality in rhesus monkeys*. Science, 2009. **325**(5937): p. 201-4.
3. Masoro, E.J., *Overview of caloric restriction and ageing*. Mech Ageing Dev, 2005. **126**(9): p. 913-22.
4. Speakman, J.R. and S.E. Mitchell, *Caloric restriction*. Molecular Aspects of Medicine, 2011. **32**(3): p. 159-221.
5. Weindruch, R., et al., *The retardation of aging in mice by dietary restriction: longevity, cancer, immunity and lifetime energy intake*. J Nutr, 1986. **116**(4): p. 641-54.
6. Fontana, L., L. Partridge, and V.D. Longo, *Extending healthy life span--from yeast to humans*. Science, 2010. **328**(5976): p. 321-6.
7. Mattison, J.A., et al., *Caloric restriction improves health and survival of rhesus monkeys*. Nature Communications, 2017. **8**(1): p. 14063.
8. Flanagan, E.W., et al., *Calorie Restriction and Aging in Humans*. Annual Review of Nutrition, 2020. **40**(1): p. 105-133.
9. Zhang, C., et al., *Structural modulation of gut microbiota in life-long calorie-restricted mice*. Nature Communications, 2013. **4**(1): p. 2163.
10. David, L.A., et al., *Diet rapidly and reproducibly alters the human gut microbiome*. Nature, 2014. **505**(7484): p. 559-563.
11. Marchesi, J.R., et al., *The gut microbiota and host health: a new clinical frontier*. Gut, 2016. **65**(2): p. 330-9.
12. Ravussin, E., et al., *A 2-Year Randomized Controlled Trial of Human Caloric Restriction: Feasibility and Effects on Predictors of Health Span and Longevity*. The Journals of Gerontology: Series A, 2015. **70**(9): p. 1097-1104.
13. Pietrocola, F., et al., *Caloric Restriction Mimetics Enhance Anticancer Immunosurveillance*. Cancer Cell, 2016. **30**(1): p. 147-160.
14. Lee, J., et al., *2-Deoxy-D-glucose protects hippocampal neurons against excitotoxic and oxidative injury: evidence for the involvement of stress proteins*. J Neurosci Res, 1999. **57**(1): p. 48-61.
15. Guarente, L., *Calorie restriction and sirtuins revisited*. Genes Dev, 2013. **27**(19): p. 2072-85.

16. Xu, C., et al., *Calorie Restriction Prevents Metabolic Aging Caused by Abnormal SIRT1 Function in Adipose Tissues*. Diabetes, 2014. **64**(5): p. 1576-1590.
17. Cantó, C. and J. Auwerx, *Calorie Restriction: Is AMPK a Key Sensor and Effector?* Physiology, 2011. **26**(4): p. 214-224.
18. You, M., et al., *Sirtuin 1 signaling and alcoholic fatty liver disease*. Hepatobiliary surgery and nutrition, 2015. **4**(2): p. 88-100.
19. Speakman, J.R. and S.E. Mitchell, *Caloric restriction*. Mol Aspects Med, 2011. **32**(3): p. 159-221.
20. Madeo, F., et al., *Caloric Restriction Mimetics against Age-Associated Disease: Targets, Mechanisms, and Therapeutic Potential*. Cell Metabolism, 2019. **29**(3): p. 592-610.
21. Jones, J.M., *CODEX-aligned dietary fiber definitions help to bridge the 'fiber gap'*. Nutrition Journal, 2014. **13**(1): p. 34.
22. Sawicki, C.M., et al., *Dietary Fiber and the Human Gut Microbiota: Application of Evidence Mapping Methodology*. Nutrients, 2017. **9**(2).
23. Jha, R. and J.D. Berrocoso, *Review: Dietary fiber utilization and its effects on physiological functions and gut health of swine*. Animal, 2015. **9**(9): p. 1441-52.
24. Zhang, L., et al., *Effects of dietary fibre source on microbiota composition in the large intestine of suckling piglets*. FEMS Microbiology Letters, 2016. **363**(14): p. fnw138.
25. Graf, D., et al., *Contribution of diet to the composition of the human gut microbiota*. Microb Ecol Health Dis, 2015. **26**: p. 26164.
26. Gill, S.K., et al., *Dietary fibre in gastrointestinal health and disease*. Nature Reviews Gastroenterology & Hepatology, 2021. **18**(2): p. 101-116.
27. Reynolds, A., et al., *Carbohydrate quality and human health: a series of systematic reviews and meta-analyses*. The Lancet, 2019. **393**(10170): p. 434-445.
28. Wong, C., P.J. Harris, and L.R. Ferguson, *Potential Benefits of Dietary Fibre Intervention in Inflammatory Bowel Disease*. International Journal of Molecular Sciences, 2016. **17**(6): p. 919.
29. Grunberger, G., K.-L.C. Jen, and J.D. Artiss, *The benefits of early intervention in obese diabetic patients with FBCx™ — a new dietary fibre*. Diabetes/Metabolism Research and Reviews, 2007. **23**(1): p. 56-62.
30. Neyrinck, A.M., et al., *Prebiotic dietary fibre intervention improves fecal markers related to inflammation in obese patients: results from the Food4Gut randomized placebo-controlled trial*. European Journal of Nutrition, 2021. **60**(6): p. 3159-3170.

31. Sender, R., S. Fuchs, and R. Milo, *Revised Estimates for the Number of Human and Bacteria Cells in the Body*. PLOS Biology, 2016. **14**(8): p. e1002533.
32. Qin, J., et al., *A human gut microbial gene catalogue established by metagenomic sequencing*. Nature, 2010. **464**(7285): p. 59-65.
33. Sommer, F. and F. Bäckhed, *The gut microbiota — masters of host development and physiology*. Nature Reviews Microbiology, 2013. **11**(4): p. 227-238.
34. Faith, J.J., et al., *The long-term stability of the human gut microbiota*. Science, 2013. **341**(6141): p. 1237439.
35. Hoy, Y.E., et al., *Variation in Taxonomic Composition of the Fecal Microbiota in an Inbred Mouse Strain across Individuals and Time*. PLoS One, 2015. **10**(11): p. e0142825.
36. Hufeldt, M.R., et al., *Variation in the gut microbiota of laboratory mice is related to both genetic and environmental factors*. Comp Med, 2010. **60**(5): p. 336-47.
37. Lozupone, C.A., et al., *Diversity, stability and resilience of the human gut microbiota*. Nature, 2012. **489**(7415): p. 220-30.
38. Conlon, M.A. and A.R. Bird, *The impact of diet and lifestyle on gut microbiota and human health*. Nutrients, 2014. **7**(1): p. 17-44.
39. Round, J.L. and S.K. Mazmanian, *The gut microbiota shapes intestinal immune responses during health and disease*. Nature Reviews Immunology, 2009. **9**(5): p. 313-323.
40. Koh, A., et al., *From Dietary Fiber to Host Physiology: Short-Chain Fatty Acids as Key Bacterial Metabolites*. Cell, 2016. **165**(6): p. 1332-1345.
41. Jandhyala, S.M., et al., *Role of the normal gut microbiota*. World J Gastroenterol, 2015. **21**(29): p. 8787-803.
42. Swann, J.R., et al., *Systemic gut microbial modulation of bile acid metabolism in host tissue compartments*. Proceedings of the National Academy of Sciences, 2011. **108**(Supplement 1): p. 4523.
43. Chiang, J.Y., *Recent advances in understanding bile acid homeostasis*. F1000Research, 2017. **6**: p. 2029-2029.
44. Ramírez-Pérez, O., et al., *The Role of the Gut Microbiota in Bile Acid Metabolism*. Annals of Hepatology, 2017. **16**: p. S21-S26.
45. Russell, D.W., *The enzymes, regulation, and genetics of bile acid synthesis*. Annu Rev Biochem, 2003. **72**: p. 137-74.
46. Singh, J., et al., *Review on Bile Acids: Effects of the Gut Microbiome, Interactions with Dietary Fiber, and Alterations in the Bioaccessibility of Bioactive Compounds*. J Agric Food Chem, 2019. **67**(33): p. 9124-9138.

47. Long, S.L., C.G.M. Gahan, and S.A. Joyce, *Interactions between gut bacteria and bile in health and disease*. Mol Aspects Med, 2017. **56**: p. 54-65.
48. Cariou, B., et al., *The Farnesoid X Receptor Modulates Adiposity and Peripheral Insulin Sensitivity in Mice* . Journal of Biological Chemistry, 2006. **281**(16): p. 11039-11049.</sup>
49. Abdelkarim, M., et al., *The Farnesoid X Receptor Regulates Adipocyte Differentiation and Function by Promoting Peroxisome Proliferator-activated Receptor- α ; and Interfering with the Wnt/ β -Catenin Pathways* . Journal of Biological Chemistry, 2010. **285**(47): p. 36759-36767.</sup>
50. McCusker, S., et al., *Amino acid content of selected plant, algae and insect species: a search for alternative protein sources for use in pet foods*. J Nutr Sci, 2014. **3**: p. e39.
51. Chandini, S., et al., *Seaweeds as a source of nutritionally beneficial compounds - A review*. Journal of Food Science and Technology -Mysore-, 2008. **45**: p. 1-13.
52. Huxtable, R.J., *Physiological actions of taurine*. Physiol Rev, 1992. **72**(1): p. 101-63.
53. Abebe, W. and M.S. Mozaffari, *Role of taurine in the vasculature: an overview of experimental and human studies*. Am J Cardiovasc Dis, 2011. **1**(3): p. 293-311.
54. Wang, Y., et al., *Crystal structure of human cysteamine dioxygenase provides a structural rationale for its function as an oxygen sensor*. Journal of Biological Chemistry, 2021. **297**(4).
55. Gupta, R.C., Y. Seki, and J. Yosida, *Role of taurine in spinal cord injury*. Curr Neurovasc Res, 2006. **3**(3): p. 225-35.
56. Anderson, C.M., et al., *Taurine uptake across the human intestinal brush-border membrane is via two transporters: H⁺-coupled PAT1 (SLC36A1) and Na⁺- and Cl⁻-dependent TauT (SLC6A6)*. J Physiol, 2009. **587**(Pt 4): p. 731-44.
57. Jakaria, M., et al., *Taurine and its analogs in neurological disorders: Focus on therapeutic potential and molecular mechanisms*. Redox Biol, 2019. **24**: p. 101223.
58. Ripps, H. and W. Shen, *Review: taurine: a "very essential" amino acid*. Mol Vis, 2012. **18**: p. 2673-86.
59. Danielsson, H., *PRESENT STATUS OF RESEARCH ON CATABOLISM AND EXCRETION OF CHOLESTEROL*. Adv Lipid Res, 1963. **1**: p. 335-85.
60. Park, E., et al., *Development of a novel cysteine sulfinic Acid decarboxylase knockout mouse: dietary taurine reduces neonatal mortality*. J Amino Acids, 2014. **2014**: p. 346809.

61. Jeong-Ah, Y., et al., *Neuroprotective Effect of Taurine against Oxidative Stress-Induced Damages in Neuronal Cells*. *Biomolecules & Therapeutics*, 2010. **18**(1): p. 24-31.
62. Ashkani-Esfahani, S., et al., *Taurine improves the wound healing process in cutaneous leishmaniasis in mice model, based on stereological parameters*. *Adv Biomed Res*, 2014. **3**: p. 204.
63. Miyamoto, T.A., et al., *Taurine-mediated cardioprotection is greater when administered upon reperfusion than prior to ischemia*. *Adv Exp Med Biol*, 2009. **643**: p. 27-36.
64. Sirdah, M.M., *Protective and therapeutic effectiveness of taurine in diabetes mellitus: a rationale for antioxidant supplementation*. *Diabetes Metab Syndr*, 2015. **9**(1): p. 55-64.
65. Schaffer, S.W., et al., *Impaired energy metabolism of the taurine-deficient heart*. *Amino Acids*, 2016. **48**(2): p. 549-58.
66. Terrill, J.R., et al., *Increasing taurine intake and taurine synthesis improves skeletal muscle function in the mdx mouse model for Duchenne muscular dystrophy*. *J Physiol*, 2016. **594**(11): p. 3095-110.
67. Ahmadian, M., et al., *Taurine supplementation has anti-atherogenic and anti-inflammatory effects before and after incremental exercise in heart failure*. *Ther Adv Cardiovasc Dis*, 2017. **11**(7): p. 185-194.
68. Solís, J., et al., *Does taurine act as an osmoregulatory substance in the rat brain?* *Neuroscience Letters*, 1988. **91**(1): p. 53-58.
69. El Idrissi, A., L. Boukarrou, and W. L'Amoreaux, *Taurine supplementation and pancreatic remodeling*. *Adv Exp Med Biol*, 2009. **643**: p. 353-8.
70. Schaffer, S. and H.W. Kim, *Effects and Mechanisms of Taurine as a Therapeutic Agent*. *Biomol Ther (Seoul)*, 2018. **26**(3): p. 225-241.
71. Hwang, C., A.J. Sinskey, and H.F. Lodish, *Oxidized redox state of glutathione in the endoplasmic reticulum*. *Science*, 1992. **257**(5076): p. 1496-502.
72. Pai, E.F. and G.E. Schulz, *The catalytic mechanism of glutathione reductase as derived from x-ray diffraction analyses of reaction intermediates*. *J Biol Chem*, 1983. **258**(3): p. 1752-7.
73. Cooper, A.J.L. and M.H. Hanigan, *Metabolism of Glutathione S-Conjugates: Multiple Pathways*. *Comprehensive Toxicology*, 2018: p. 363-406.
74. Kim, Y. and H.H. Jang, *Role of Cytosolic 2-Cys Prx1 and Prx2 in Redox Signaling*. *Antioxidants*, 2019. **8**: p. 169.

75. Hoensch, H., et al., *Influence of clinical factors, diet, and drugs on the human upper gastrointestinal glutathione system*. Gut, 2002. **50**(2): p. 235-40.
76. van Lieshout, E.M. and W.H. Peters, *Age and gender dependent levels of glutathione and glutathione S-transferases in human lymphocytes*. Carcinogenesis, 1998. **19**(10): p. 1873-5.
77. Wang, H., H. Liu, and R.-M. Liu, *Gender difference in glutathione metabolism during aging in mice*. Experimental Gerontology, 2003. **38**(5): p. 507-517.
78. Lyons, J., et al., *Blood glutathione synthesis rates in healthy adults receiving a sulfur amino acid-free diet*. Proc Natl Acad Sci U S A, 2000. **97**(10): p. 5071-6.
79. Lauterburg, B.H. and M.E. Velez, *Glutathione deficiency in alcoholics: risk factor for paracetamol hepatotoxicity*. Gut, 1988. **29**(9): p. 1153-7.
80. Wu, W.-H., C.-C. Chao, and F.-S. Wang, *Reducing the effects of drug toxicity on glutathione metabolism*. Journal of the Taiwan Institute of Chemical Engineers, 2016. **60**: p. 113-118.
81. Wang, Y., et al., *Bile acids regulate cysteine catabolism and glutathione regeneration to modulate hepatic sensitivity to oxidative injury*. JCI Insight, 2018. **3**(8).
82. Weckwerth, W., K. Wenzel, and O. Fiehn, *Process for the integrated extraction, identification and quantification of metabolites, proteins and RNA to reveal their co-regulation in biochemical networks*. Proteomics, 2004. **4**(1): p. 78-83.
83. Doerfler, H., et al., *Granger causality in integrated GC-MS and LC-MS metabolomics data reveals the interface of primary and secondary metabolism*. Metabolomics, 2013. **9**(3): p. 564-574.
84. Obermeyer, G., et al., *Dynamic adaption of metabolic pathways during germination and growth of lily pollen tubes after inhibition of the electron transport chain*. Plant Physiol, 2013. **162**(4): p. 1822-33.
85. Klymiuk, I., et al., *The Human Gastric Microbiome Is Predicated upon Infection with Helicobacter pylori*. Front Microbiol, 2017. **8**: p. 2508.
86. Afgan, E., et al., *The Galaxy platform for accessible, reproducible and collaborative biomedical analyses: 2018 update*. Nucleic Acids Res, 2018. **46**(W1): p. W537-w544.
87. Yilmaz, P., et al., *The SILVA and "All-species Living Tree Project (LTP)" taxonomic frameworks*. Nucleic Acids Res, 2014. **42**(Database issue): p. D643-8.
88. Adler, L.W. and B.P. Rosen, *Properties of Escherichia coli mutants with alterations in Mg²⁺-adenosine triphosphatase*. J Bacteriol, 1976. **128**(1): p. 248-56.

89. Veillette, A., et al., *Expression of the lck tyrosine kinase gene in human colon carcinoma and other non-lymphoid human tumor cell lines*. *Oncogene Res*, 1987. **1**(4): p. 357-74.
90. Ito, T., et al., *Mass spectrometry-based metabolomics to identify taurine-modified metabolites in heart*. *Amino Acids*, 2018. **50**(1): p. 117-124.
91. Budinska, E., et al., *Microbiome and Metabolome Profiles Associated With Different Types of Short Bowel Syndrome: Implications for Treatment*. *Journal of Parenteral and Enteral Nutrition*, 2020. **44**(1): p. 105-118.
92. Wegner, K., et al., *Rapid analysis of bile acids in different biological matrices using LC-ESI-MS/MS for the investigation of bile acid transformation by mammalian gut bacteria*. *Analytical and Bioanalytical Chemistry*, 2017. **409**(5): p. 1231-1245.
93. Zaunschirm, M., et al., *Contribution of the Ratio of Tocopherol Homologs to the Oxidative Stability of Commercial Vegetable Oils*. *Molecules*, 2018. **23**(1): p. 206.
94. Sun, X. and W. Weckwerth, *COVAIn: a toolbox for uni- and multivariate statistics, time-series and correlation network analysis and inverse estimation of the differential Jacobian from metabolomics covariance data*. *Metabolomics*, 2012. **8**(1): p. 81-93.
95. Girvan, M. and M.E. Newman, *Community structure in social and biological networks*. *Proc Natl Acad Sci U S A*, 2002. **99**(12): p. 7821-6.
96. Duszka, K., et al., *Complementary intestinal mucosa and microbiota responses to caloric restriction*. *Scientific Reports*, 2018. **8**(1): p. 11338.
97. Cummings, J.H. and A.M. Stephen, *The role of dietary fibre in the human colon*. *Canadian Medical Association journal*, 1980. **123**(11): p. 1109-1114.
98. Kim, C. and Y.-N. Cha, *Taurine chloramine produced from taurine under inflammation provides anti-inflammatory and cytoprotective effects*. *Amino Acids*, 2014. **46**(1): p. 89-100.
99. Chupel, M.U., et al., *Exercise and taurine in inflammation, cognition, and peripheral markers of blood-brain barrier integrity in older women*. *Applied Physiology, Nutrition, and Metabolism*, 2018. **43**(7): p. 733-741.
100. Sakai, K., et al., *Decreased plasma amino acid concentrations in cats with chronic gastrointestinal diseases and their possible contribution in the inflammatory response*. *Veterinary Immunology and Immunopathology*, 2018. **195**: p. 1-6.
101. Jong, C.J., J. Azuma, and S. Schaffer, *Mechanism underlying the antioxidant activity of taurine: prevention of mitochondrial oxidant production*. *Amino Acids*, 2012. **42**(6): p. 2223-2232.

102. Jong, C.J., et al., *Role of Mitochondria and Endoplasmic Reticulum in Taurine-Deficiency-Mediated Apoptosis*. *Nutrients*, 2017. **9**(8): p. 795.
103. Schaffer, S.W., et al., *Impaired energy metabolism of the taurine-deficient heart*. *Amino Acids*, 2016. **48**(2): p. 549-558.
104. Nishizono, S., et al., *Mechanisms of action of compounds that mimic beneficial effects of calorie restriction such as lifespan extension: Is taurine a promising candidate?* *The Journal of Physical Fitness and Sports Medicine*, 2017. **6**(4): p. 201-207.
105. Yanar, K., et al., *Caloric restriction and redox homeostasis in various regions of aging male rat brain: Is caloric restriction still worth trying even after early-adulthood?* *Journal of Food Biochemistry*, 2019. **43**(3): p. e12740.
106. Fabbiano, S., et al., *Functional Gut Microbiota Remodeling Contributes to the Caloric Restriction-Induced Metabolic Improvements*. *Cell Metabolism*, 2018. **28**(6): p. 907-921.e7.
107. Wang, S., et al., *Gut microbiota mediates the anti-obesity effect of calorie restriction in mice*. *Scientific Reports*, 2018. **8**(1): p. 13037.
108. Boyer, J.L., *Bile Formation and Secretion*, in *Comprehensive Physiology*. p. 1035-1078.

7. Further Publications and Conference Proceedings

7.1. Publications

Duszka K, Gregor A, Reichel MW, Baierl A, Fahrngruber C, König J. Visual stimulation with food pictures in regulation of hunger hormones and nutrient deposition, a potential contributor to the obesity crisis. *PloS One*. 2020 Jun 10.

Duszka K, Gregor A, Guillou H, König J, Wahli W. Peroxisome Proliferator-Activated Receptors and Caloric Restriction-Common Pathways Affecting Metabolism, Health, and Longevity. *Cells*. 2020 Jul 16.

Gregor A, Fragner L, Trajanoski S, Li W, Sun X, Weckwerth W, König J & Duszka K. Cage bedding modifies metabolic and gut microbiota profiles in mouse studies applying dietary restriction. *Scientific Reports*. 2020 Oct 30.

Gregor A, Pignitter M, Fahrngruber C, Bayer S, Somoza V, König J, Duszka K. Caloric restriction increases levels of taurine in the intestine and stimulates taurine uptake by conjugation to glutathione. *J Nutr Biochem*. 2021 May 20.

Gregor A, Pignitter M, Trajanoski S, Auernigg-Haselmaier S, Somoza V, König J, Duszka K. Microbial contribution to the caloric restriction-triggered regulation of the intestinal levels of glutathione transferases, taurine, and bile acid. *Gut Microbes*. 2021 Oct 25.

Gregor A, Auernigg-Haselmaier S, Trajanoski S, König J, Duszka K. Colonic Medium-Chain Fatty Acids Act as a Source of Energy and for Colon Maintenance but Are Not Utilized to Acylate Ghrelin. *Nutrients*. 2021 Oct 26.

Locker F, Szarzynski A, Beikbaghban T, Gregor A, Duszka K, Ingrid W, Kofler B, Pohl E. Triglyceride mediated upregulation of UCP3 in murine heart. *Biophysical Journal*. 2022 Feb 11.

Gregor A, Huber L, Auernigg-Haselmaier S, Sternberg F, Billerhart M, Dunkel A, Somoza V, Ogris M, Kofler B, Longo VD, König J, Duszka K. A Comparison of the Impact of Restrictive Diets on the Gastrointestinal Tract of Mice. *Nutrients*. 2022.07.29

7.2. Oral/Poster Presentations

13. European Nutrition Conference, FENS

Poster title: "Cage bedding affects intestinal microbiota and metabolism in mice"

11. ÖGMBT Annual Meeting: Inside the World of Biomolecules

Poster title: "Cage bedding affects intestinal microbiota in mice"

56. Wissenschaftlichen Kongress der Deutschen Gesellschaft für Ernährung

Poster title: "The impact of cage bedding on microbial caprylate production"

Received a poster award in the category "Physiologie und Biochemie der Ernährung".

Original Article 1



OPEN

Cage bedding modifies metabolic and gut microbiota profiles in mouse studies applying dietary restriction

A. Gregor¹, L. Fragner^{2,3}, S. Trajanoski⁴, W. Li³, X. Sun³, W. Weckwerth^{2,3}, J. König^{1,3} & K. Duszka^{1,3}✉

Experiments involving food restriction are common practice in metabolic research. Under fasted conditions, mice supplement their diet with cage bedding. We aimed at identifying metabolic and microbiota-related parameters affected by the bedding type. We exposed mice housed with wooden, cellulose, or corncob cage beddings to ad libitum feeding, caloric restriction (CR), or over-night (ON) fasting. Additionally, two subgroups of the ON fast group were kept without any bedding or on a metal grid preventing coprophagy. Mice under CR supplemented their diet substantially with bedding; however, the amount varied depending on the kind of bedding. Bedding-related changes in body weight loss, fat loss, cecum size, stomach weight, fecal output, blood ghrelin levels as well as a response to glucose oral tolerance test were recorded. As fiber is fermented by the gut bacteria, the type of bedding affects gut bacteria and fecal metabolites composition of CR mice. CR wood and cellulose groups showed distinct cecal metabolite and microbiome profiles when compared to the CR corncob group. While all ad libitum fed animal groups share similar profiles. We show that restriction-related additional intake of bedding-derived fiber modulates multiple physiological parameters. Therefore, the previous rodent studies on CR, report the combined effect of CR and increased fiber consumption.

It is commonly agreed that mice need to be housed with bedding and nesting material to fulfill the animals' welfare requirements. Cage bedding is an important factor for animal well-being. It provides nesting material, helps to keep warmth, provides a proper walking surface, and buffers air ammonia content¹. However, mice and rats fed at ad libitum and, even more, under dietary restrictions tend to consume cage bedding². Moreover, multiple metabolic tests involving rodents are preceded by over-night (ON) fasting. Thus, the type of bedding and mice's ability to extract energy from the bedding will impact the results of the metabolic tests. An even bigger impact is expected in the case of caloric restriction (CR). CR requires daily delivery of a limited, accurately dosed amount of food. In animal as well as in human studies CR has been shown to increase lifespan and health-span. It prevents the development of various diseases including age-related, neurological, and metabolic diseases as well as cancer^{3,4}. For a successful CR experimental protocol, mice energy intake has to be strictly adjusted. Thus, uncontrolled energy uptake and fiber supplementation by consuming cage bedding can substantially influence the experimental outcome. Accordingly, in our previous publication⁵, we showed that mice submitted to CR develop an increased cecum size. We concluded that the enlarged cecum results from the accumulation of indigestible fiber as a consequence of bedding consumption. The enlarged cecum is observed upon consumption of a high-fiber diet^{6–8} but it is also a phenotype typical to germ-free mice and indicates aggregation of fiber mass as well as disturbed nitrogen reabsorption in the small intestine^{9–11}. Importantly, fiber can also reduce nutrient digestibility as it limits the access of enzymes to nutrients and it may also affect the passage rate of the digesta, especially if consumed in high amounts¹². Accordingly, it has been noticed that feed conversion is reduced from animals housed on corncob (CC) bedding¹³. Two previous publications addressed the issue of the impact of the CC bedding on mice body weight and gut microbiota concluding that application of the CC bedding may

¹Department of Nutritional Sciences, University of Vienna, Althanstrasse 14 (UZA II), 1090 Wien, Austria. ²Molecular Systems Biology, Department of Functional and Evolutionary Ecology, University of Vienna, Vienna, Austria. ³Vienna Metabolomics Center, University of Vienna, Vienna, Austria. ⁴Core Facility Computational Bioanalytics, Medical University of Graz, Graz, Austria. ✉email: kalina.duszka@univie.ac.at

confound study results^{13,14}. However, no one, thus far, compared different types of bedding considering metabolic research and microbiota.

Bedding consumption is particularly important in the context of the rapidly developing field of gut microbiota. Dietary fibers, including those present in cage bedding, may undergo complete or partial fermentation by the gut microbes¹⁵, leading to the production of short-chain fatty acids (SCFA) and stimulating the growth of certain bacterial species¹⁶. The metabolic end products of colonic microbiota play an important role in the maintenance of health and the development of disease^{15,17}. Succeeding inconsistencies in scientific outcomes, the issue of reproducibility in microbiota research was inevitably raised^{18,19}. We aim at studying the variability in research outcomes introduced by cage beddings as well as bringing awareness to the reproducibility of the studies involving fasting and CR by stressing the importance of bedding.

Results

Cage bedding affects mice body and organ weight. To assay the impact of cage bedding we submitted mice to two kinds of dietary restrictions in different housing conditions. The mice were held with one of the cage beddings: wooden (W), cellulose (C), or corncob (CC). The animals from over-night fasted (ON) groups were housed with one of three cage beddings (ON-W, ON-C, ON-CC) and additional groups without bedding (no bedding, ON-NB) or on a metal grid (ON-G). The grid was preventing the animals from contact with the cage bottom, thus limiting coprophagy. In parallel, to assess the long-term effects of bedding consumption we submitted mice to 14 days CR using the three kinds of cage bedding: wooden (CR-W), cellulose (CR-C), and corncob (CR-CC). Corresponding control groups (W, C, CC) were housed ad libitum with one of the assigned cage beddings. The mice housed with wooden bedding ate the biggest amount of bedding while mice on cellulose bedding ate the least of bedding (all groups $p < 0.001$; Fig. 1a). With similar starting bodyweight (Supplementary Fig. S1), overnight-fasted mice from ON-W, ON-C, ON-CC, ON-NB groups lost 13–14% body weight (Fig. 1b) while ON-G mice lost 16% body weight suggesting the impact of coprophagy and/or cage bedding consumption on body weight. CR mice lost 20–22% body weight within 14 days with the CR-CC group losing the most. At the same time, all ad libitum mice gained 6–8% body weight. There were no differences in the weight of the stomach with its content between the ad libitum and CR groups (Fig. 1c) indicating comparable consumption in hours prior to the dissection, even though CR mice had access to food for the last time the evening preceding the dissection. Mice from all ON groups had lighter stomachs than ad libitum fed and CR mice proving diminished consumption (W vs ON-W $p = 0.004$, C vs ON-C $p = 0.006$). Both ON-G (ON-W vs ON-G $p = 0.002$, ON-C vs ON-G $p < 0.001$, ON-CC vs ON-G $p < 0.001$) and ON-NB (ON-CC vs ON-NB $p = 0.002$) groups had smaller stomachs than other ON groups suggesting the lowest food intake. Among ON fasted groups, CC group had the heaviest stomach and its content implying increased consumption or slower digestibility of CC bedding compared to W and C. CR mice, which experienced long-lasting dietary restriction, had heavier stomach with its content than ON mice suggesting that long-term food restriction enhances supplementation with cage bedding and/or feces. Mice from all CR groups showed an increased weight of cecum with its content compared to ad libitum mice (Fig. 1d) pointing toward an accumulation of indigestible fiber. The cecum of the CR-CC group was significantly smaller than the cecum of CR-W mice ($p = 0.005$) suggesting less fiber deposition. All ON fast mice showed decreased cecum weight compared to ad libitum mice. ON-G group had a statistically significantly lighter cecum than any other ON mice (ON-G vs ON-W $p < 0.01$, ON-G vs ON-C $p < 0.01$, ON-G vs ON-CC $p < 0.01$, ON-G vs ON-NB $p = 0.007$). All CR and ON mice had smaller liver than corresponding control mice (Supplementary Fig. S1). However, there was no impact of the type of bedding or lack of bedding on the liver size in relation to their body size in ON as well as CR groups. Similarly, CR mice had less epididymal white adipose tissue (eWAT) (Supplementary Fig. S1) and subcutaneous white adipose tissue (sWAT) (Supplementary Fig. S1) than control groups, however, there was no impact of the bedding type. Despite comparable total body weight loss between the different ON groups, the ON-NB group showed higher sWAT content compared to the ON-W, ON-C, and ON-CC groups.

Cage bedding impacts ghrelin and glucose levels in plasma. Mice from CR and ON groups showed increased plasma total ghrelin levels compared to ad libitum groups (Fig. 1e; all groups $p < 0.005$). CR-W had a lower level of total ghrelin compared to CR-CC, however, the difference was not statistically significant ($p = 0.06$). The more pronounced pattern was measured for active ghrelin with values for CR-W stronger contrasting other CR groups and showing significant difference when compared to CR-C ($p = 0.004$; Fig. 1f). However, each day of CR, mice from all CR groups took a similar time to reach for a daily food portion suggesting equal hunger level (Supplementary Fig. S2). Additionally, the expression of Neuropeptide Y (Npy), leptin receptor (Lepr), and cholecystokinin receptor (Cckr) genes is modified by CR and ON fasting but not affected by the type of bedding (Supplementary Fig. S2). Concerning the ON groups, the type of bedding or lack thereof did not influence plasma active ghrelin levels (Fig. 1f).

CR and ON groups had generally lower plasma glucose levels compared to ad libitum fed groups (Supplementary Fig. S2). Glucose concentration was lower in ON-NB and ON-G than other ON groups; however, due to multiple groups, not statistically significant in all instances (ON-W vs ON-NB $p = 0.008$, ON-C vs ON-NB $p = 0.03$, ON-CC vs ON-NB $p = 0.05$, ON-W vs ON-G $p = 0.01$, ON-C vs ON-G $p = 0.04$, ON-CC vs ON-G $p = 0.03$). Upon glucose load mice from ON-NB and ON-G groups showed decreased blood glucose levels starting from 30 min after glucose administration (Fig. 1g, Supplementary Fig. S2) suggesting increased uptake in peripheral tissues. The area under the curve of plasma glucose levels was smaller for ON-NB and ON-G compared to other ON groups (ON-W vs ON-NB $p = 0.004$, ON-C vs ON-NB $p = 0.008$, ON-CC vs ON-NB $p = 0.003$, ON-W vs ON-G $p = 0.009$, ON-C vs ON-G $p = 0.01$, ON-CC vs ON-G $p = 0.004$; Supplementary Fig. S2).

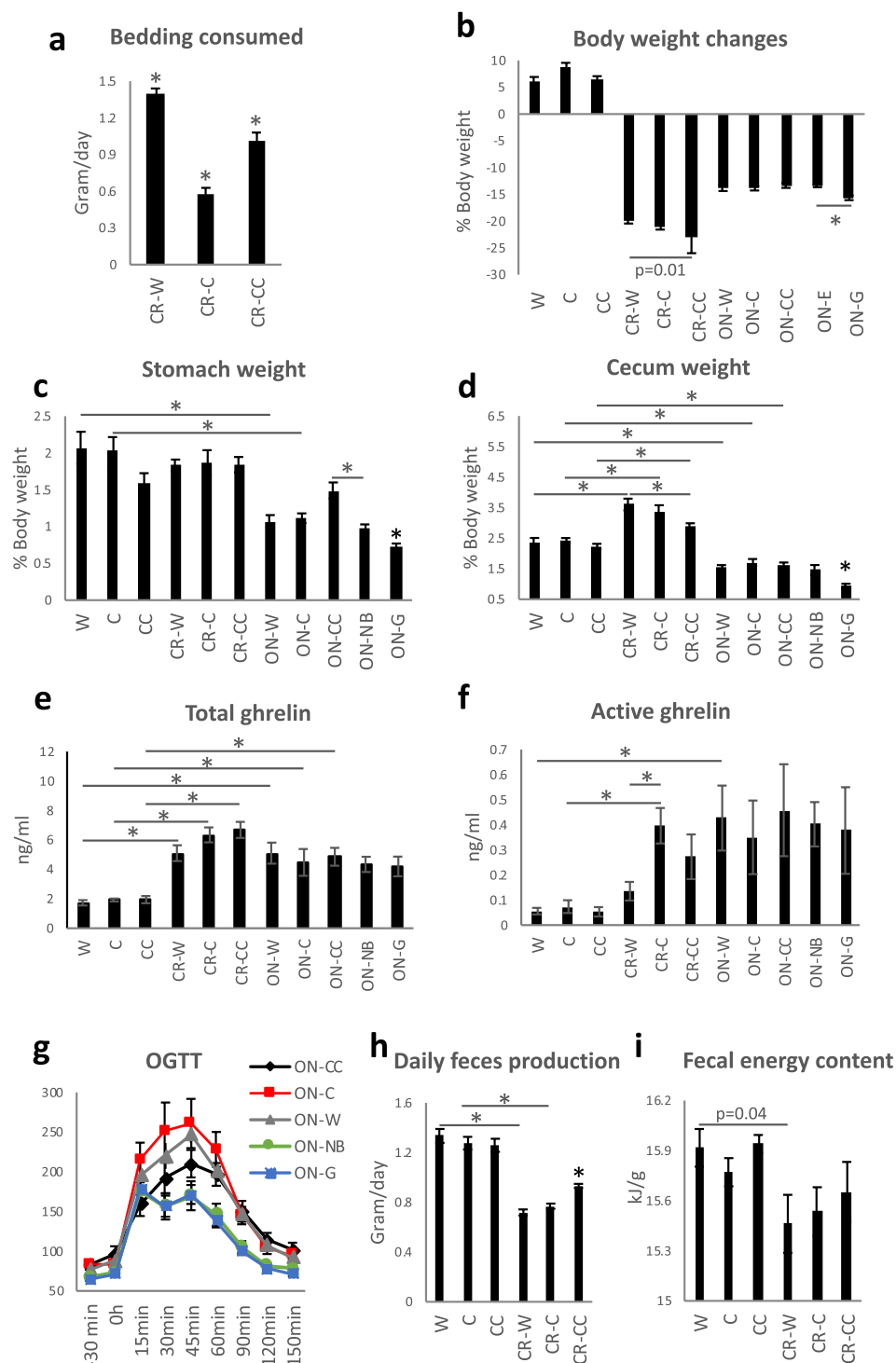


Figure 1. Cage bedding affects body parameters in dietary restricted mice. The amount of bedding consumed by mice submitted caloric restriction (CR) was measured daily between days 11 and 13 of the CR (a). Bodyweight changes were recorded for ad libitum, CR mice as well as over-night (ON) fasted mice and expressed as % change (b). Stomach (c) and cecum (d) weight were measured. Total (e) and active (f) ghrelin concentrations were analyzed in the mice plasma. Oral glucose tolerance test (OGTT) was performed after ON fasting (g). CR mice feces were collected and its weight (h), as well as energy content (i), was assessed. One-way ANOVA was applied to verify statistical significance. Asterisk (*) indicates statistical significance between the indicated groups after Bonferroni correction for multiple testing. The bars indicate the mean of eight to ten biological replicates \pm SEM.

Cage bedding affects energy content, microbiota, and metabolites in CR mice cecum. To investigate the impact on the gastrointestinal tract we measured gene expression in the intestinal mucosa. As we previously published⁵, CR tends to increase the expression of metabolic genes (*Ppara α* , *Acot4*, *Scd1*) and decrease the expression of inflammatory genes (*MyD88*, *Rsd2*, *Oasl1a*, *Irf7*) (Supplementary Fig. S3). However, the type of bedding did not affect gene expression.

The bedding was collected from CR mice cages every 24 h for three consecutive days and feces were separated, dried, and weighed. The CR mice produced fewer feces than ad libitum groups (for all groups $p < 0.001$; Fig. 1h) and the feces contained less energy; however the difference was not statistically significant when correcting for the number of experimental groups (W vs CR-W $p = 0.04$; Fig. 1i). Importantly, CR-CC produced more feces compared to the other CR groups (for both groups comparison $p < 0.001$; Fig. 1h). Further, we analyzed cecal microbiota as fermentation of indigestible food in mice is compartmentalized in the cecum. At the same time, microbiota and metabolites share similarities between cecum, colon, and feces^{20,21}. All ad libitum fed mice groups shared similar microbial composition (Fig. 2a). We observed a strong shift in cecal bacteria composition from ad libitum to CR mice (Fig. 2a). In general, among the CR groups, CR-W and CR-C bacteria composition overlapped while CR-CC was distinct (Fig. 2b–c). CR was accompanied by a non-statistically significant shift in the ratio of *Firmicutes* to *Bacteroidetes* (CC vs CR-CC $p = 0.01$; Supplementary Fig. S4). The strongest differences on the phylum level were recorded for *Proteobacteria* (all ad libitum vs CR groups $p < 0.001$; Fig. 2d, Supplementary Fig. S4) and *Deferribacteres* (all ad libitum vs CR groups $p < 0.001$; Supplementary Fig. S4). The sequencing results were compared to published CR reports^{22–26} and the previously observed decrease in abundance of *Roseburia* (C vs CR-C $p = 0.004$, CC vs CR-CC $p < 0.055$), *Butyricoccus* (all ad libitum vs CR groups $p < 0.001$), *Streptococcus* (W vs CR-W $p = 0.005$, C vs CR-C $p < 0.001$, CC vs CR-CC $p < 0.001$), *Anaerotruncus* (C vs CR-C $p = 0.001$), and *Lachnospiraceae* (all ad libitum vs CR groups $p < 0.001$; Supplementary Fig. S4) as well as an increase in *Lactobacillus* (all ad libitum vs CR groups $p < 0.001$), *Parabacteroides* (W vs CR-W $p = 0.02$, C vs CR-C $p < 0.001$, CC vs CR-CC $p < 0.01$), and *Odoribacter* (W vs CR-W $p = 0.02$, C vs CR-C $p = 0.03$, CC vs CR-CC $p < 0.001$) in CR compared to ad libitum (Fig. 2e,f, Supplementary Fig. S4) were observed. In other reported CR-affected Operational Taxonomic Units (OTU) (e.g. *Alistipes*, *Alloprevotella*, *Erysipelotrichaceae*, *Intestinimonas*, *Lachnospiraceae*, *Marvinbryantia*, *Roseburia*, *Ruminococcaceae*)^{23–26} we observed inverse or no effect of CR (Supplementary Fig. S5). Importantly, there has also been little overlap between different published data sets. We identified phylum *Deferribacteres* (CR-W vs CR-CC $p < 0.001$, CR-C vs CR-CC $p = 0.003$), genus *Lactobacillus* (CR-W vs CR-CC $p < 0.006$, CR-C vs CR-CC $p = 0.03$) as well as the families *Marinifilaceae* (CR-W vs CR-CC $p < 0.001$, CR-C vs CR-CC $p < 0.001$), *Clostridiales XIII UCG-001* (CR-W vs CR-CC $p < 0.001$, CR-C vs CR-CC $p < 0.001$), *Deferribacteraceae* (CR-W vs CR-CC $p < 0.001$, CR-C vs CR-CC $p = 0.008$), *Burkholderiaceae* (CR-W vs CR-CC $p = 0.009$, CR-C vs CR-CC $p < 0.001$), and *Tannerellaceae* (CR-C vs CR-CC $p = 0.008$) as bacteria affected the strongest (based on p -value) by the bedding type in CR mice, particularly by the difference between CC versus C and W beddings (Fig. 2e,g–k, Supplementary Fig. S4). Moreover, OTUs *Odoribacter* (CR-W vs CR-CC $p < 0.001$, CR-C vs CR-CC $p < 0.001$), *Mucispirillum* (phylum *Deferribacteres*) (CR-W vs CR-CC $p < 0.001$, CR-C vs CR-CC $p = 0.003$), *Parasutterella* (CR-W vs CR-CC $p = 0.02$, CR-C vs CR-CC $p = 0.002$), and *Erysipelatoclostridium* (CR-W vs CR-CC $p < 0.001$, CR-C vs CR-CC $p = 0.007$), *Eubacterium* (from *Xylanophilum* group; CR-W vs CR-CC $p = 0.019$, CR-C vs CR-CC $p = 0.007$), *Ruminoclostridium 6* (CR-W vs CR-CC $p = 0.03$, CR-C vs CR-CC $p = 0.002$) and *Ruminococcus 1* (CR-W vs CR-CC $p = 0.05$, CR-C vs CR-CC $p = 0.001$) distinguished CR-CC from CR-W and CR-C (Supplementary Figs. S4 and S6). Correspondingly, the composition of cecal metabolites was affected by the restriction and bedding type (Fig. 3a). The metabolites composition was similar in the mice groups fed ad libitum while among CR groups, CR-W and CR-C were distinct from CR-CC. Variable importance for prediction (VIP) scores were calculated from the PLS and the top 25 highly significant metabolites that cause the difference between the groups have been identified (Fig. 3b). The hierarchical clustering of metabolites further visualized the differences between the groups (Fig. 3c). Among the metabolites setting the CR groups apart, fumaric acid (CR-W vs CR-CC $p = 0.03$, CR-C vs CR-CC $p = 0.002$), fructose (CR-W vs CR-CC $p = 0.001$, CR-C vs CR-CC $p = 0.001$), and phosphoric acid monomethyl ester (CR-W vs CR-CC $p = 0.02$, CR-C vs CR-CC $p = 0.001$) were identified (Fig. 3c–f). The levels of SCFAs acetate (CR-W vs CR-CC $p = 0.01$, CR-C vs CR-CC $p = 0.006$) and butyrate (CR-W vs CR-CC $p = 0.001$, CR-C vs CR-CC $p = 0.002$), as well as medium-chain fatty acids (MCFAs), were decreased in all CR groups regardless of the type of bedding (Fig. 3g–i, Supplementary Fig. S7). The levels of propionate were significantly downregulated only for the CR-CC group (CC vs CR-CC $p = 0.001$, CR-W vs CR-CC $p = 0.001$, CR-C vs CR-CC $p = 0.001$; Fig. 3i). Further, we sought to identify which bacteria could contribute to the observed metabolomic changes. A correlation between changes in bacteria composition and metabolites occurrence revealed the co-dependence of multiple factors (Fig. 4, Table 1). Correlation coefficients were calculated for the CR groups and depicted by Cytoscape into clusterings of cecal bacterial families and metabolites indicating strong interaction (Fig. 4).

Discussion

Previously we showed that mice submitted to CR increased their cecum weight as a likely result of the accumulation of indigestible fiber from bedding⁵. In the current project, we investigated the consequences of the increased consumption of cage bedding and how it influences the outcome of animal studies. We show the impact of cage bedding in restrictive dietary protocols, reflected by differences in body weight, adiposity, cecum size, glucose, and ghrelin levels in plasma as well as cecal microbiota and metabolites profile.

All CR mice consumed bedding, however, the amounts of eaten beddings varied suggesting a difference in preference (olfactory and gustatory properties), the capacity of the bedding to deliver energy, or offer satiety. The CR groups showed bedding-dependent variability in weight loss. The difference may be explained by the availability of fiber which, especially the soluble one, can serve as a source of energy (2 kcal/100 g)²⁷. CR-W and CR-C

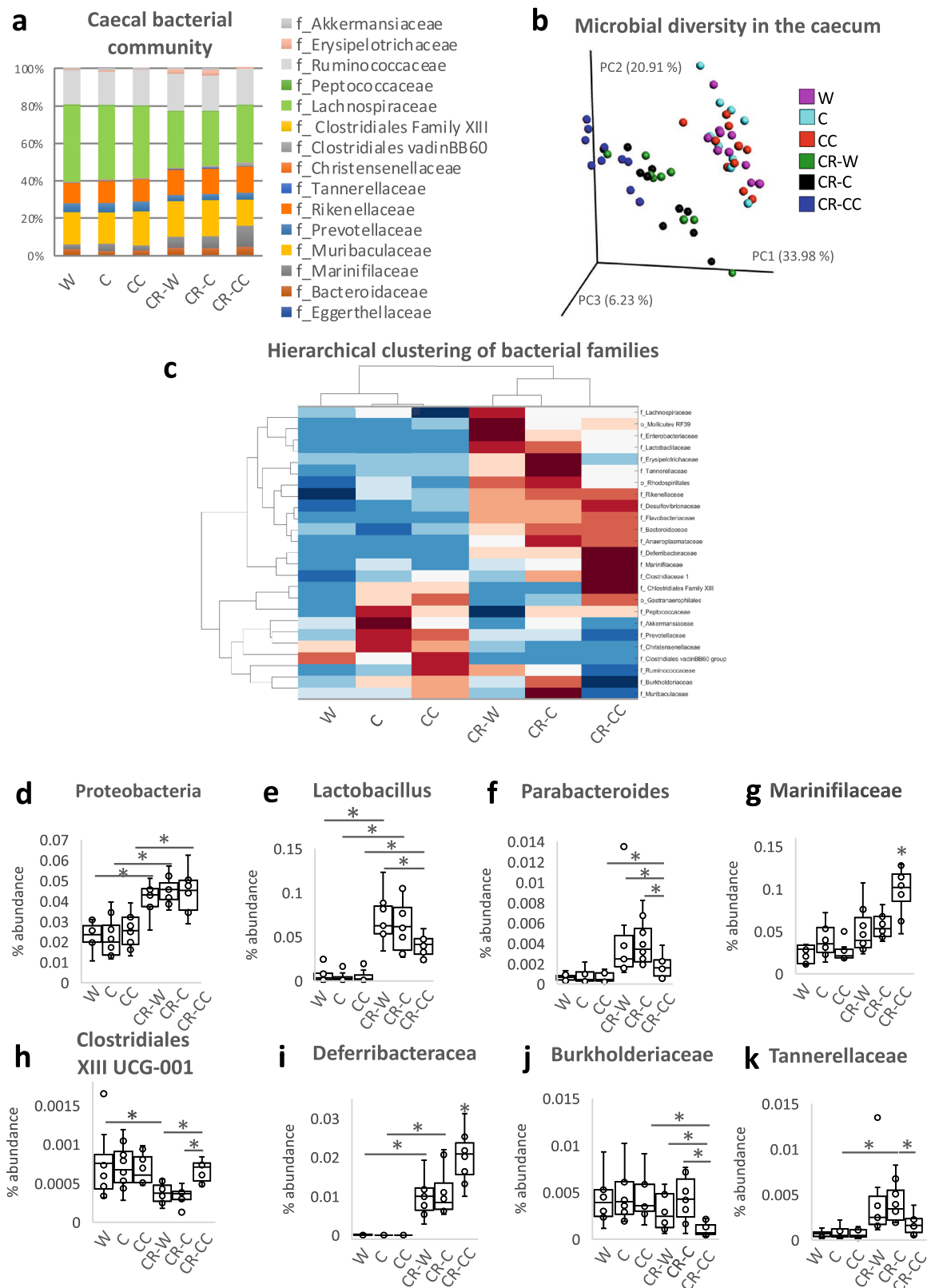


Figure 2. Cage bedding impacts the composition of cecal microbiota. The composition of bacterial families (a) and microbial diversity (b) in the cecum was analyzed in ad libitum and CR fed mice. The data was presented as a heatmap of the hierarchical clustering analysis of bacterial families using COVAIN (c). The abundance of bacteria in the cecum was expressed as % (d–k). Asterisk (*) indicates statistical significance after Bonferroni correction for multiple testing. Groups were compared using one-way ANOVA. Error bars stand for the mean \pm SEM. The data represents nine to ten biological replicates per experimental group.

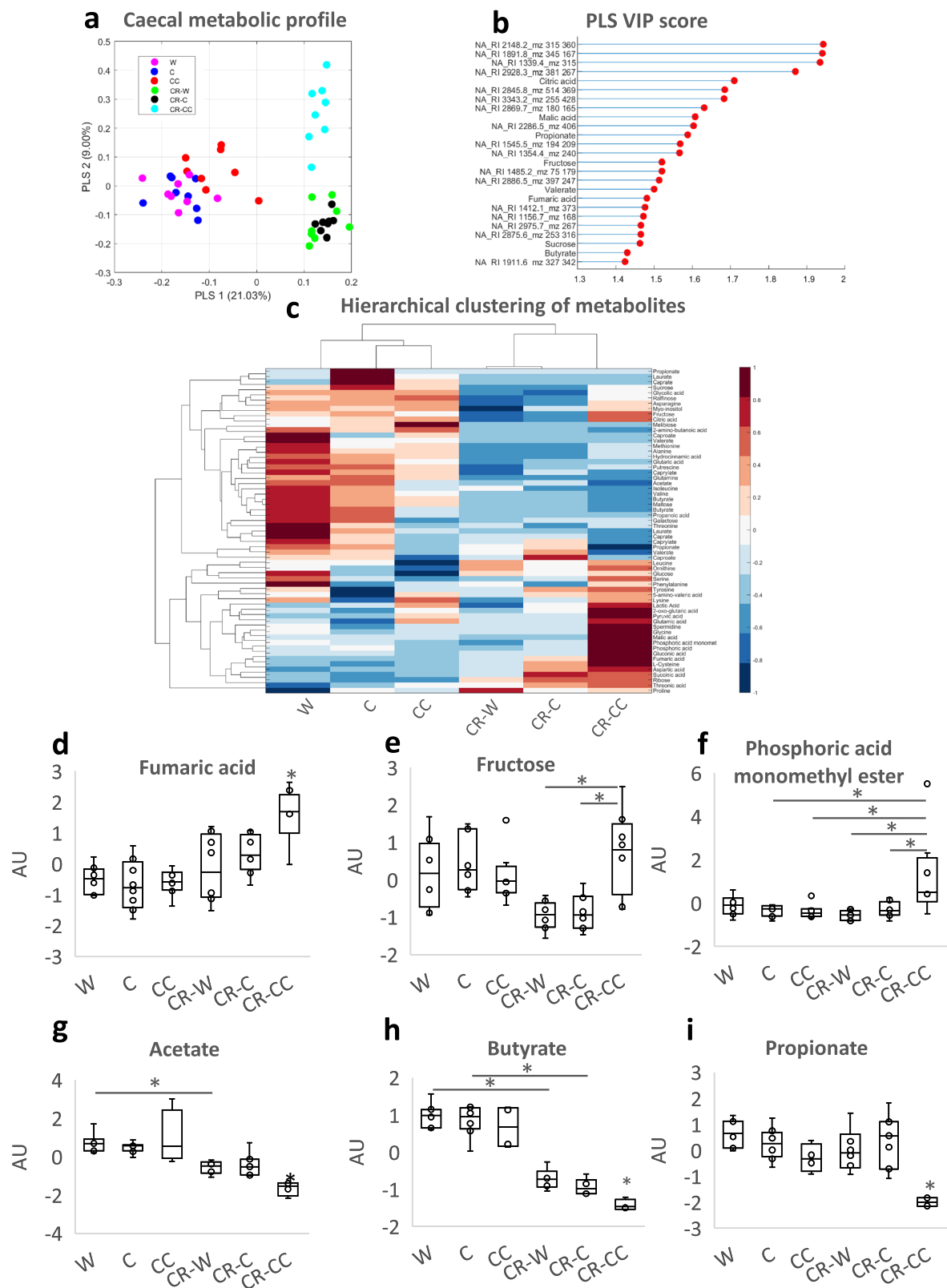


Figure 3. Cage bedding impacts the composition of cecal metabolites. The metabolome of cecal content was analyzed (a) and the most important variables were summarized (b). Heatmap of hierarchical clustering analysis of annotated metabolites was created using COVAIN (c). Z-Scored metabolites figures show the relative deviation from the groups mean value (0) for fumaric acid (d), fructose (e), and phosphoric acid monomethyl ester (f) represent the most important annotated metabolites contributing to a distinct metabolic profile within the CR group. The cecum content of SCFAs was analyzed (g–i). Single data points are indicated by circles and medians as horizontal lines within each box. One-way ANOVA was applied to verify statistical significance. Asterisk (*) indicates statistical significance after Bonferroni post-hoc analysis. Error bars stand for \pm SEM; $n=8-10$.

Network of bacteria and metabolites

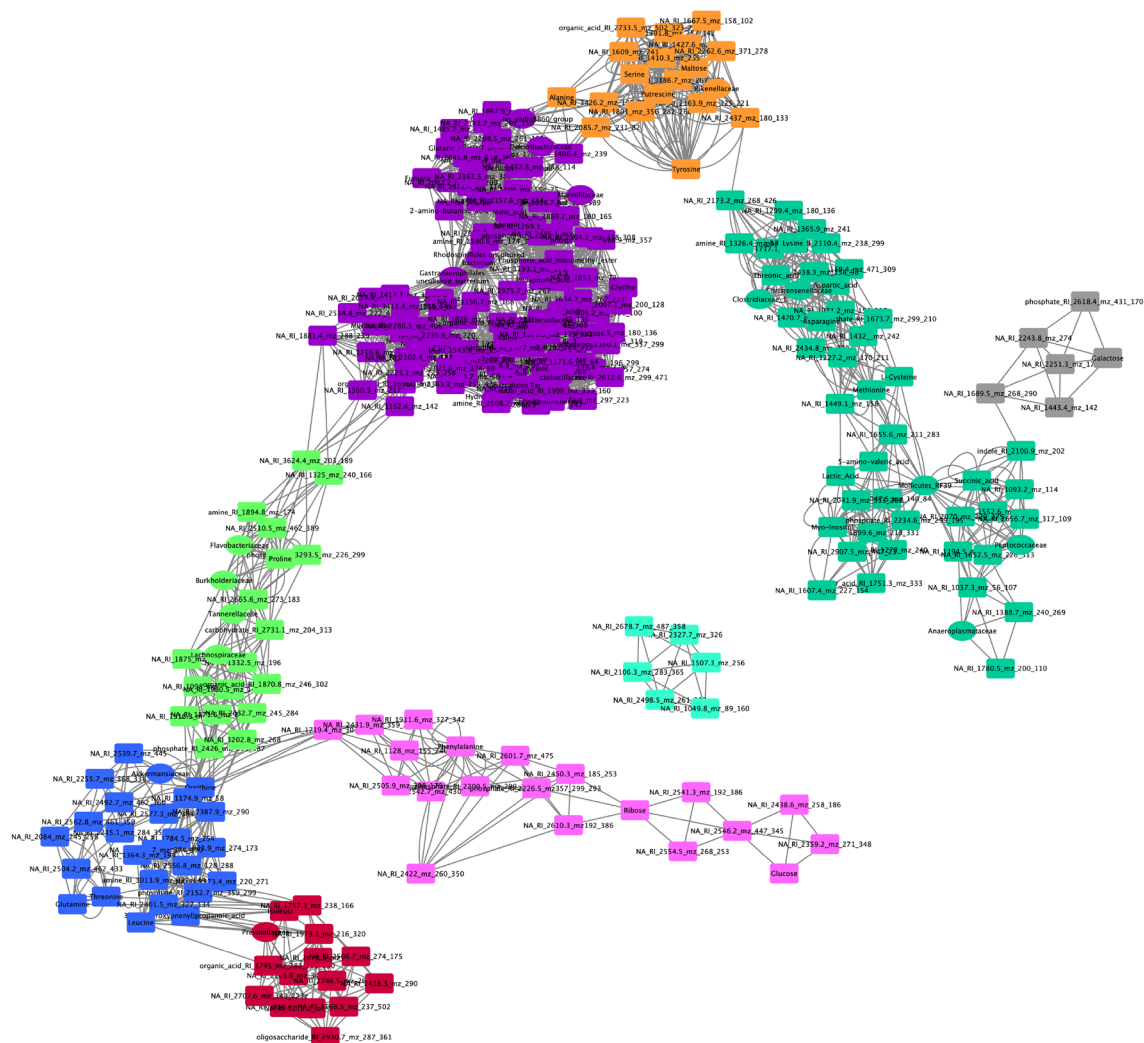


Figure 4. Correlation network of bacteria with metabolites in the cecum. The correlation network depicts changes in bacterial families composition and metabolites occurrence characteristic to CR. Each node represents one metabolite (ellipse) or a bacterial family-level OUT (V-shape) and each edge represents a statistically significant correlation where the Pearson's correlation coefficient ≥ 0.8 . Girven–Newman algorithm was applied in network clustering analysis where modules (clusters, denoted by different colors) depict association patterns between metabolites and bacteria. The visualization was performed with Cytoscape v3.7.2. (<http://www.cytoscape.org/>).

groups consumed mostly cellulose which is fermentable to some extent (up to 70%–80%), even in humans^{28,29}. Similarly, hemicellulose can be bacterially digested²⁹ and it might improve the fermentability of cellulose³⁰. While lignin is indigestible by human enzymes²⁹, it was shown in vitro to be partially digestible by the human microbiome³¹ and in vivo by rats³². In order to compare the amount of energy taken up and extracted by mice from the ingested beddings energy content in feces was measured. We were not able to detect differences in fecal energy content (kJ/g) between the CR groups, however, it is important to notice that the CR-CC group produced more feces (g/day) and therefore secreted more total energy (kJ/day). This result is accompanied by the highest body weight loss for the CR-CC group. Therefore, we suspect that of the three beddings CC was the source of which the mice were able to absorb the least of energy. Importantly, it is impossible to state whether the differences in the measured amounts of feces result from disparities in the production or the consumption of feces.

The weight of the stomach with its content was considered in our study as an indicator of the scale of consumption within the last hours prior to the dissection. The smaller stomach size in the animals housed on the grids proved our concept. Interestingly, although ON fasted animals consumed bedding their stomachs were much smaller than the stomachs of CR mice, whereas the difference between ad libitum and CR mice was minor. Therefore, prolonged restriction favors enhanced bedding consumption. Similarly to the stomach, the weight of the cecum with its content reflected the amount of fiber consumption. However, this was more specific in a way that it also pictured the intake over a prolonged period, fiber accumulation, and digestibility of the fiber in

	g_Bacteroides	g_Rikenellaceae RC9 gut group	g_Parabacteroides	f_Flavobacteriaceae	g_Lactobacillus	g_Lachnospirillum	g_Tyzzerella	f_Ruminococcaceae	g_[Eubacterium] coprostanoligenes	g_Candidatus Soleaferrea	g_Intestinimonas	g_Ruminiclostridium	g_Ruminococcaceae UCG-010	f_Erysipelotrichaceae	o_Rhodospirillales	f_Desulfovibrionaceae	f_Flavobacteriaceae	f_Desulfovibrionaceae
Alanine	0.0420	0.0353	0.0079	0.0279	0.0091	0.0244	0.0084	0.0171	0.0113	0.0751	0.0255	0.0782	0.0103	0.0595	0.0238	0.0363	0.0191	0.0370
Asparagine	0.1260	0.0861	0.0017	0.0513	0.0029	0.1496	0.0238	0.1365	0.0091	0.1895	0.1326	0.2716	0.0000	0.1968	0.1477	0.1110	0.0279	0.1189
Glutamine	0.0025	0.0008	0.0308	0.0019	0.0097	0.0365	0.0151	0.0250	0.0143	0.0045	0.0138	0.0223	0.0634	0.0399	0.0580	0.0015	0.0018	0.0018
Isoleucine	0.0146	0.0221	0.1479	0.0490	0.1385	0.0307	0.0606	0.0036	0.1632	0.0061	0.0137	0.0015	0.3008	0.0049	0.0046	0.0128	0.0769	0.0079
Valine	0.0006	0.0038	0.0811	0.0146	0.0502	0.0050	0.0146	0.0004	0.0484	0.0026	0.0012	0.0004	0.1405	0.0051	0.0072	0.0009	0.0180	0.0004
Putrescine	0.0111	0.0154	0.0200	0.0192	0.0064	0.0563	0.0002	0.0334	0.0107	0.0438	0.0353	0.0530	0.0187	0.0297	0.0516	0.0143	0.0073	0.0144
Maltose	0.0006	0.0019	0.0367	0.0067	0.0195	0.0082	0.0046	0.0012	0.0225	0.0039	0.0022	0.0036	0.0726	0.0068	0.0083	0.0006	0.0068	0.0003
Raffinose	0.1200	0.0638	0.0054	0.0300	0.0019	0.1737	0.0580	0.1947	0.0056	0.1567	0.1415	0.2975	0.0022	0.2932	0.2542	0.0985	0.0156	0.1123
Ribose	0.0114	0.0010	0.0405	0.0003	0.0142	0.0269	0.0755	0.0423	0.0128	0.0046	0.0119	0.0423	0.0880	0.1309	0.1119	0.0046	0.0019	0.0069
Threonic acid	0.0075	0.0156	0.1552	0.0401	0.1283	0.0143	0.0549	0.0014	0.1344	0.0038	0.0058	0.0002	0.2865	0.0058	0.0058	0.0072	0.0614	0.0043
2-amino-butyric acid	0.0098	0.0034	0.0684	0.0025	0.0245	0.0023	0.0793	0.0234	0.0086	0.0105	0.0024	0.0319	0.0926	0.1433	0.1030	0.0054	0.0038	0.0089
Hydrocinnamic acid	0.0148	0.0114	0.0040	0.0101	0.0023	0.0301	0.0010	0.0138	0.0064	0.0343	0.0188	0.0468	0.0096	0.0290	0.0204	0.0126	0.0053	0.0123
Glutaric acid	0.0065	0.0135	0.0309	0.0210	0.0176	0.0139	0.0009	0.0045	0.0184	0.0287	0.0097	0.0187	0.0392	0.0115	0.0118	0.0086	0.0131	0.0077
Glycolic acid	0.0900	0.0397	0.0003	0.0162	0.0008	0.1221	0.0402	0.1111	0.0069	0.0987	0.0906	0.2067	0.0029	0.1904	0.1325	0.0656	0.0116	0.0718
Butyrate	0.0011	0.0029	0.0343	0.0082	0.0189	0.0073	0.0036	0.0010	0.0213	0.0061	0.0024	0.0047	0.0653	0.0068	0.0070	0.0012	0.0076	0.0008
Valerate	0.0402	0.0598	0.1020	0.0775	0.0950	0.0090	0.0354	0.0045	0.0809	0.0680	0.0156	0.0289	0.1291	0.0322	0.0097	0.0420	0.0756	0.0387
Propanoic acid	0.0122	0.0277	0.0794	0.0544	0.0702	0.0622	0.0051	0.0102	0.1009	0.0256	0.0330	0.0117	0.1402	0.0002	0.0060	0.0165	0.0528	0.0110

Table 1. Correlation of bacteria with metabolites in the cecum. Correlation p-values between annotated metabolites and the bacterial genus in the cecum of CR mice were calculated. For Operational Taxonomic Units (OTU) that could not be assigned on the genus level, the closest taxonomical level of identification was used. Characters before the name of the bacteria represent family (f), genus (g), and order (o). Coloured cells show statistically significant differences; red = negative correlation; green = positive correlation. Correlation coefficient analysis using Pearson's correlation ($r=0.8$) was done in COVAIN; $p < 0.0083$.

the given beddings. Interestingly, the size of the cecum reversely correlated with the amount of feces produced as CR mice had a smaller cecum when housed on CC bedding.

Since bedding and feces ingestion influence the outcomes of metabolic studies^{14,33,34} rodents may be kept on a metal grid short-term³⁵ to prevent bedding consumption as well as limit coprophagy. However, this experimental setup cannot stop mice from eating feces directly from the anus. To completely cease coprophagy, the use of anal cups or neck restrainers would be necessary, which would be distressing to the animal and could interfere with normal feeding behavior. In our study, mice housed on the grid showed higher body weight loss as well as lighter stomach and cecum compared to conventionally fasted mice, indicating less consumption. It has previously been shown that rats housed in wire-bottom cages do not show any clinical pathology symptoms when compared to rats from solid bottom cages³⁶. However, housing rats in wire-bottom cages overnight leads to immediate alterations of heart rate, body weight, and locomotor activity, which might be related to stress response³⁷. Therefore, the bodyweight loss in the mice fasted on the grid may also indicate the impact of additional stress or energy loss required for body temperature regulation when deprived of nesting material. When coprophagy was permitted, ON fasted mice did not differ in cecum and body weight from mice with access to bedding indicating the importance and scale of coprophagy. Coprophagy occurs not only to compensate for energy during deprivation but also to supplement the diet with various nutrients of gut microbiota origin. Choline, cysteine, thiamine, iron, vitamin K, B₁₂, and essential fatty acids are sourced from feces and if the animals are not allowed to consume feces, chow needs to be supplemented^{38–46}. However, on an ad libitum balanced laboratory diet coprophagy might not be crucial, as its absence does not result in lower body weight or less progeny⁴⁷. Most importantly, coprophagy leads to the re-inoculation of the gut, therefore, it is an important factor in microbiota composition. Moreover, bedding presence and not coprophagy was the deciding factor concerning glucose tolerance. Both groups, housed without bedding or kept on the grid showed lower glucose levels compared to any group submitted to ON in the presence of bedding despite the fact that the initial, fasting glucose levels were comparable between all the groups.

Since CR results in hunger, the impact of supplementation with different beddings on hunger was tested by assessing the speed of meal initiation. Bedding did not influence how rapidly the mice started consumption of the daily portion of chow. Nevertheless, after day two of CR, all groups ate nearly immediately following access to food, therefore, beyond this point small differences in the speed of the meal initiation were difficult to detect. Moreover, basal blood glucose levels and gene expression in the hypothalamus were comparable between the animals of different CR and ON groups. Importantly, the levels of active ghrelin, the “hunger hormone”, were increased in CR-CC and CR-C compared to CR-W. This indicates that the type of bedding may influence hunger perception.

Several publications reported changes in microbiota composition in CR compared to ad libitum fed mice. Data comparison revealed a few similarities of our results with previous studies^{22–26} concerning consistent trends in the abundance of selected OTUs, regardless of the type of bedding. Nevertheless, numerous differences in bacteria occurrence were found between ours and the published sequencing results. Obviously, microbiota

composition depends on multiple factors including different types of cage bedding, contributing to the differences in outcomes of similar experiments. Accordingly, strong differences in gut bacteria and metabolites were observed between beddings having the most distinct fiber profile (CC vs C and W), while C and W bedding, which stem from the same initial material, resulted in comparable microbiota composition. Fittingly, *Ruminococcus*, which abundance raises in response to high-cellulose diet⁴⁸, was increased in CR-C and CR-W versus corresponding ad libitum groups but this was not present in CR-CC. Consequently, *Ruminococcus* was identified as one of the OTUs distinguishing CR-CC versus both CR-W and CR-C. Therefore, it is important to consider that the main trigger of microbiota composition changes in CR animal trials is not the nutrient restriction but the bedding consumption.

Lactobacillus which is known to mitigate inflammation and improve gut barrier function is stimulated by CR^{22,49}. Also in our study CR strongly increased the abundance of *Lactobacillus* in mice cecum. This result corresponds well with our previous report⁵ showing a decrease in expression of the immune function-related gene in the intestine of CR mice. Importantly, the type of bedding affected the extent to which the bacteria levels increased, therefore, likely modulating inflammatory status.

A high-fiber diet affects body weight, GI-tract and liver status, microbiota composition, fiber fermentation, and general health^{8,50,51}. However, most of the studies point toward a stronger impact of soluble versus insoluble fiber since these are the vital substrates for SCFA production^{16,50,52,53}. Despite high fiber intake and cecum enlargement suggesting an elevated fermentation, CR mice showed lowered levels of all short to medium-chain fatty acids. The lowered levels of SCFA may be associated with the decrease in the relative abundance of enzymes involved in butyrogenesis and acetogenesis upon CR²³. However, an increase in propiogenesis-related enzymes has been reported in parallel²³. Moreover, supplementation with fiber including cellulose or corn fiber does not result in an increased SCFA in the cecum^{54,55}. The knowledge concerning insoluble fiber fermentation by gut microbiota is very limited. In general, compared to soluble fiber, cellulose is poorly fermented, it yields mostly acetate and less propionate or butyrate^{54,55}, and the process takes place mostly in the distal colon where transit time is slower, and bacterial densities are higher⁵⁶. There are multiple fecal strains digesting cellulose from both major phyla *Bacteroidetes* and *Firmicutes*⁵⁷ and the main cellulolytic strains isolated from human feces have been classified as *Ruminococcus* sp, *Clostridium* sp, *Eubacterium* sp, and *Bacteroides* sp.^{57–60}. Therefore, despite the lower fermentability of cellulose compared to soluble fiber, we assume that SCFA production increased in CR mice supplementing themselves with cage bedding. We propose that the produced metabolites are likely taken up more efficiently and utilized by the host due to CR-related energy shortage. Additionally, the levels of fumaric acid, an intermediate product of bacterial fermentation are increased in all CR groups and highest in CR-CC. This implies an increased fermentation particularly strongly stimulated by CC bedding.

We analyzed the correlation between the occurrence of the detected cecal microbiota and corresponding metabolites. We could confirm the previously published negative correlation between *Bacteroides* and fatty acids^{61,62}, *Oscillibacter* and isoleucine⁶³ and positive correlation between *Alistipes* and proline⁶², *Lachnospirillum* and glutaric acid⁶⁴, *Bacteroides* and spermidine⁶⁵ as well as *Blautia* and malic acid and myo-inositol⁶². However, most of the observed correlations have not been reported before.

To summarize, based on the differences between mice kept with or without cage bedding we can conclude that mice consume bedding and feces during dietary restrictions and this influences their body, WAT, stomach and cecum weight, cecal microbiota and metabolites profile as well as plasma glucose and ghrelin level. Therefore, we propose that the amount of energy extracted from fiber depends on the bedding type and contributes to the bodyweight differences. Moreover, in the to-date published reports on the effect of CR, particularly on microbiota, in mice or rats, it is impossible to distinguish between the effect of CR or the supplemented bedding making the results not comparable to human CR studies. The reproducibility of published results is a major issue in the scientific community. Our data indicate an important factor that needs to be taken into account when interpreting and designing experiments, particularly important when restrictive diets are considered. With great progress in the field of microbiota within the last few years and knowing the importance of dietary fiber as a source of prebiotics, it is important to indicate that gut bacteria composition is affected by the type of fiber present in mice cage bedding. We propose that for short-term restrictions, cages with grid floors are used. Due to ethical concerns, this approach cannot be applied to long-term experiments, instead it should be encouraged to routinely report not only the type of the diet but also cage bedding.

Materials and methods

Animal experiments. Male C57BL/6NRj mice purchased from Janvier Inc. Labs (Le Genest, France) were housed in standard SPF conditions using a Tecniplast IVC system (cage type 2L, blue line). Mice were fed a standard chow (V1535 R/M-H Extrudate; ssniff Spezialdiäten GmbH, Soest, Germany). The animals were divided into control ad libitum, CR, and ON fast groups (Supplementary Table S1). Each of these groups was separated into three subgroups by the bedding type: wooden (Lignocel select), corncob (RehoFix MK 3500), cellulose (Arborcel Performance Small; all beddings from J. Rettenmaier & Söhne GmbH + Co KG; Vienna, Austria). The fiber composition of the beddings is presented in the Supplementary Fig. S1A. Additionally, two subgroups of the ON fast group were housed without any cage bedding or on a metal grid to prevent contact with cage bottom and coprophagy. The control group mice were kept ad libitum on each of the bedding. Each group of mice contained 10 animals; however, during the dissection some of the tissues were lost resulting in 8–10 replicates for the presented results. Mice from CR groups were submitted to two weeks CR with 75% of normal food intake. Mice body weight was measured daily during the CR protocol. To estimate the hunger of the CR mice, a daily food pellet was placed in the cage and the time it took the mice to initiate the meal was measured with a stopwatch. Cage bedding was changed daily from the 11th day of CR for three consecutive days to assess the amount of bedding eaten. The harvested bedding was dried and feces were separated. The feces were dried

and used for verification of daily fecal mass production and energy content measurement by direct calorimetry (IKA-Kalorimeter C2000; IKA-Werke GmbH & Co. KG; Staufen, Germany). Fresh fecal samples were collected on days 12 and 13 of CR and from ad libitum fed mice. The feces were snap-frozen and stored at -80°C .

For the ON fasted groups, food was removed in the evening and the mice were fasted 16 h with free water access. After ON fast, mice were submitted to an oral glucose tolerance test (OGTT) by gavaging 3 mg glucose per gram body weight. Afterward, the mice were fed ad libitum. One week later the ON fasting procedure was repeated and mice were sacrificed and dissected in the morning. Food from the cages of control mice was removed 2 h before the dissection. All mice were euthanized by isoflurane overdose, with blood drawn by cardiac puncture. The stomach and cecum with their content as well as adipose tissue and liver weight were recorded. Blood was mixed with 10 $\mu\text{l/ml}$ EDTA, 20 $\mu\text{l/ml}$ aprotinin, and 10 $\mu\text{l/ml}$ dipeptidyl peptidase (DPP) IV. Plasma was separated from the blood cells by centrifugation for 10 min at $3,600\times g$ 4°C and was stored at -80°C . Stomach, small intestine, and colon scrapings as well as cecum content were snap-frozen and stored at -80°C until use.

All animal experimentation protocols were approved by the Federal Ministry of Science, Research and Economy, Unit for Animal Experiments and Genetic Engineering in Austria (BMVFW-66.006/0017-WF/V/3b/2016). The experiments were performed in agreement with the Austrian Federal Act on Animal Welfare.

Sequencing the 16S rDNA genes and metataxonomic analysis. The samples for sequencing were processed according to the previously published protocol⁶⁶. Cecum samples were homogenized in MagNA Pure Bacteria Lysis Buffer from the MagNA Pure LC DNA Isolation Kit III (Bacteria, Fungi) in MagNA Lyser green beads tubes at 6,500 rpm for three 30 s cycles in a MagNA Lyser Instrument (all from Roche, Mannheim, Germany). The homogenized samples were mixed with 25 μl lysozyme (100 mg/ml), incubated at 37°C for 30 min followed by adding 43.4 μl Proteinase K (20 mg/ml) and incubation at 65°C overnight. Afterwards, the enzymes were heat-inactivated at 95°C for 10 min and 250 μl lysed supernatant was used for DNA extracted on a MagNA Pure LC 2.0 following the instructions for the MagNA Pure LC DNA Isolation Kit III (Bacteria, Fungi) (Roche). PCR reactions were run in triplicates using a FastStart High Fidelity PCR system and contained 5 μl of total DNA, $1\times$ Fast Start High Fidelity Buffer, 1.25 U High Fidelity Enzyme, 200 μM dNTPs, 0.4 μM primers, and PCR-grade water in 25 μl reaction volume (all reagents from Roche, Mannheim, Germany). The following target primers were applied for the amplification of phylogenetic informative hypervariable regions V1-V2: 27F—AGA GTTTGATCCTGGCTCAG and 375R—CTGCTGCCTYCCGTA. The primers were used with Illumina adapters for indexing PCR reaction according to Illumina's 16S metagenomic sequencing library preparation guide. The PCR temperature cycles were as follows: initial denaturation at 95°C for 3 min, 30 cycles of denaturation at 95°C for 45 s, annealing of primers at 55°C for 45 s and extension at 72°C for 1 min, final extension step at 72°C for 7 min and cooling to 4°C . The PCR reaction triplicates were pooled and checked using 1% agarose gel and subsequent normalization of 20 μl PCR products was performed on a SequalPrep Normalization Plate (LifeTechnologies, Germany). Of the normalized PCR products, 15 μl was used as a template in a single 50 μl indexing PCR reaction for 8 cycles; the temperature cycles conditions were as described above for the targeted PCR. For the final sequencing library, 5 μl of PCR products from each sample were pooled and 30 μl of the library was purified using a 1% agarose gel and the QIAquick gel extraction kit (Qiagen, Germany). The obtained library was quantified with QuantiFluor ONE dsDNA Dye on Quantus Fluorometer (Promega, Germany), its quality was verified using an Agilent BioAnalyzer 2100 (Waldbronn, Germany) and the 6 pM library was sequenced on a MiSeq desktop sequencer (Illumina, Netherlands) containing 20% PhiX control DNA (Illumina) with v2 chemistry for 500 cycles. FastQ raw reads were used for subsequent data analysis.

Raw sequencing data in fastq format was imported in Galaxy web-based platform⁶⁷ and analyzed with the QIIME2 2018.4 microbiome analysis pipeline. After initial quality control data was preprocessed with DADA2⁶⁸ using default parameters and removing specific primer sequences. The resulting feature representative sequences were classified with the QIIME2 pre-fitted sklearn-based taxonomy classifier against SILVA 16S rRNA database version 132 at 99% identity⁶⁹. The resulting feature abundance table, also known as OTUs table over all samples including taxonomy information was used for all subsequent analyses. For the phylogenetic methods, representative sequences were aligned with MAFFT de novo multiple sequence aligner⁷⁰ followed by the creation of a phylogenetic tree with FastTree⁷¹.

Metabolomics. Extraction and analysis of cecal metabolites were performed according to Weckwerth et al.⁷² with slight modifications. Frozen samples (~ 30 mg) were transferred into "Precellys lysis kit" homogenizing tubes with 1.4 mm ceramic beads and 800 μl ice-cold MCW extraction buffer (methanol:chloroform:water = 2.5:1:0.5) was added. The samples were homogenized in a Precellys24 Tissue Homogenizer (Bertin Instruments) twice for 15 s at 5000 rpm and were incubated on ice for 15 min. Next, samples were vortexed and centrifuged for 5 min at 10,500 rpm at 4°C then the supernatant was transferred to a 2 ml Eppendorf tube. The extraction step was repeated by short vortexing the pellet with 400 μl ice-cold MCW followed with 15 min incubation on ice and centrifugation for 5 min at 10,500 rpm at 4°C . The two supernatants were combined and to separate chloroform phase from the water/methanol phase 400 μl H_2O was added. After vortexing and centrifuging the samples for another 5 min at 14,000 rpm at 4°C , the upper polar phase was transferred to a new Eppendorf tube and both fractions were dried in a speed vac using an optimized pressure gradient to prevent boiling retardation. The polar fraction was dissolved in 50 μl of methoxamine hydrochloride solution (20 mg/ml pyridine) and incubated at 30°C for 90 min with continuous shaking. Then 80 μl of *N*-methyl-*N*-trimethylsilyltrifluoroacetamid (MSTFA) was added to derivatize polar functional groups at 37°C for 30 min. The derivatized samples were stored at room temperature for 120 min before injection. Gas chromatography–mass spectrometry (GC–MS) analysis was performed using a Leco Pegasus BT-TOF (Leco Instrumente GmbH, Mönchengladbach, Germany)

equipped with a PAL3 Autosampler (CTC Analytics AG, Zwingen, Switzerland). Chromatographic separation and data validation were conducted as published earlier with slight modifications^{73,74}. Derivatized extract (1 µl) was injected on an HP-5MS column (30 m × 0.25 mm × 0.25 µm) (Agilent Technologies) in split less mode. Mass spectral data acquisition was performed using the following instrument parameters. Electron impact ionization was conducted at 70 eV and 1 mA emission current. Ion source and transferline temperature were set to 250 °C. Mass spectra were collected at an acquisition rate of 10 spectra/sec and a mass range of 40–600 Th using a relative detector voltage with an offset of – 100 V from optimized detector voltage. Mass spectrometry data are stored at MetaboLights (<https://www.ebi.ac.uk/metabolights/>).

Statistical analysis. OTUs table was reduced by removing all OTUs present in less than three samples per group. The obtained data of GC–MS and LC–MS were normalized to fresh weight, then annotated and classified according to the Metabolomics Standards Initiative (MSI). Data transformation, alignment, and integrative analysis including correlation coefficient, partial least square (PLS) regression, one-way ANOVA, hierarchical clustering, and correlation network analysis were performed with the statistical software COVAIN⁷⁵ under MATLAB environment. The amount of each metabolite and bacteria OTUs were z-scored across all samples. The correlation network associating metabolites (classified as MSI 1 and 2) and bacteria OTUs was constructed by Pearson's correlation coefficients (cutoff value = 0.8). For network visualization, Girven-Newman algorithm⁷⁶ was applied and visualization was performed with Cytoscape v3.7.2. (<http://www.cytoscape.org/>).

Concerning other data sets, the experimental groups were compared applying one-way ANOVA with Bonferroni post-hoc corrections for multiple testing. Where applicable, differences between two experimental groups were analyzed using Student's t-test with statistical significance threshold set at $p < 0.05$. Each of the groups contained 8–10 biological replicates.

Data availability

The microbiota and metabolomics datasets generated during and analyzed during the current study are available in the European Nucleotide Archive [<https://www.ebi.ac.uk/ena/browser/view/PRJEB37837>] and MetaboLights repository, [www.ebi.ac.uk/metabolights/MTBLS1631] respectively.

Received: 19 August 2020; Accepted: 17 November 2020

Published online: 30 November 2020

References

1. Ferrecchia, C. E., Jensen, K. & Van Andel, R. Intracage ammonia levels in static and individually ventilated cages housing C57BL/6 mice on 4 bedding substrates. *J. Am. Assoc. Lab. Anim. Sci.* **53**, 146–151 (2014).
2. Jensen, T. L., Kiersgaard, M. K., Sorensen, D. B. & Mikkelsen, L. F. Fasting of mice: a review. *Lab. Anim.* **47**, 225–240 (2013).
3. Weindruch, R., Walford, R. L., Fligiel, S. & Guthrie, D. The retardation of aging in mice by dietary restriction: longevity, cancer, immunity and lifetime energy intake. *J. Nutr.* **116**, 641–654 (1986).
4. Masoro, E. J. Caloric restriction and aging: an update. *Exp. Gerontol.* **35**, 299–305 (2000).
5. Duszka, K. *et al.* Complementary intestinal mucosa and microbiota responses to caloric restriction. *Sci. Rep.* **8**, 11338 (2018).
6. Moen, B. *et al.* Effect of dietary fibers on cecal microbiota and intestinal tumorigenesis in azoxymethane treated A/J min/+ mice. *PLoS ONE* **11**, e0155402 (2016).
7. Hoover, W. H. & Heitmann, R. N. Effects of dietary fiber levels on weight gain, cecal volume and volatile fatty acid production in rabbits. *J. Nutr.* **102**, 375–379 (1972).
8. Drew, J. E. *et al.* Dietary fibers inhibit obesity in mice, but host responses in the cecum and liver appear unrelated to fiber-specific changes in cecal bacterial taxonomic composition. *Sci. Rep.* **8**, 15566 (2018).
9. Wostmann, B. S., Bruckner-Kardoss, E. & Knight, P. L. Jr. Cecal enlargement, cardiac output, and O₂ consumption in germfree rats. *Proc. Soc. Exp. Biol. Med.* **128**, 137–141 (1968).
10. Loesche, W. J. Accumulation of endogenous carbohydrate-containing compounds in the cecum of the germfree rat. *Proc. Soc. Exp. Biol. Med.* **131**, 387–392 (1969).
11. Konishi, F., Oku, T. & Hosoya, N. Hypertrophic effect of unavailable carbohydrate on cecum and colon in rats. *J. Nutr. Sci. Vitaminol. (Tokyo)* **30**, 373–379 (1984).
12. Zijlstra, R. T., Jha, R., Woodward, A. D., Fouchse, J. & van Kempen, T. A. Starch and fiber properties affect their kinetics of digestion and thereby digestive physiology in pigs. *J. Anim. Sci.* **90**(Suppl 4), 49–58 (2012).
13. Ambery, A. G., Tackett, L., Penque, B. A., Hickman, D. L. & Elmendorf, J. S. Effect of Corn cob bedding on feed conversion efficiency in a high-fat diet-induced prediabetic model in C57BL/6J mice. *J. Am. Assoc. Lab. Anim. Sci.* **53**, 449–451 (2014).
14. Le Leu, R. K., Conlon, M. A., Bird, A. R. & Clarke, J. M. Housing experimental rats in solid-based cages with digestible bedding may confound outcomes of nutritional studies. *J. Sci. Food Agric.* **95**, 2155–2158 (2015).
15. Topping, D. L. & Clifton, P. M. Short-chain fatty acids and human colonic function: roles of resistant starch and nonstarch polysaccharides. *Physiol. Rev.* **81**, 1031–1064 (2001).
16. Macfarlane, S. & Macfarlane, G. T. Regulation of short-chain fatty acid production. *Proc. Nutr. Soc.* **62**, 67–72 (2003).
17. Tan, J. *et al.* The role of short-chain fatty acids in health and disease. *Adv. Immunol.* **121**, 91–119 (2014).
18. Franklin, C. L. & Ericsson, A. C. Microbiota and reproducibility of rodent models. *Lab. Anim. (NY)* **46**, 114–122 (2017).
19. Schloss, P. D. Identifying and overcoming threats to reproducibility, replicability, robustness, and generalizability in microbiome research. *mBio* **9**, e00525 (2018).
20. Gu, S. *et al.* Bacterial community mapping of the mouse gastrointestinal tract. *PLoS ONE* **8**, e74957 (2013).
21. Zeng, H. *et al.* Integrating multiple analytical datasets to compare metabolite profiles of mouse colonic-cecal contents and feces. *Metabolites* **5**, 489–501 (2015).
22. Fraumene, C. *et al.* Caloric restriction promotes rapid expansion and long-lasting increase of *Lactobacillus* in the rat fecal microbiota. *Gut Microbes* **9**, 104–114 (2018).
23. Tanca, A. *et al.* Caloric restriction promotes functional changes involving short-chain fatty acid biosynthesis in the rat gut microbiota. *Sci. Rep.* **8**, 14778 (2018).
24. Zhang, C. *et al.* Structural modulation of gut microbiota in life-long calorie-restricted mice. *Nat. Commun.* **4**, 2163 (2013).
25. Liu, T. *et al.* A more robust gut microbiota in calorie-restricted mice is associated with attenuated intestinal injury caused by the chemotherapy drug cyclophosphamide. *mBio* **10**, e02903 (2019).

26. Wang, S. *et al.* Gut microbiota mediates the anti-obesity effect of calorie restriction in mice. *Sci. Rep.* **8**, 13037 (2018).
27. Hervik, A. K. & Svihus, B. The role of fiber in energy balance. *J. Nutr. Metab.* **2019**, 4983657 (2019).
28. Slavin, J. L., Brauer, P. M. & Marlett, J. A. Neutral detergent fiber, hemicellulose and cellulose digestibility in human subjects. *J. Nutr.* **111**, 287–297 (1981).
29. Holloway, W. D., Tasman-Jones, C. & Lee, S. P. Digestion of certain fractions of dietary fiber in humans. *Am. J. Clin. Nutr.* **31**, 927–930 (1978).
30. Crawford, D. F., Anthony, W. B. & Harris, R. R. Evaluation of concentrated hemicellulose extract as cattle feed. *J. Anim. Sci.* **46**, 32–40 (1978).
31. Niemi, P. *et al.* Interactions of a lignin-rich fraction from brewer's spent grain with gut microbiota in vitro. *J. Agric. Food Chem.* **61**, 6754–6762 (2013).
32. Begum, A. N. *et al.* Dietary lignins are precursors of mammalian lignans in rats. *J. Nutr.* **134**, 120–127 (2004).
33. Potgieter, F. J., Wilke, P. I., van Jaarsveld, H. & Alberts, D. W. The in vivo effect of different bedding materials on the antioxidant levels of rat heart, lung and liver tissue. *J. S. Afr. Vet. Assoc.* **67**, 27–30 (1996).
34. Buddaraju, A. K. & Van Dyke, R. W. Effect of animal bedding on rat liver endosome acidification. *Comp. Med.* **53**, 616–621 (2003).
35. National Research Council. *Guide for the Care and Use of Laboratory Animals* 8th edn. (National Academies Press, New York, 2011).
36. Sauer, M. B. *et al.* Clinical pathology laboratory values of rats housed in wire-bottom cages compared with those of rats housed in solid-bottom cages. *J. Am. Assoc. Lab. Anim. Sci.* **45**, 30–35 (2006).
37. Giral, M., Garcia-Olmo, D. C. & Kramer, K. Effects of wire-bottom caging on heart rate, activity and body temperature in telemetry-implanted rats. *Lab. Anim.* **45**, 247–253 (2011).
38. Barnes, R. H., Kwong, E. & Fiala, G. Effects of the prevention of coprophagy in the rat. III. Digestibility of protein and fat. *J. Nutr.* **65**, 251–258 (1958).
39. Barnes, R. H., Tuthill, S., Kwong, E. & Fiala, G. Effects of the prevention of coprophagy in the rat. V. Essential fatty acid deficiency. *J. Nutr.* **68**, 121–130 (1959).
40. Barnes, R. H. & Kwong, E. Choline biosynthesis and choline requirement in the rat as affected by coprophagy. *J. Nutr.* **92**, 224–232 (1967).
41. Barnes, R. H. & Fiala, G. Effects of the prevention of coprophagy in the rat. II. Vitamin B12 requirement. *J. Nutr.* **65**, 103–114 (1958).
42. Barnes, R. H., Fiala, G. & Kwong, E. Prevention of coprophagy in the rat and the growth-stimulating effects of methionine, cystine and penicillin when added to diets containing unheated soybeans. *J. Nutr.* **85**, 127–131 (1965).
43. Barnes, R. H., Kwong, E. & Fiala, G. Effects of the prevention of coprophagy in the rat. IV. Biotin. *J. Nutr.* **67**, 599–610 (1959).
44. Kwong, E. & Barnes, R. H. Role of coprophagy in masking dietary deficiencies of cystine in the rat. *J. Nutr.* **105**, 1457–1465 (1975).
45. Schulze, J. & Haenel, H. Relationships between coprophagia, intestinal flora and vitamins in experimental animals. *Z. Versuchstierkd* **11**, 190–206 (1969).
46. Neale, R. J. Coprophagy in iron-deficient rats. *Lab. Anim.* **16**, 204–207 (1982).
47. Ebino, K. Y., Yoshinaga, K., Saito, T. R. & Takahashi, K. W. A simple method for prevention of coprophagy in the mouse. *Lab. Anim.* **22**, 1–4 (1988).
48. Liu, T. W. *et al.* Nondigestible fructans alter gastrointestinal barrier function, gene expression, histomorphology, and the microbiota profiles of diet-induced obese C57BL/6J mice. *J. Nutr.* **146**, 949–956 (2016).
49. Pan, F. *et al.* Predominant gut *Lactobacillus murinus* strain mediates anti-inflammatory effects in calorie-restricted mice. *Microbiome* **6**, 54 (2018).
50. Zou, J. *et al.* Fiber-mediated nourishment of gut microbiota protects against diet-induced obesity by restoring IL-22-Mediated Colonic Health. *Cell Host Microbe* **23**, 41–53 (2018).
51. Desai, M. S. *et al.* A dietary fiber-deprived gut microbiota degrades the colonic mucus barrier and enhances pathogen susceptibility. *Cell* **167**, 1339–1353 (2016).
52. Weitkunat, K. *et al.* Effects of dietary inulin on bacterial growth, short-chain fatty acid production and hepatic lipid metabolism in gnotobiotic mice. *J. Nutr. Biochem.* **26**, 929–937 (2015).
53. Chassaing, B. *et al.* Lack of soluble fiber drives diet-induced adiposity in mice. *Am. J. Physiol. Gastrointest. Liver Physiol.* **309**, G528–541 (2015).
54. Knapp, B. K. *et al.* Soluble fiber dextrin and soluble corn fiber supplementation modify indices of health in cecum and colon of Sprague-Dawley rats. *Nutrients* **5**, 396–410 (2013).
55. Vince, A. J., McNeil, N. I., Wager, J. D. & Wrong, O. M. The effect of lactulose, pectin, arabinogalactan and cellulose on the production of organic acids and metabolism of ammonia by intestinal bacteria in a faecal incubation system. *Br. J. Nutr.* **63**, 17–26 (1990).
56. Stark, A. H. & Madar, Z. In vitro production of short-chain fatty acids by bacterial fermentation of dietary fiber compared with effects of those fibers on hepatic sterol synthesis in rats. *J. Nutr.* **123**, 2166–2173 (1993).
57. Chassard, C., Delmas, E., Robert, C. & Bernalier-Donadille, A. The cellulose-degrading microbial community of the human gut varies according to the presence or absence of methanogens. *FEMS Microbiol. Ecol.* **74**, 205–213 (2010).
58. Wedekind, K. J., Mansfield, H. R. & Montgomery, L. Enumeration and isolation of cellulolytic and hemicellulolytic bacteria from human feces. *Appl. Environ. Microbiol.* **54**, 1530–1535 (1988).
59. Robert, C. & Bernalier-Donadille, A. The cellulolytic microflora of the human colon: evidence of microcrystalline cellulose-degrading bacteria in methane-excreting subjects. *FEMS Microbiol. Ecol.* **46**, 81–89 (2003).
60. Betian, H. G., Linehan, B. A., Bryant, M. P. & Holdeman, L. V. Isolation of a cellulolytic *Bacteroides* sp. from human feces. *Appl. Environ. Microbiol.* **33**, 1009–1010 (1977).
61. Neis, E. P., Dejong, C. H. & Rensen, S. S. The role of microbial amino acid metabolism in host metabolism. *Nutrients* **7**, 2930–2946 (2015).
62. Cheng, W. *et al.* Effects of a galacto-oligosaccharide-rich diet on fecal microbiota and metabolite profiles in mice. *Food Funct.* **9**, 1612–1620 (2018).
63. Han, J., Meng, J., Chen, S. & Li, C. Integrative analysis of the gut microbiota and metabolome in rats treated with rice straw biochar by 16S rRNA gene sequencing and LC/MS-based metabolomics. *Sci. Rep.* **9**, 17860 (2019).
64. Tang, Z. Z. *et al.* Multi-omic analysis of the microbiome and metabolome in healthy subjects reveals microbiome-dependent relationships between diet and metabolites. *Front. Genet.* **10**, 454 (2019).
65. Tofalo, R., Cocchi, S. & Suzzi, G. Polyamines and gut microbiota. *Front. Nutr.* **6**, 16 (2019).
66. Klymiuk, I. *et al.* The human gastric microbiome is predicated upon infection with *Helicobacter pylori*. *Front. Microbiol.* **8**, 2508 (2017).
67. Afgan, E. *et al.* The Galaxy platform for accessible, reproducible and collaborative biomedical analyses: 2018 update. *Nucleic Acids Res.* **46**, W537–W544 (2018).
68. Callahan, B. J. *et al.* DADA2: High-resolution sample inference from Illumina amplicon data. *Nat. Methods* **13**, 581–583 (2016).
69. Yilmaz, P. *et al.* The SILVA and “All-species Living Tree Project (LTP)” taxonomic frameworks. *Nucleic Acids Res.* **42**, D643–648 (2014).
70. Katoh, K., Misawa, K., Kuma, K. & Miyata, T. MAFFT: a novel method for rapid multiple sequence alignment based on fast Fourier transform. *Nucleic Acids Res.* **30**, 3059–3066 (2002).

71. Price, M. N., Dehal, P. S. & Arkin, A. P. FastTree 2—approximately maximum-likelihood trees for large alignments. *PLoS ONE* **5**, e9490 (2010).
72. Weckwerth, W., Wenzel, K. & Fiehn, O. Process for the integrated extraction, identification and quantification of metabolites, proteins and RNA to reveal their co-regulation in biochemical networks. *Proteomics* **4**, 78–83 (2004).
73. Obermeyer, G., Fragner, L., Lang, V. & Weckwerth, W. Dynamic adaption of metabolic pathways during germination and growth of lily pollen tubes after inhibition of the electron transport chain. *Plant Physiol.* **162**, 1822–1833 (2013).
74. Doerfler, H. *et al.* Granger causality in integrated GC-MS and LC-MS metabolomics data reveals the interface of primary and secondary metabolism. *Metabolomics* **9**, 564–574 (2013).
75. Sun, X. & Weckwerth, W. COVAIN: a toolbox for uni- and multivariate statistics, time-series and correlation network analysis and inverse estimation of the differential Jacobian from metabolomics covariance data. *Metabolomics* **8**, 81–93 (2012).
76. Girvan, M. & Newman, M. E. Community structure in social and biological networks. *Proc. Natl. Acad. Sci. USA* **99**, 7821–7826 (2002).

Acknowledgements

Open access funding provided by the University of Vienna.

Author contributions

A.G. performed animal experiments, samples and data analysis as well as contributed to the manuscript writing; L.F. performed GC–MS metabolites analysis; S.T. and W.L. performed the bioinformatical analysis of microbiota composition; W.L. analyzed GC–MS experiments data; X.L. provided statistical analysis tool and methods; W.W. contributed with metabolomics platform, expert advice and supervised metabolomics analysis; J.K. contributed expert advice; K.D. designed and performed the experiments, analyzed samples and wrote the manuscript. All authors approved the final manuscript.

Competing interests

The authors declare no competing interests.

Additional information

Supplementary information is available for this paper at <https://doi.org/10.1038/s41598-020-77831-3>.

Correspondence and requests for materials should be addressed to K.D.

Reprints and permissions information is available at www.nature.com/reprints.

Publisher's note Springer Nature remains neutral with regard to jurisdictional claims in published maps and institutional affiliations.



Open Access This article is licensed under a Creative Commons Attribution 4.0 International License, which permits use, sharing, adaptation, distribution and reproduction in any medium or format, as long as you give appropriate credit to the original author(s) and the source, provide a link to the Creative Commons licence, and indicate if changes were made. The images or other third party material in this article are included in the article's Creative Commons licence, unless indicated otherwise in a credit line to the material. If material is not included in the article's Creative Commons licence and your intended use is not permitted by statutory regulation or exceeds the permitted use, you will need to obtain permission directly from the copyright holder. To view a copy of this licence, visit <http://creativecommons.org/licenses/by/4.0/>.

© The Author(s) 2020

Original Article 2

RESEARCH PAPER

Caloric restriction increases levels of taurine in the intestine and stimulates taurine uptake by conjugation to glutathione

András Gregor^a, Marc Pignitter^b, Christine Fahrngruber^a, Sebastian Bayer^b, Veronika Somoza^{b,c},
Jürgen König^a, Kalina Duszka^{a,*}

^a Department of Nutritional Sciences, University of Vienna, Vienna, Austria

^b Department of Physiological Chemistry, University of Vienna, Vienna, Austria

^c Leibniz-Institut für Food Systems Biology, Technical University of Munich, Freising, Germany

Received 13 November 2020; received in revised form 30 March 2021; accepted 29 April 2021

Abstract

Our previous study indicated increased levels of taurine-conjugated bile acids (BA) in the intestine content of mice submitted to caloric restriction (CR). In the current project, we found increased levels of free taurine and taurine conjugates, including glutathione (GSH)-taurine, in CR compared to *ad libitum* fed animals in the mucosa along the intestine but not in the liver. The levels of free GSH were decreased in the intestine of CR compared to *ad libitum* fed mice. However, the levels of oxidized GSH were not affected and were complemented by the lack of changes in the antioxidative parameters. Glutathione-S transferases (GST) enzymatic activity was increased as was the expression of GST genes along the gastrointestinal tract of CR mice. In the CR intestine, addition of GSH to taurine solution enhanced taurine uptake. Accordingly, the expression of taurine transporter (TauT) was increased in the ileum of CR animals and the levels of free and BA-conjugated taurine were lower in the feces of CR compared to *ad libitum* fed mice. Fittingly, BA- and GSH-conjugated taurine levels were increased in the plasma of CR mice, however, free taurine remained unaffected. We conclude that CR-triggered production and release of taurine-conjugated BA in the intestine results in increased levels of free taurine what stimulates GST to conjugate and enhance uptake of taurine from the intestine.

© 2021 The Author(s). Published by Elsevier Inc.

This is an open access article under the CC BY license (<http://creativecommons.org/licenses/by/4.0/>)

Keywords: Caloric restriction; Bile acids; Taurine; Glutathione; Intestine.

1. Introduction

Caloric restriction (CR) is one of the primary intervention tools applied for weight loss and health maintenance, showing remarkable health benefits. CR lowers the incidence of multiple diseases and diminishes the rate of age-specific mortality, resulting in extended lifespan [1–5]. The metabolic adaptation to CR and the origin of its beneficial effects stem from a synchronized response of a composite network of pathways which results in multiple whole-body outcomes including reduction of inflammation, resting metabolic rate, body temperature, fat metabolism, and enhanced insulin sensitivity [1,6–8]. A reduction of oxidative stress is claimed to be among the factors contributing to the beneficial outcomes of CR [9–11]. Reduced glutathione (GSH) is one of the most important non-enzymatic antioxidants which

serves as a scavenger of free radicals, aids in the reduction of H₂O₂, and takes part in detoxification. Together with glutathione peroxidases (GPx) and glutathione S-transferases (GSTs), GSH forms the glutathione system, which is abundant in the gastrointestinal (GI) tract [12,13]. GPx catalyzes the reduction of reactive oxygen species, mainly hydrogen peroxide on the cost of oxidation of GSH to GSH disulfide (GSSG) [14]. Afterward, to complete the cycle and maintain oxidative balance, GSH reductase (GR) converts GSSG back to GSH [15]. GSTs function as a family of enzymes, which catalyze the conjugation of GSH to different electrophilic substrates, thereby producing water-soluble compounds that are further directed to excretion via urine and bile [16]. The expression of GSTs is directly regulated by nuclear factor erythroid-derived 2-like 2 (Nrf2) which is one of the primary transcription factor modulating responses to oxidative stress on the gene expression level. Nrf2 controls also the production of GSH by stimulating the expression of rate-limiting enzymes in GSH synthesis: GSH synthetase (GS) as well as a glutamate-cysteine ligase (GCL) composed of catalytic (GCLC) and a modifier unit (GCLM) [17–20]. Similarly, Nrf2 induces the expression of γ -glutamyl transpep-

* Corresponding author at: Kalina Duszka, Althanstrasse 14, 1090 Vienna, Austria, Tel. 43-14-27754992

E-mail address: kalina.duszka@univie.ac.at (K. Duszka).

tidase (GGT), an enzyme present in cell membranes of many organs including the intestine, and taking part in GSH metabolism [20,21].

Bile is produced by the liver and mainly consists of water, bilirubin, and bile acids (BAs). Upon secretion to the small intestines, BAs enhance lipid uptake. Once formed by activation of the key enzyme of the classic synthesis pathway Cyp7a1, BAs are conjugated to glycine or taurine. Contrary to humans, in mice, only a minor fraction (ca. 5%) of BAs is conjugated to glycine and the majority (ca. 95%) to taurine [22]. Taurine is one of the most abundant free amino acids in the body [23]. It has anti-inflammatory [24–27], antioxidative [26,28–31], and osmoprotective [30,32] properties. In the intestine of an immunosuppressive mouse model, taurine increases the number of some immune cells and total cells in Payer's patches [33], it reduces the growth of harmful bacteria, increases the production of short-chain fatty acids [34], and attenuates induced colitis [35,36]. In human intestinal epithelial Caco-2 cells, taurine stimulates the expression of anti-inflammatory factors [37]. The impact of taurine is primarily controlled by its concentration, which relies on TauT transporter as well as biosynthetic enzymes cysteine dioxygenase (CDO) and cysteine sulfinate decarboxylase (CSAD) [38]. Therefore, taurine can be also synthesized and the process takes place mainly in the liver [39]; however, the main source of taurine is dietary protein [40].

As reported previously [41], we measured increased levels of the taurine-conjugated BA taurocholic acid (TCA) and tauroursodeoxycholic acid (TUDCA) in the intestinal content of mice submitted to CR compared to *ad libitum* feeding. In the current study, we explored the consequences of a CR-triggered increase in the levels of intestinal taurine-conjugated BA. We hypothesized that CR-associated elevated levels of taurine-conjugated BAs are accompanied by increased levels of free taurine that stems from deconjugation in the intestine.

2. Materials and Methods

2.1. Animal care and experimental procedures

Male C57Bl/6 mice purchased from Janvier Labs (Le Genest-Saint-Isle, France) were kept under a 12-h light/12-h dark cycle in standard specific-pathogen-free (SPF) conditions. The animals were fed a V153x R/M-H auto diet from SNIFF-Spezialitäten GmbH (Soest, Germany) and housed with free water access. Mice aged 12 weeks were randomly divided into experimental groups of control *ad libitum* fed (*ad lib*) or CR mice. The study was confirmed on a second independent group of animals. During the dissection, some samples were lost resulting in seven to nine biological replicates in the first group and eight biological replicates in the second group. The animals were assigned ID not associated with the experimental group; therefore, throughout sample and data analysis group assignment was not known. The groups did not differ significantly in body weight when starting the experimental procedures. Animal food intake was measured for one week prior to the intervention to determine the amount of chow diet to be given under CR. The mice from the CR group underwent 14 days of CR that consisted of a ~25% reduction of daily food intake. The CR mice were fed one time per day with the defined amount of chow. This extent of CR is efficient in triggering CR-related phenotypes but prevents excessive body weight loss as presented previously [41]. The samples of the stomach and intestinal mucosa as well as the liver were collected during dissection, snap-frozen, and stored at -80°C until use.

During the design and performance of the experiment the ARRIVE guidelines have been followed. All animal experimentation protocols were approved by the Bundesministerium für Wissenschaft, Forschung und Wirtschaft, Referat für Tierversuche und Gentechnik (BMWF-66.006/0008-V/3b/2018). All experiments were carried out according to animal experimentation Animal Welfare Act guidelines.

2.2. Intestinal sacs assay

The freshly dissected small intestine was divided into five even parts. Part four, counting from the duodenum was flushed with PBS, and ends were loosely tied with a thread leaving a four cm-long sac. A blunted needle was introduced and the intestine was filled with 200 μ l of taurine (25 mg/ml) or taurine (25 mg/ml) and GSH (61.5 mg/ml) solutions. The sacs were closed tightly and incubated in a 37°C water bath in 10 ml of prewarmed Dulbecco's Modified Eagle Medium (DMEM,

Sigma-Aldrich, St. Louis, MO, USA). Three 200 μ l medium samples were collected over 1.5 h for measurement of taurine transport.

2.3. Protein concentration and activity assays

The levels of GSH and GSSG, as well as the activity of GST, GR, GPx (all from BioVision, Milpitas, CA, USA), and Nrf2 (Abcam, Cambridge, UK), were assessed using commercial assay kits according to the manufacturer's indications.

2.4. Electron spin resonance

Frozen samples were cut into 15 μ g pieces and 144 μ l of oxygen-free KHB and 6 μ l of oxygen-free 10 mM CMH solution were added. The samples were incubated for 60 min in a 37°C shaking incubator and quickly spun down. 100 μ l of the solution from each sample was transferred to a fresh tube and snap-frozen in liquid nitrogen until measuring. Electron spin resonance (ESR) measurements were performed at 150 K in a capillary tube (100 μ l), which was placed into a high sensitivity resonator (Bruker ER 4122SHQE), using an X-band Bruker Elexsys-II E500 EPR spectrometer (Bruker BioSpin GmbH, Rheinstetten, Germany) with a modulation frequency of 100 kHz and a microwave frequency of 9.4 GHz. Spectra were recorded every 20 s, averaging every 10 consecutive spectra. The sweep width was 450 G, the sweep time 20 s, the modulation amplitude 5 G, the center field 3400 G, the microwave power 20 mW, and the resolution was 1024 points. EPR spectra were simulated and the area under the curve was determined by double integration of the spectrum. A reference-free quantitation of the number of spins was performed, as has been described previously [42].

2.5. Gene expression

RNA was isolated from intestinal scrapings using the RNeasy mini kit (Qiagen, Hilden, Germany). Samples were thawed in lysis buffer, disrupted using a syringe and needle, and processed following the manufacturer's recommendations. SuperScript II Reverse Transcriptase (Invitrogen, Life Technologies, Carlsbad, CA, USA) was used for the reverse transcription step. Quantitative real-time PCR (qRT-PCR) reactions were carried out using the QuantStudio 6 Flex Real-Time PCR System with the SYBR Green PCR Master Mix (both from Applied Biosystems, Life Technologies, Carlsbad, CA, USA). The primers used are listed in the supplementary data file. The Ct values for each tested gene were normalized to Ct values of Eef1a1. The presented results show $\Delta\Delta$ Ct averaged for biological replicates for each experimental group.

2.6. GSH and taurine conjugates detection

The protocol was adapted from the method of Ito et al. [43] and Budinska et al. [44]. Frozen liver and intestinal mucosa samples were cut on dry ice to the size of 7–10 mg and homogenized. Liver samples were transferred into Precellys homogenizing tubes with 1.4 mm ceramic beads and according to the sample weight nine times the volume of ethanol absolute at -20°C was added. Liver samples were homogenized in the Precellys 24 Tissue Homogenizer (Bertin Instruments, Montigny-Le Bretonneux, France) twice for 15 s at 5000 rpm, vortexed for 30 s, and incubated at -20°C. Intestinal samples were transferred into 1.5 ml Eppendorf tubes and were disrupted in five thawing and freezing cycles. Next, nine times the volume of ethanol absolute -20°C was added, samples were vortexed for 30 s. After the homogenization, liver and intestinal samples were handled alike. Samples were incubated at -20°C for 24 h and centrifuged for 10 min at 18000 g, the supernatants were transferred to new tubes, and, to remove the remaining debris, the centrifugation step was repeated. The supernatants were transferred into HPLC vials in a thermostatic autosampler kept at 4°C. 60 μ l of intestinal sacs samples were diluted with 600 μ l ethanol, vortexed, incubated for 20 min at -20°C, and centrifuged at 15000 g for 15 min at 4°C. The supernatant was dried in a SpeedVac concentrator for 45 min at 60°C, then dissolved in 70 μ l ethanol. Samples (10 μ l) were analyzed by LCMS in negative modus using an LCMS-8040 Liquid Chromatograph Mass Spectrometer (Shimadzu Corporation, Kyoto, Japan) with an Atlantis T3 3 μ m column (2.1 \times 150 mm, Waters, Milford, MA, USA). The column temperature was 40°C. The mobile phases consisted of 0.1% formic acid in water (eluent A) and 0.1% formic acid in acetonitrile (eluent B). The gradient was maintained at an initial 5% B for 2.5 min, to 20% B at 8 min, and was set back to 5% B at 9 min with a hold for one minute. The area under the curve (AUC) corresponding to each molecule was quantified and used to compare samples.

2.7. Identification of conjugates

Standards of GSH and taurine (both from Sigma-Aldrich, St. Louis, MO, USA) were prepared in 70% ethanol. To induce the conjugation of taurine to GSH 150 mmol of each was weighted in the same 2 ml Eppendorf tube, 70% ethanol was added, vortexed shortly, and was incubated for 30 min at room temperature. Standards were separated with the column and HPLC gradient described above and

were fragmented with an LC-MS system (LCMS-80-40, Shimadzu, Korneuburg, Austria). The MS instrument was operated in multiple reaction mode (MRM) with the following settings: nebulizing gas flow 3L/min, drying gas flow 12L/min, desolvation line temperature 250°C, and heat block temperature 350°C. Argon was used as the collision-induced dissociation (CID) gas with a collision energy of 20eV. The fragmentation pattern was compared to METLIN database. To identify GSH and taurine conjugates, samples were screened for precursor ions producing similar fragmentation patterns to GSH and taurine. For validation that the identified compound contains taurine or GSH, samples were analyzed with the multiple reaction monitoring (MRM) setting. For example, the fragmentation pattern of metabolite m/z 249 shows taurine and the specific taurine fragment, according to the METLIN database. The exact mass of the selected precursor ions was measured using an LC-ESI-TOF-system consisting of an Ultimate 3000 (Thermo Fischer Scientific, Waltham, MA, US) and a micrOTOF-Q II (Bruker Daltonics, Bremen, Germany) with an Atlantis T3 3 μ m column (2.1 \times 150 mm, Waters, Milford, MA, USA). The column temperature was 40°C. The mobile phases consisted of 0.1% formic acid in water (eluent A) and 0.1% formic acid in acetonitrile (eluent B). The gradient was maintained at an initial 5% B for 2.5 min, to 20% B at 8 min, and was set back to 5% B at 9 min with a hold for one minute. The exact mass and fragmentation pattern of the selected precursor ions were checked against the METLIN database. The compounds identified as GSH or taurine conjugates are listed in supplementary table 2.

2.8. Bile acid analysis

Sample extraction and measurement of bile acids were carried out using a modified method by Rohn et al. [45]. Shortly, feces samples were weighted in Precellys homogenizing tubes with 1.4 mm ceramic beads, and nine times the volume of methanol absolute at -20°C was added. Samples were homogenized in the Precellys 24 Tissue Homogenizer (Bertin Instruments, Montigny-le Bretonneux, France) twice for 15 s at 5000 rpm, vortexed for 30 s, and centrifuged for 10 min at 5000 g at 4°C. The supernatants were transferred to new 1.5 ml Eppendorf tubes, and, to remove the remaining debris, the centrifugation step was repeated this time at 12000 g. Supernatants were transferred into new Eppendorf tubes and after third centrifugation, supernatants were directly transferred into an HPLC vial. Samples (10 μ l) were analyzed by LCMS in positive modus using an LCMS-8040 Liquid Chromatograph Mass Spectrometer (Shimadzu Corporation, Kyoto, Japan) with an Atlantis T3 3 μ m column (2.1 \times 150 mm, Waters, Milford, MA, USA). The column temperature was 30°C. The mobile phase A consisted of water and eluent B was acetonitrile/methanol (3/1, v/v), both containing 0.1% formic acid and a concentration of 20mM ammonium acetate. The gradient was maintained from an initial 30% B for 5 min, to 100% B at 25 min, which was kept constant for 20 min. Afterward, the composition was set back to the initial ratio of 30% B within 2 min, followed by 10 min of re-equilibration.

2.9. Statistics

The differences in the intestine mucosa GST expression between the experimental groups were used to calculate the sample size. Within the study, data sets with two groups (CR and *ad libitum*) of seven to nine biological replicates were compared using a two-sided student's t-test to verify statistical significance. Additionally, for the *ex vivo* assay, statistical significance was assessed using one-way ANOVA with Bonferroni post-hoc corrections for four groups of five to seven replicates using SPSS Statistics 26 (IBM Corp., Armonk, NY, USA). A p-value lower than 0.05 was considered statistically significant. The presented data stems from two technical replicates.

3. Results

3.1. CR increases the levels of free taurine and its conjugates along the intestinal mucosa but not in the liver

As we previously published, CR is associated with increased levels of taurine-conjugated BAs in the intestine [41]. To further explore this phenomenon, we studied the impact of CR on intestinal taurine levels. In order to mirror previous experimental conditions, male C57Bl/6 mice were submitted to 14 days caloric restriction receiving 75% of the amount of standard chow that the animals would voluntarily consume. The levels of taurine were measured in the mucosa along the small intestine. We detected increased levels of free taurine in the duodenum of CR compared to *ad libitum* fed mice (Fig. 1A). To verify how taurine could be utilized in the intestine, compounds containing taurine were analyzed. Multiple conjugates of taurine were detected and, accordingly, their levels were increased in the mucosa of CR animals (conjugate with molecular

mass 249 is presented) (Fig. 1B). Among the compounds detected, we identified a GSH-*taurine* conjugate. The conjugate showed an increased concentration in intestinal mucosa samples of CR compared to *ad libitum* fed mice. However, in the duodenum, this difference was not statistically significant (Fig. 1C). The levels of free taurine, taurine conjugates, and GSH-*taurine* were statistically significantly elevated in the jejunum (Fig. 1D-F), and the ileum of CR animals (Fig. 1G-I). The differences in the amounts of the metabolites were more pronounced in the distal compared to the proximal intestine and the concentration of taurine was the highest in the ileum. The level of one of the taurine metabolites, taurine chloramine (TauCl), a compound with strong anti-inflammatory properties, was also increased in the ileum (Fig. 1J). While glycine levels were not affected by the diet (Fig. 1K). We further verified if CR also affects the liver in a similar way, but there was no difference in free taurine (Fig. 2A), conjugated taurine (Fig. 2B), or GSH-*taurine* conjugates (Fig. 2C) levels between CR and *ad libitum* mice. Importantly, the expression of genes associated with BAs synthesis (Cyp7a1), transport (Ntcp), and cysteine metabolism (Cdo) was up-regulated in CR liver while that of TauT was not affected by the restriction (Fig. 2D). Contrary to the liver, the mRNA expression of Cdo was not affected by CR in the mucosa of the ileum (Suppl Fig. 1A).

3.2. CR impacts GSH and GST but does not influence REDOX response in the jejunum mucosa

Since one of the identified taurine conjugates contained GSH, we verified the levels of reduced (GSH) and oxidized (GSSG) glutathione in the jejunum mucosa. The levels of GSH were significantly decreased in the CR compared to *ad libitum* fed mice (Fig. 3A), while GSSG concentration was not affected by CR (Fig. 3B). To validate whether the rate of *de novo* synthesis or utilization of GSH is modified during CR, expression of genes connected with GSH synthesis (Nrf2, Ggt, Gclc, and Gs) and antioxidant activity (Grx1, Grx2, GPx1, and GPx2), as well as activity of several of the factors, were measured in the mucosa of the jejunum. The mRNA level of Nrf2 was downregulated in the CR mice (Fig. 3C), although its transcriptional activity was not changed (Fig. 1D). Also, the expression of Ggt was downregulated (Fig. 3C). The expression of other genes connected with GSH synthesis and its anti-oxidative role was not affected (Fig. 3C). The activity of GR which is responsible for the conversion of GSSG to GSH was increased in the CR animals (Fig. 3E), whereas the activity of GPx was not significantly affected and showed high variability (Suppl Fig. 1B). To verify the functional outcome of the anti-oxidative role of GSH in the CR intestine, the total antioxidant capacity was assessed (Fig. 3F) and the levels of reactive oxygen species were measured by means of ESR (Fig. 3G) in the intestinal mucosa. Both of the parameters were not affected. Additionally, the expression on manganese superoxide dismutase (MnSOD), catalase (Cat), thioredoxin 1, and 2 (Trx1 and Trx2) were decreased in the intestinal mucosa of CR mice (Suppl Fig. 1C). Therefore, we decided to focus on the conjugating function of GSH and found increased activity of GST in the intestine of CR compared to *ad libitum* fed mice (Fig. 3H). We also measured gene expression in six distinct parts of the GI tract (stomach, duodenum, jejunum, ileum, proximal colon, and distal colon) (Fig. 3I). Fittingly with the enzymatic activity results, the expression of Gst genes was consistently increased in mucosa of the different parts of the GI tract. However, the range of upregulation varied between different forms of Gst. Additionally, Gsta4 showed the opposite trend of decreased expression in CR compared to *ad libitum* mice in jejunum; however, not statistically significant.

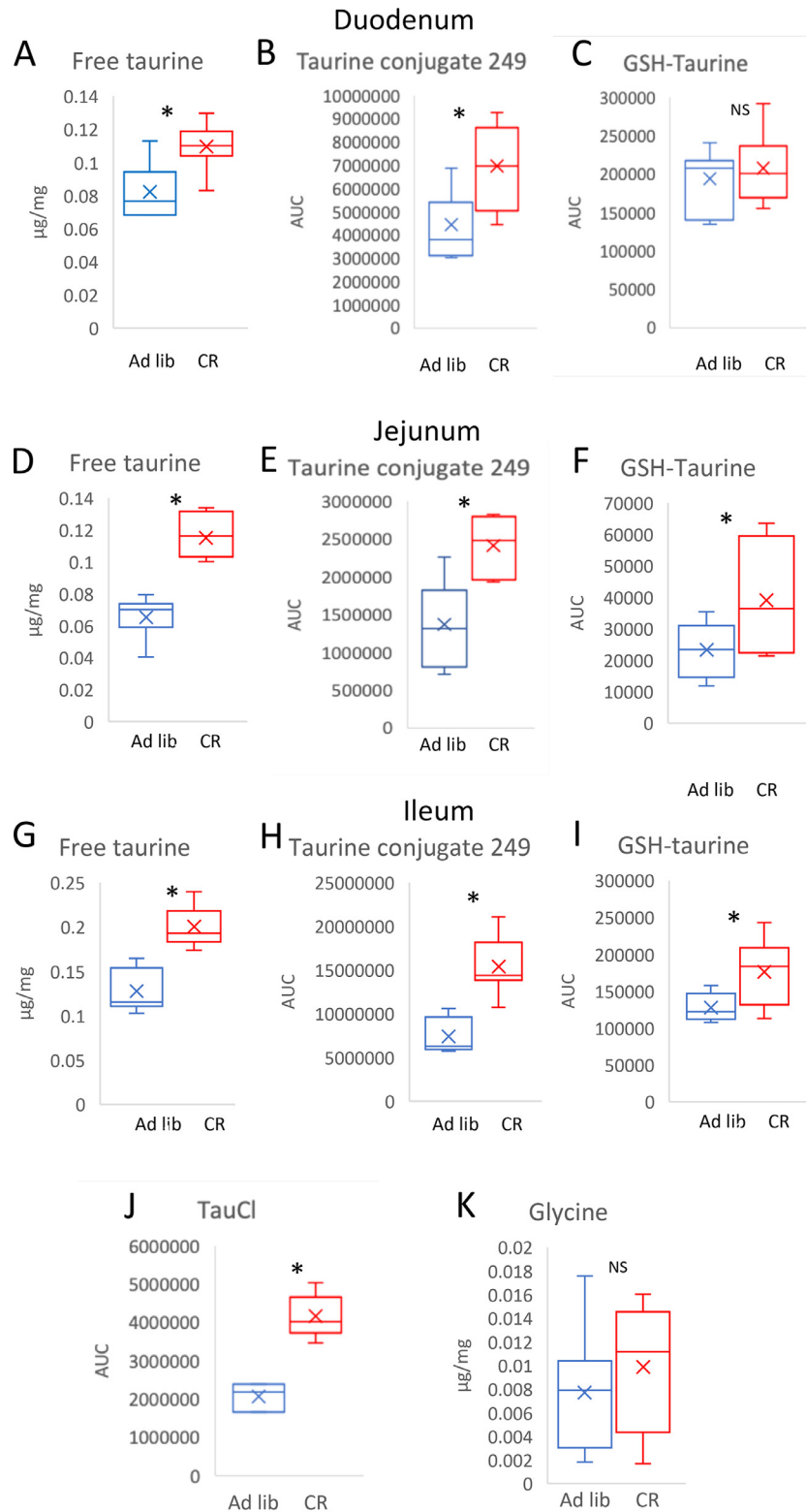


Fig. 1. Caloric restriction (CR) increases the levels of free taurine and its conjugates along the intestinal mucosa. The levels of free taurine (A, D, G), taurine conjugate with m/z 249 (B, E, H), and GSH-tyrosine conjugate (C, F, I) were measured in the mucosa of the duodenum (A-C), jejunum (D-F), and ileum (G-I). Similarly, the levels of taurine chloramine (TauCl; J) and glycine (K) were assessed in the mucosa of ileum. Statistical significance was assessed using a two-tailed Student's t-test; * $P < .05$; $n=6-8$. Error bars stand for \pm SEM.

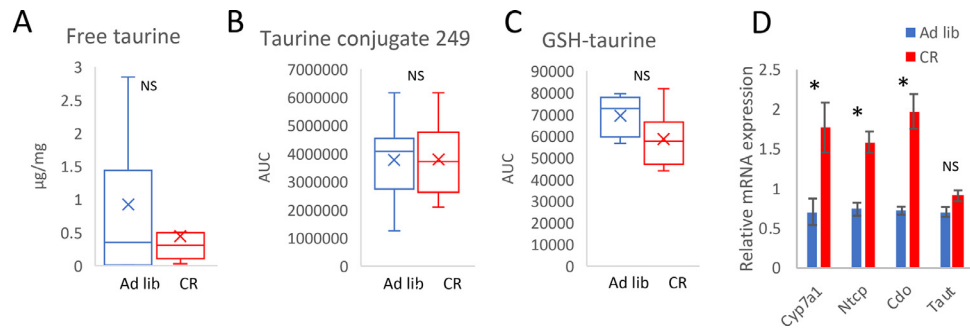


Fig. 2. CR does not affect the levels of taurine and its conjugates in the liver but regulates BA production and cysteine-related gene expression. The levels of free taurine (A), taurine conjugate with m/z 249 (B), and GSH-aurine conjugate (C) were measured in the liver. Gene expression was assessed in the liver of CR and *ad libitum* fed mice (D). Cyp7a1: cholesterol 7 α -hydroxylase; Ntcp: Na⁺/taurocholate cotransporting polypeptide; Cdo: cysteine dioxygenase; TauT: taurine transporter. Two-tailed Student's t-test was applied to assess statistical differences between the groups; * P <.05. Bars indicate the mean of eight to nine biological replicates \pm SEM.

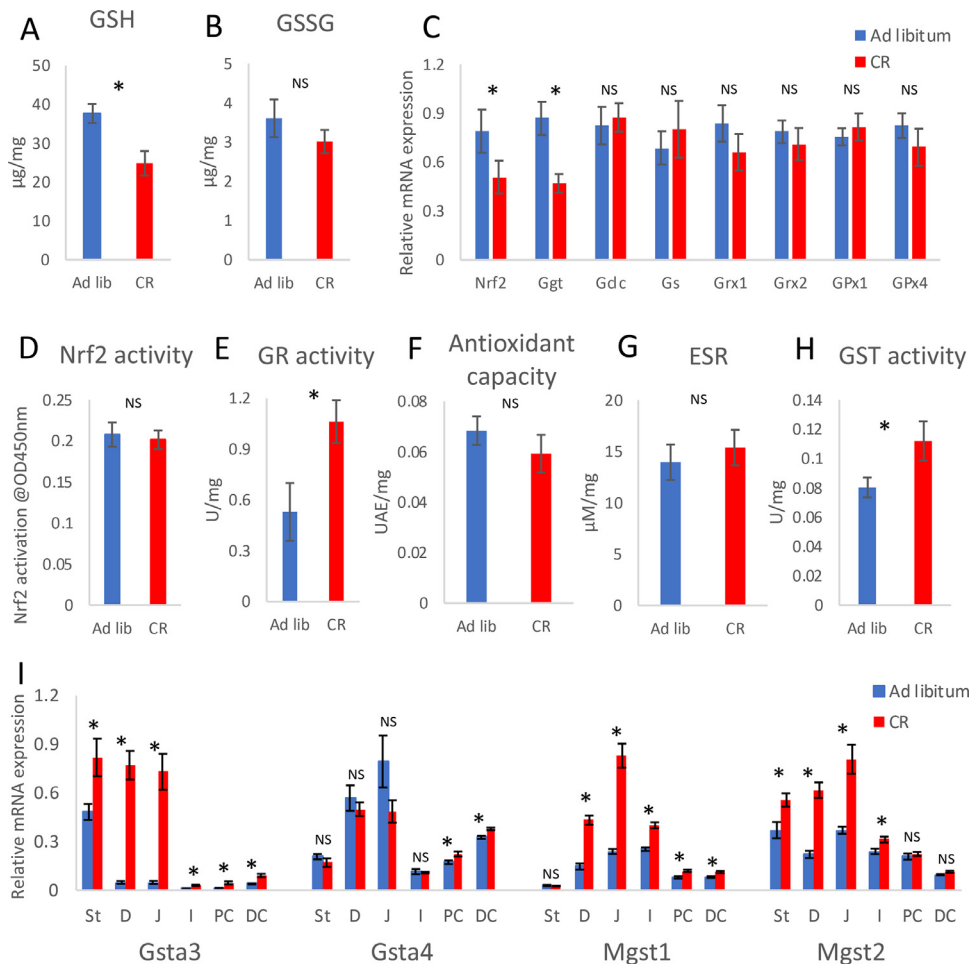


Fig. 3. CR impacts glutathione (GSH) and glutathione-S transferase (GST) in the jejunum mucosa. The levels of reduced GSH (A) and oxidized GSH (GSSG) (B) were measured in the jejunum mucosa using commercial assays. Gene expression was measured in the mucosa of the jejunum of CR and *ad libitum* mice (C). The activity of nuclear factor erythroid 2-related factor 2 (Nrf2) (D) and glutathione reductase (GR) (E) as well as antioxidant capacity (F), were measured in the mucosa of the jejunum utilizing commercial assays. Electron spin resonance (ESR) was applied to assess the levels of reactive oxygen species in the mucosa of the jejunum (G). GST activity was measured in the jejunum mucosa using commercial assays (H). Gene expression of the different GST subtypes was measured in the mucosa of six parts of the GI tract (St-stomach, D-duodenum, J-jejunum, I-ileum, PC-proximal colon, DC-distal colon) of CR and *ad libitum* fed mice (I). Nrf2: nuclear factor erythroid 2-related factor 2; Ggt: gamma-glutamyl transpeptidase; Gcl: glutamate-cysteine ligase; Gs: glutathione synthase; Grx1: glutathione reductase 1; Grx2: glutathione reductase 2; GPx1: glutathione peroxidase 1; GPx2: glutathione peroxidase 2; Gsta3: GSH S-transferase α 3; Gsta4: GSH S-transferase α 4; Mgst1: microsomal GSH S-transferase 1; Mgst2: microsomal GSH S-transferase 2. Two-tailed Student's t-test was applied to assess statistical differences between the groups; * P <.05. Error bars indicate \pm SEM. Figures in panels A-I represent the mean of eight to nine biological replicates.

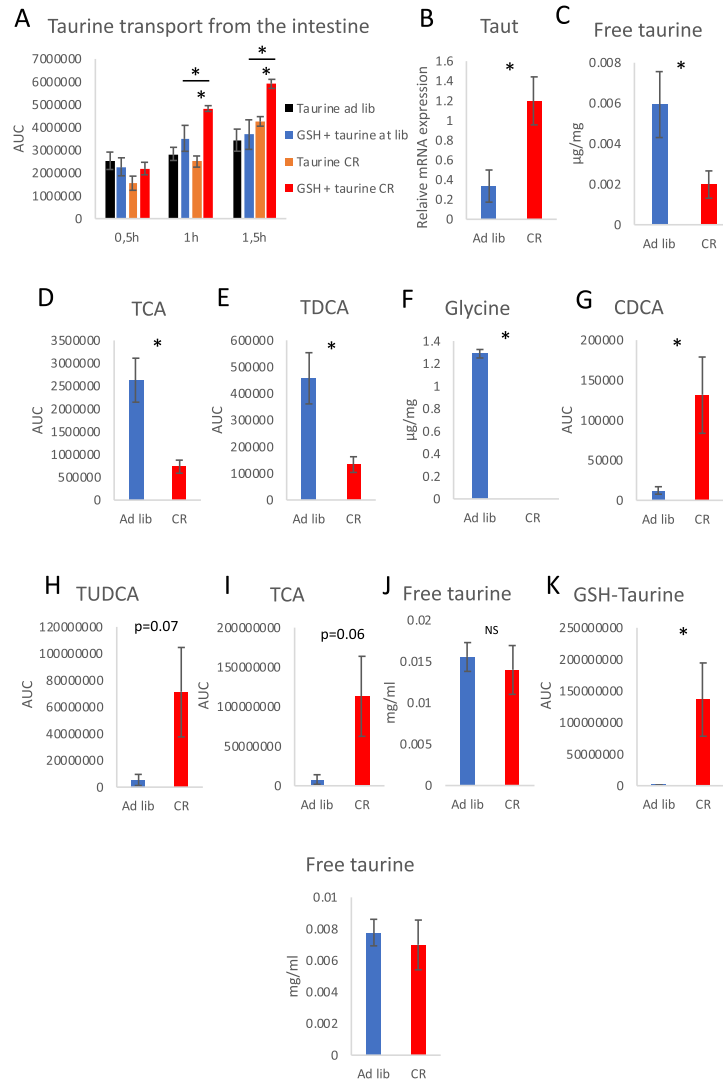


Fig 4. Both GSH and CR stimulate uptake of taurine in the intestine. Taurine uptake was assessed using *ex vivo* intestine sacs infused with a solution containing taurine or taurine and GSH. The concentration of transported taurine was measured in the surrounding medium at the indicated time points (A). The expression of *TauT* mRNA was measured in the mucosa of the ileum (B). Feces were analyzed for the levels of free taurine (C) and bile acids conjugated with taurine: TCA (D) and TDCA (E) and glycine (F). The levels of chenodeoxycholic acid (CDCA; G), TUDCA (H), TCA (I), free taurine (J), and GSH-conjugated taurine (K) were measured in mice plasma. The groups presented in panel A were compared using ANOVA. Student's t-test was applied to assess statistical differences between the groups in panels B-E; * $P < .05$. Error bars indicate \pm SEM. The figure in panel A represents the mean of five to seven replicates while in panels B-E eight biological replicates.

3.3. GSH and CR stimulate uptake of taurine in the intestine

The strongest difference between CR and ad libitum mice in the expression of GSTs was observed in the duodenum and jejunum (Fig. 3I), however, the difference in taurine and its conjugates increased along the small intestine and peaked in the ileum (Fig. 1). Therefore, for the next experiments, ileum was applied. To verify the functionality of the occurrence of GSH-*taurine* conjugates, we incubated *ex vivo* intestinal sacs of CR and ad libitum fed mice which were infused with taurine or a mix of taurine and GSH solutions to measure uptake of taurine. The levels of taurine in the surrounding medium were measured at three time points over 1.5 h of incubation. The uptake of taurine did not change between CR and ad libitum fed mice when sacs were infused with a taurine solution (Fig. 4A). Similarly, a solution containing taurine and GSH did not impact taurine uptake in ad libitum fed mice. However, incubation of the intestine of CR mice with taurine and GSH solution strongly increased the concentration of taurine in the surrounding

medium. Therefore, CR and GSH jointly increased the uptake of taurine. Correspondingly, the mRNA expression of *TauT*, the main intestinal transporter responsible for capturing taurine between the meals [46], was higher in ileum mucosa of CR compared to ad libitum fed mice (Fig. 4B). In accordance, the levels of free taurine and taurine-conjugated BA (TCA and TDCA) were lower in the feces of CR compared to ad libitum fed mice (Fig. 4C-E). CR completely removed glycine from feces (Fig. 4F). Furthermore, the levels of chenodeoxycholic acid (CDCA; Fig. 4G) and taurine conjugated BAs TUDCA and TCA (Fig. 4H-I) were higher in the plasma of CR compared to ad libitum mice corresponding well the suggested increased BA synthesis in the liver and enhanced intestinal uptake. Despite TUDCA and TCA showing a very strong trend towards increased levels in CR mice the results were not statistically significant ($P = .07$ and $P = .06$ respectively). Importantly, CR did not affect the plasma levels of free taurine (Fig. 4J) but strongly increased the levels of GSH-*taurine* (Fig. 4K) confirming that the conjugation by GSH is necessary for the uptake of taurine.

4. Discussion

To contribute to building the full picture of the molecular mechanism of intestinal response to CR we focused on one of the previously reported by us phenotypes [41] connected with increased levels of taurine-conjugated BAs in the intestinal contents. In the current study, we prove that CR is associated with increased levels of free and conjugated taurine in the intestinal mucosa. The increased level of intestinal and plasma BAs matches well with elevated expression of BA synthesis- and transport-related genes in the liver of CR mice presented in this study. Correspondingly, based on gene expression data, the synthesis of taurine is likely to increase in the cysteine dioxygenase-associated cysteine metabolic pathways in the liver but not in the intestinal epithelium. However, the expression of the TauT in the liver was not affected, suggesting that taurine is not exported from the liver as free taurine but as bile conjugate. Further, we report that during CR, the levels of taurine increase along the small intestine but not in the liver. Our results show that the amount of BA-derived taurine increases in the CR intestine and various types of conjugates are created to bind taurine. Conjugation of taurine to GSH enhances taurine re-uptake from the intestine and CR affects plasma levels of GSH-conjugated but not free taurine. Importantly, the impact of GSH on taurine uptake has never been described before and the molecular background of this interaction is not known. Correspondingly, we showed that the level of taurine bound to BAs as well as free taurine is lower in the feces and higher in plasma of CR compared to *ad libitum* mice indicating increased efficiency of uptake in the small intestine.

The BAs are secreted to the proximal intestine upon lipid consumption and travel along the GI tract to solubilize lipids aiding digestion and absorption. However, the secretion of motilin, a hormone stimulating BAs secretion, increases also during fasting [47], which likely triggers the observed phenotype. Once reaching the distal intestine, 95% of BAs are reabsorbed and recirculated to the liver [48]. The amount of free taurine, GSH-*taurine*, and other taurine conjugates are increased in all parts of the intestinal mucosa in CR compared to *ad libitum* mice. However, in this study, the differences between CR and *ad libitum* fed mice are stronger in the distal intestine compared to the duodenum. Most likely, this is due to increased BA reabsorption and high expression of TauT in the ileum [46].

While, as we showed previously, CR results in the reduction of levels of multiple metabolites in the GI tract [41], taurine is an intriguing example of a molecule with an increased concentration, suggesting a physiological role. The role of enterohepatic circulation or accumulation of taurine during CR has never been investigated. However, we hypothesize that taurine could serve as a regulator of metabolic adjustment as it had been shown to reduce the hepatic secretion of lipids while enhancing fatty acid oxidation and ketogenesis which are processes characteristic to fasting and CR [49]. Additionally, as published before [41], CR results in the downregulation of the immune and anti-microbial genes in the intestine. Fittingly, taurine [24–27, 34], as well as BAs [50–52] are known for their anti-inflammatory role and impact on microbiota. Therefore, the increased levels of BAs and taurine in the intestine during CR could contribute to the previously described phenotype. Importantly, taurine supplementation, similarly to CR has been shown to reduce endoplasmic reticulum stress and extend lifespan in *C. elegans* [53]. Consequently, taurine has already been suggested as a supplement mimicking the beneficial outcomes of CR [54]. An important aspect of mimicking CR is the enhancement of mitochondrial function. Taurine reduces the generation of superoxide in mitochondria and is required for normal mitochondrial structure and metabolism. This is likely a consequence of creating

5-*taurinomethyluridine*-tRNA^{Leu} conjugate which is vital for mitochondrial protein expression [55–58]. Therefore, compartmentalization of taurine and organelle-specific biological activity may be a key to unveiling its contribution to the beneficial outcomes of CR.

Seeing the changes of GSH levels in the context of CR we, first, hypothesized changes in the REDOX response, which are often associated with CR. However, contradictory data concerning oxidative stress in CR have been reported [59–63]. Our results show that intestinal mucosa does not respond to CR by modulating the levels of reactive oxygen species or anti-oxidative capacity. Surprisingly, the shifted ratio of GSH/GSSG was not reflected in the total oxidative stress. Assuming diminished oxidative stress during CR, as reflected by MnSOD, Cat, and Trx expression, the requirement for GSH is reduced, and therefore, the level of GSH would not influence the oxidative stress balance. We conclude that it is not the oxidative but the conjugative activity of GSH that is involved in the intestinal response to CR and that GST is activated during CR to conjugate taurine which is likely released from BAs. We show that GST gene expression increases and accordingly, the activity of GST and the occurrence of GSH conjugate are elevated in the mucosa of CR mice. Due to the higher demand from the GST side, the level of free GSH decreases. Consequently, the GSSG/GSH ratio is elevated, and this activates GR which converts GSSG to GSH and reestablishes the basic state ratio. It is, however, possible that the decreased level of GSH could also partly result from the CR-accompanied shortage of nutrients, substrates to synthesize GSH, and food-derived GSH. The reduced expression of *Ggt*, coding for GSH hydroxylase which digests external GSH in order to deliver amino acids for absorption and intracellular GSH synthesis, may reflect the reduced availability of the extracellular GSH.

In summary, we describe a novel role of GSH in the handling of CR-associated abundance of taurine in the small intestine. Interestingly, the role of BAs secreted not in the context of food consumption is not known. Importantly, the here described CR-triggered upregulation of GST expression and activity, a link between intestinal GSH and BA-derived taurine as well as the impact of GSH on taurine absorption has never been established before. With this and future studies, we build upon our previous publications, focusing on a specific novel piece of regulation and aiming at the development of a more detailed molecular picture of the response of the intestine to CR. Currently, the mechanism behind the remarkable health benefits of CR is largely undetermined, particularly in the GI tract. Based on our previous work we speculate that BA and taurine could contribute to the CR-triggered reduction of intestinal inflammation or increased efficiency of nutrient uptake. However, the exact physiological purpose and consequences of this regulation and its relevance to human physiology need to be further investigated.

Author Contributions

AG: data curation, investigation, writing-review and editing; MP: methodology, writing-review and editing; CF: methodology; SB: methodology; VS: conceptualization, writing-review and editing; JK conceptualization, writing-review and editing; KD conceptualization, data curation, investigation, supervision, visualization, writing-original draft. All authors have read and agreed to the published version of the manuscript.

Declaration of Competing Interest

The authors have no competing interest to declare.

Funding

This research did not receive any specific grant from funding agencies in the public, commercial, or not-for-profit sectors.

Availability of data and materials

All data generated or analysed during this study are included in this published article and its supplementary information files.

Acknowledgments

The authors would like to thank Dr. Barbara Lieder for her input in the discussions concerning the publication. Open access funding provided by the University of Vienna.

Supplementary materials

Supplementary material associated with this article can be found, in the online version, at doi:[10.1016/j.jnutbio.2021.108781](https://doi.org/10.1016/j.jnutbio.2021.108781).

References

- [1] Speakman JR, Mitchell SE. Caloric restriction. *Mol Aspects Med* 2011;32:159–221.
- [2] Weindruch R, Walford RL, Fligiel S, Guthrie D. The retardation of aging in mice by dietary restriction: longevity, cancer, immunity and lifetime energy intake. *J Nutr* 1986;116:641–54.
- [3] Anderson RM, Shanmuganayagam D, Weindruch R. Caloric restriction and aging: studies in mice and monkeys. *Toxicol Pathol* 2009;37:47–51.
- [4] Fontana L, Partridge L, Longo VD. Extending healthy life span—from yeast to humans. *Science* 2010;328:321–6.
- [5] Mattison JA, Colman RJ, Beasley TM, Allison DB, Kemnitz JW, Roth GS, et al. Caloric restriction improves health and survival of rhesus monkeys. *Nat Commun* 2017;8:14063.
- [6] Duszka K, Wahli W. Peroxisome proliferator-activated receptors as molecular links between caloric restriction and circadian rhythm. *Nutrients* 2020;12.
- [7] Duszka K, Gregor A, Guillou H, König J, Wahli W. Peroxisome proliferator-activated receptors and caloric restriction-common pathways affecting metabolism. *Cells* 2020;9.
- [8] Redman LM, Ravussin E. Caloric restriction in humans: impact on physiological, psychological, and behavioral outcomes. *Antioxid Redox Signal* 2011;14:275–87.
- [9] Merry BJ. Molecular mechanisms linking calorie restriction and longevity. *Int J Biochem Cell Biol* 2002;34:1340–54.
- [10] Sanz A, Caro P, Ibanez J, Gomez J, Gredilla R, Barja G. Dietary restriction at old age lowers mitochondrial oxygen radical production and leak at complex I and oxidative DNA damage in rat brain. *J Bioenerg Biomembr* 2005;37:83–90.
- [11] Yu BP. Aging and oxidative stress: modulation by dietary restriction. *Free Radic Biol Med* 1996;21:651–68.
- [12] Siegers CP, Riemann D, Thies E, Younes M. Glutathione and GSH-dependent enzymes in the gastrointestinal mucosa of the rat. *Cancer Lett* 1988;40:71–6.
- [13] Hoensch H, Morgenstern I, Peterleit G, Siepmann M, Peters WH, Roelofs HM, et al. Influence of clinical factors, diet, and drugs on the human upper gastrointestinal glutathione system. *Gut* 2002;50:235–40.
- [14] Bhabak KP, Mughes G. Functional mimics of glutathione peroxidase: bioinspired synthetic antioxidants. *Acc Chem Res* 2010;43:1408–19.
- [15] Couto N, Wood J, Barber J. The role of glutathione reductase and related enzymes on cellular redox homeostasis network. *Free Radic Biol Med* 2016;95:27–42.
- [16] Hinchman CA, Ballatori N. Glutathione conjugation and conversion to mercapturic acids can occur as an intrahepatic process. *J Toxicol Environ Health* 1994;41:387–409.
- [17] Chen B, Lu Y, Chen Y, Cheng J. The role of Nrf2 in oxidative stress-induced endothelial injuries. *J Endocrinol* 2015;225:R83–99.
- [18] Solis WA, Dalton TP, Dieter MZ, Freshwater S, Harrer JM, He L, et al. Glutamate-cysteine ligase modifier subunit: mouse Gclm gene structure and regulation by agents that cause oxidative stress. *Biochem Pharmacol* 2002;63:1739–54.
- [19] Lu SC. Glutathione synthesis. *Biochim Biophys Acta* 2013;1830:3143–53.
- [20] Morales Pantoja IE, Hu CL, Perrone-Bizzozero NI, Zheng J, Bizzozero OA. Nrf2-dysregulation correlates with reduced synthesis and low glutathione levels in experimental autoimmune encephalomyelitis. *J Neurochem* 2016;139:640–50.
- [21] Zhang H, Liu H, Dickinson DA, Liu RM, Postlethwait EM, Laperche Y, et al. gamma-Glutamyl transpeptidase is induced by 4-hydroxynonenal via EpRE/Nrf2 signaling in rat epithelial type II cells. *Free Radic Biol Med* 2006;40:1281–92.
- [22] Ibrahim E, Diakonov I, Arunthavarajah D, Swift T, Goodwin M, McIlvride S, et al. Bile acids and their respective conjugates elicit different responses in neonatal cardiomyocytes: role of Gi protein, muscarinic receptors and TGR5. *Sci Rep* 2018;8:7110.
- [23] Schuller-Levis GB, Park E. Taurine: new implications for an old amino acid. *FEMS Microbiol Lett* 2003;226:195–202.
- [24] Kim C, Cha YN. Taurine chloramine produced from taurine under inflammation provides anti-inflammatory and cytoprotective effects. *Amino Acids* 2014;46:89–100.
- [25] Marcinkiewicz J, Mak M, Bobek M, Biedron R, Bialecka A, Koprowski M, et al. Is there a role of taurine bromamine in inflammation? Interactive effects with nitrite and hydrogen peroxide. *Inflamm Res* 2005;54:42–9.
- [26] Niu X, Zheng S, Liu H, Li S. Protective effects of taurine against inflammation, apoptosis, and oxidative stress in brain injury. *Mol Med Rep* 2018;18:4516–22.
- [27] Chupel MU, Minuzzi LG, Furtado G, Santos ML, Hogervorst E, Filaire E, et al. Exercise and taurine in inflammation, cognition, and peripheral markers of blood-brain barrier integrity in older women. *Appl Physiol Nutr Metab* 2018;43:733–41.
- [28] Silva LA, Silveira PC, Ronsani MM, Souza PS, Scheffer D, Vieira LC, et al. Taurine supplementation decreases oxidative stress in skeletal muscle after eccentric exercise. *Cell Biochem Funct* 2011;29:43–9.
- [29] Thirupathi A, Freitas S, Sorato HR, Pedrosa GS, Effting PS, Damiani AP, et al. Modulatory effects of taurine on metabolic and oxidative stress parameters in a mice model of muscle overuse. *Nutrition* 2018;54:158–64.
- [30] Bucolo C, Fidilio A, Platania CBM, Geraci F, Lazzara F, Drago F. Antioxidant and Osmoprotecting Activity of Taurine in Dry Eye Models. *J Ocul Pharmacol Ther* 2018;34:188–94.
- [31] Lee DS, Jo HG, Kim MJ, Lee H, Cheong SH. Antioxidant and anti-stress effects of taurine against electric foot-shock-induced acute stress in rats. *Adv Exp Med Biol* 2019;1155:185–96.
- [32] Trachtman H, Barbour R, Sturman JA, Finberg L. Taurine and osmoregulation: taurine is a cerebral osmoprotective molecule in chronic hypernatremic dehydration. *Pediatr Res* 1988;23:35–9.
- [33] Fang H, Meng F, Piao F, Jin B, Li M, Li W. Effect of Taurine on Intestinal Microbiota and Immune Cells in Peyer's Patches of Immunosuppressive Mice. *Adv Exp Med Biol* 2019;1155:13–24.
- [34] Yu H, Guo Z, Shen S, Shan W. Effects of taurine on gut microbiota and metabolism in mice. *Amino Acids* 2016;48:1601–17.
- [35] Shimizu M, Zhao Z, Ishimoto Y, Satsu H. Dietary taurine attenuates dextran sulfate sodium (DSS)-induced experimental colitis in mice. *Adv Exp Med Biol* 2009;643:265–71.
- [36] Zhao Z, Satsu H, Fujisawa M, Hori M, Ishimoto Y, Totsuka M, et al. Attenuation by dietary taurine of dextran sulfate sodium-induced colitis in mice and of THP-1-induced damage to intestinal Caco-2 cell monolayers. *Amino Acids* 2008;35:217–24.
- [37] Gondo Y, Satsu H, Ishimoto Y, Iwamoto T, Shimizu M. Effect of taurine on mRNA expression of thioredoxin interacting protein in Caco-2 cells. *Biochem Biophys Res Commun* 2012;426:433–7.
- [38] Tappaz ML. Taurine biosynthetic enzymes and taurine transporter: molecular identification and regulations. *Neurochem Res* 2004;29:83–96.
- [39] Stipanuk MH, Londono M, Lee JL, Hu M, Yu AF. Enzymes and metabolites of cysteine metabolism in nonhepatic tissues of rats show little response to changes in dietary protein or sulfur amino acid levels. *J Nutr* 2002;132:3369–78.
- [40] Yamori Y, Taguchi T, Hamada A, Kunimasa K, Mori H, Mori M. Taurine in health and diseases: consistent evidence from experimental and epidemiological studies. *J Biomed Sci* 2010;17(Suppl 1):S6.
- [41] Duszka K, Ellero-Simatos S, Ow GS, Defernez M, Paramalingam E, Tett A, et al. Complementary intestinal mucosa and microbiota responses to caloric restriction. *Sci Rep* 2018;8:11338.
- [42] Zaunschirm M, Pignitter M, Kienesberger J, Hernler N, Riegger C, Eggersdorfer M, et al. Contribution of the ratio of tocopherol homologs to the oxidative stability of commercial vegetable oils. *Molecules* 2018;23.
- [43] Ito T, Okazaki K, Nakajima D, Shibata D, Murakami S, Schaffer S. Mass spectrometry-based metabolomics to identify taurine-modified metabolites in heart. *Amino Acids* 2018;50:117–24.
- [44] Budinska E, Gojda J, Heczkova M, Bratova M, Dankova H, Wohl P, et al. Microbiome and metabolome profiles associated with different types of short bowel syndrome: implications for treatment. *JPEN J Parenter Enteral Nutr* 2020;44:105–18.
- [45] Wegner K, Just S, Gau L, Mueller H, Gerard P, Lepage P, et al. Rapid analysis of bile acids in different biological matrices using LC-ESI-MS/MS for the investigation of bile acid transformation by mammalian gut bacteria. *Anal Bioanal Chem* 2017;409:1231–45.
- [46] Anderson CM, Howard A, Walters JR, Ganapathy V, Thwaites DT. Taurine uptake across the human intestinal brush-border membrane is via two transporters: H⁺-coupled PAT1 (SLC36A1) and Na⁺- and Cl⁻-dependent TauT (SLC6A6). *J Physiol* 2009;587:731–44.
- [47] Peeters TL, Vantrappen G, Janssens J. Fasting plasma motilin levels are related to the interdigestive motility complex. *Gastroenterology* 1980;79:716–19.
- [48] de Aguiar Vallim TQ, Tarling EJ, Edwards PA. Pleiotropic roles of bile acids in metabolism. *Cell Metab* 2013;17:657–69.
- [49] Fukuda N, Yoshitama A, Sugita S, Fujita M, Murakami S. Dietary taurine reduces hepatic secretion of cholesteryl ester and enhances fatty acid oxidation in rats fed a high-cholesterol diet. *J Nutr Sci Vitaminol (Tokyo)* 2011;57:144–9.

- [50] Torres J, Palmela C, Brito H, Bao X, Ruiqi H, Moura-Santos P, et al. The gut microbiota, bile acids and their correlation in primary sclerosing cholangitis associated with inflammatory bowel disease. *United European Gastroenterol J* 2018;6:112–22.
- [51] Hang S, Paik D, Yao L, Kim E, Jamma T, Lu J, et al. Bile acid metabolites control TH17 and Treg cell differentiation. *Nature* 2019;576:143–8.
- [52] Song X, Sun X, Oh SF, Wu M, Zhang Y, Zheng W, et al. Microbial bile acid metabolites modulate gut RORgamma(+) regulatory T cell homeostasis. *Nature* 2020;577:410–15.
- [53] Kim HM, Do CH, Lee DH. Taurine reduces ER stress in *C. elegans*. *J Biomed Sci* 2010;17(Suppl 1):S26.
- [54] Nishizono A, Wang Z, Watanabe Y, Ohata Y, Chiba T. Mechanisms of action of compounds that mimic beneficial effects of calorie restriction such as lifespan extension: Is taurine a promising candidate? *J Physic Fitness Sports Med* 2017;6:201–7.
- [55] Jong CJ, Azuma J, Schaffer S. Mechanism underlying the antioxidant activity of taurine: prevention of mitochondrial oxidant production. *Amino Acids* 2012;42:2223–32.
- [56] Shetewy A, Shimada-Takaura K, Warner D, Jong CJ, Mehdi AB, Alexeyev M, et al. Mitochondrial defects associated with beta-alanine toxicity: relevance to hyper-beta-alaninemia. *Mol Cell Biochem* 2016;416:11–22.
- [57] Jong CJ, Ito T, Prentice H, Wu JY, Schaffer SW. Role of mitochondria and endoplasmic reticulum in taurine-deficiency-mediated apoptosis. *Nutrients* 2017;9:795.
- [58] Schaffer SW, Shimada-Takaura K, Jong CJ, Ito T, Takahashi K. Impaired energy metabolism of the taurine-deficient heart. *Amino Acids* 2016;48:549–58.
- [59] Barja G. Aging in vertebrates, and the effect of caloric restriction: a mitochondrial free radical production-DNA damage mechanism? *Biol rev Camb Philos Soc* 2004;79:235–51.
- [60] Forster MJ, Sohal BH, Sohal RS. Reversible effects of long-term caloric restriction on protein oxidative damage. *J gerontol A, Biol sci med sci* 2000;55:B522–9.
- [61] Lambert AJ, Merry BJ. Lack of effect of caloric restriction on bioenergetics and reactive oxygen species production in intact rat hepatocytes. *J gerontol A, Biol sci med sci* 2005;60:175–80.
- [62] Lambert AJ, Portero-Otin M, Pamplona R, Merry BJ. Effect of ageing and caloric restriction on specific markers of protein oxidative damage and membrane peroxidizability in rat liver mitochondria. *Mec ageing dev* 2004;125:529–38.
- [63] Agarwal S, Sharma S, Agrawal V, Roy N. Caloric restriction augments ROS defense in *S. cerevisiae*, by a Sir2p independent mechanism. *Free Radic Res* 2005;39:55–62.

Original Article 3



Microbial contribution to the caloric restriction-triggered regulation of the intestinal levels of glutathione transferases, taurine, and bile acid

András Gregor, Marc Pignitter, Slave Trajanoski, Sandra Auernigg-Haselmaier, Veronika Somoza, Jürgen König & Kalina Duszka

To cite this article: András Gregor, Marc Pignitter, Slave Trajanoski, Sandra Auernigg-Haselmaier, Veronika Somoza, Jürgen König & Kalina Duszka (2021) Microbial contribution to the caloric restriction-triggered regulation of the intestinal levels of glutathione transferases, taurine, and bile acid, Gut Microbes, 13:1, 1992236, DOI: [10.1080/19490976.2021.1992236](https://doi.org/10.1080/19490976.2021.1992236)

To link to this article: <https://doi.org/10.1080/19490976.2021.1992236>



© 2021 The Author(s). Published with license by Taylor & Francis Group, LLC.



[View supplementary material](#)



Published online: 25 Oct 2021.



[Submit your article to this journal](#)



Article views: 1122



[View related articles](#)

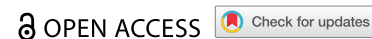


[View Crossmark data](#)




Citing articles: 1 [View citing articles](#)

BRIEF REPORT



Microbial contribution to the caloric restriction-triggered regulation of the intestinal levels of glutathione transferases, taurine, and bile acid

András Gregor^a, Marc Pignitter^b, Slave Trajanoski^c, Sandra Auernigg-Haselmaier^a, Veronika Somoza^{b,d}, Jürgen König^a, and Kalina Duszka^a 

^aDepartment of Nutritional Sciences, University of Vienna, Vienna, Austria; ^bDepartment of Physiological Chemistry, University of Vienna, Vienna, Austria; ^cCore Facility Computational Bioanalytics, Medical University of Graz, Graz, Austria; ^dLeibniz-Institut für Food Systems Biology, Technical University of Munich, Munich, Germany

ABSTRACT

Recently we showed that caloric restriction (CR) triggers an increase in the levels of free taurine, taurine-conjugated bile acids (BA), and other taurine conjugates in intestinal mucosa while decreasing glutathione (GSH) levels in wild-type male mice. In the current project, we decided to investigate whether the microbiota is involved in the response to CR by depleting gut bacteria. The antibiotics treatment diminished CR-specific increase in the levels of free taurine and its conjugates as well as upregulated expression and activity of GSH transferases (GST) in the intestinal mucosa. Further, it diminished a CR-related increase in BAs levels in the liver, plasma, and intestinal mucosa. Transplant of microbiota from CR mice to *ad libitum* fed mice triggered CR-like changes in MGST1 expression, levels of taurine and taurine conjugates in the mucosa of the ileum. We show for the first time, that microbiota contributes to the intestinal response to CR-triggered changes in BA, taurine, and GST levels.

ARTICLE HISTORY

Received 21 May 2021
Revised 1 September 2021
Accepted 28 September 2021

KEYWORDS

Caloric restriction;
microbiota; bile acids;
taurine; glutathione;
intestine


Introduction

Gut microbiota is a complex and dynamic entity characterized by its high variability in composition between different hosts. The inter-individual differences are induced by multiple factors including childbirth delivery, gender, antibiotic treatments, origin, age, and to a great extent by the diet.^{1–5} The type, amount, and timing of the meals are all factors shaping the microbiota.^{6–8} Accordingly, caloric restriction (CR) affects gut bacteria^{9–14} and the composition changes seem to mediate some of the beneficial outcomes of CR, including reduced body weight, decreased blood leptin, and insulin levels.¹⁵ Yet, the mechanism behind and functionality of CR-specific microbiota are not known. The microbiota plays a major role in numerous aspects of the host's health and disease by modulating the availability of energy and nutrients, as well as signaling molecules, e.g. hormones, neurotransmitters, ligands, etc.; thereby affecting the host on multiple levels.¹⁶ Among others, microbiota directly interacts with bile acids (BA) and submits them to various modifications, including

deconjugation of BAs and taurine.¹⁷ Multiple bacterial processes result in the generation of secondary BAs, of which the function and signaling vary from the primary BAs.¹⁸ Reversely, BAs,¹⁹ similarly to taurine^{20,21} modulate gut bacteria composition. Taurine reduces the growth of harmful bacteria and stimulates the production of short-chain fatty acids.²⁰ Taurine increases the number of selected immune cells, total cells in Payer's patches,²¹ and attenuates induced colitis in the mouse intestine.^{22,23} Besides anti-inflammatory^{24–28} activity taurine has also, antioxidant,^{27,29–32} and osmoprotective^{31,33} properties.

A complex network of enzymes and transcription factors controls BA synthesis and circulation between the liver and intestine. High levels of BAs inhibit the activity of the key enzyme of the classic synthesis pathway, cholesterol 7 α -hydroxylase (Cyp7a1) via farnesoid X receptor (FXR) or fibroblast growth factor 19 (FGF19).^{34,35} FXR is activated by BAs and, besides establishing a negative feedback loop, it regulates the expression of BA transporters and impacts inflammation.³⁶

CONTACT Kalina Duszka  kalina.duszka@univie.ac.at  Department of Nutritional Sciences, University of Vienna, Vienna, Austria.

 Supplemental data for this article can be accessed on the [publisher's website](#).

© 2021 The Author(s). Published with license by Taylor & Francis Group, LLC.

This is an Open Access article distributed under the terms of the Creative Commons Attribution License (<http://creativecommons.org/licenses/by/4.0/>), which permits unrestricted use, distribution, and reproduction in any medium, provided the original work is properly cited.

Moreover, FXR also takes input from gut microbiota thereby integrating the connection between BAs, bacteria, and inflammation. Our recent original study indicated that the liver in CR animals shows increased mRNA expression of cysteine dioxygenase (CDO), an enzyme responsible for the metabolism of cysteine to taurine.³⁷ The CR animals also show enhanced expression of Cyp7a1, Ntcp (Na⁺/taurocholate cotransporting polypeptide), which are necessary for BA synthesis and transport. Further, we demonstrated that CR results in increased levels of taurine-conjugated BAs in the intestinal content and mucosa.^{14,37} BAs in the intestine undergo deconjugation and this leads to high levels of free taurine. Simultaneously, CR stimulates the expression and activity of glutathione (GSH) S-transferases (GST) that conjugate taurine leading to an increase in GSH-aurine conjugate levels. The occurrence of GSH-aurine conjugate in conjunction with CR triggers enhanced intestinal uptake of taurine.³⁷ Knowing the vast role of gut bacteria in the metabolism of BAs, we hypothesized that microbiota may contribute to the CR-triggered phenomena. Here, we present novel results showing that microbiota is required for the CR-triggered phenotype associated with GSH and taurine conjugation as well as intestinal uptake.

Results

CR triggers strong microbiota composition changes in the cecum on multiple phylogenetic levels (Figure 1a, Suppl fig S1). We researched the impact of taurine on microbiota and compared the published results^{20,21} with our sequencing data of *ad libitum* fed and CR mice cecum. Among the bacteria already known to be affected, we found *Firmicutes*, *Clostridiales*, and *Lachnospiraceae* downregulated in the CR mice whereas *Proteobacteria*, *Bacilli*, and *Lactobacillales* were upregulated (Figure 1b-g). Interestingly, the exact opposite regulation was reported after the administration of taurine.^{20,21}

In order to assess the role of microbiota in the previously described CR-triggered intestinal phenotype,³⁷ we applied a mouse model with depleted gut microbiota by treatment with a wide spectrum antibiotic cocktail. We submitted the

antibiotics-treated mice to CR (AT CR) and control *ad libitum* feeding (AT) (Figure 2a). In accordance with our earlier report,³⁷ CR increases GST (*Mgst1* and *Gsda3*) mRNA expression and enzymatic activity (Figure 2b-c). Antibiotics treatment diminished the CR-induced changes in GST gene expression (Figure 2b-c) and prevented an increase in GST activity (Figure 2d). However, no differences were observed between *ad libitum* and AT *ad libitum* conditions (Figure 2d). CR compared to *ad libitum* conditions increased production of GSH-aurine conjugate when jejunum tissue lysate was incubated with a solution containing taurine and GSH (Figure 2e). Antibiotics treatment neutralized the impact of CR but did not affect the outcomes of *ad libitum* feeding (Figure 2e). Accordingly, the reduction in GSH level in CR compared to *ad libitum* mice was lessened by dosing antibiotics (figure 2f). The concentration of oxidized GSH (GSSG) was not affected by CR or microbiota depletion (Figure 2g). As previously shown,³⁷ the CR-triggered imbalance in GSH/GSSG ratio leads to the introduction of glutathione reductase (GR) activity (here not statistically significant after correction for multiple testing) aiming at neutralization of the disparity. The CR animals with depleted intestinal microbiota did not show differences in GR activity compared to *ad libitum* mice (Figure 2h). CR-elicited differences in intestinal mRNA expression of the factors involved in GSH synthesis, NRF2, and GGT1, were offset by bacteria depletion (Figure 2i-j). Searching for the molecular mechanism, we quantified the levels of butyrate, which is one of the short-chain fatty acids produced by microbiota and has been reported to induce GST activity.³⁸ However, in CR animals, the amount of cecal butyrate is strongly reduced compared to *ad libitum* mice (Figure 2k).

We reported previously that the levels of oxidative stress-related factors were not affected by CR in the intestinal mucosa.³⁷ Similarly, microbiota depletion did not modify it (Suppl fig S2A-B). Nevertheless, the modulation of microbiota neutralized the CR-specific differences in the expression of oxidative stress-related factors catalase, manganese superoxide dismutase (*Mn-Sod*), and thioredoxin 2 (*Trx2*) (Suppl fig S2 C-E).

As we published before,³⁷ CR elevates free taurine and taurine conjugates in the mucosa of jejunum and ileum. In the current study, the levels of

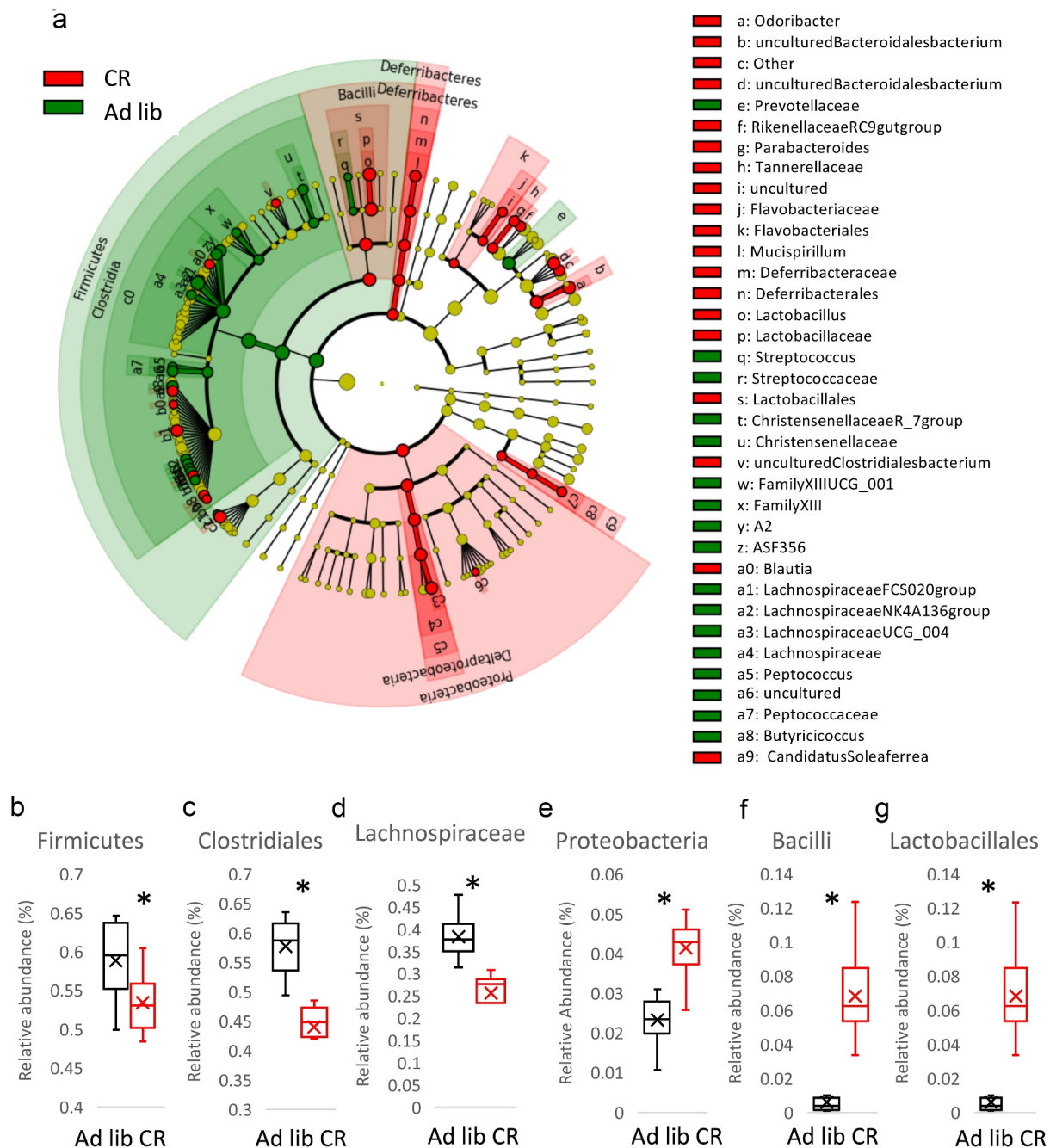


Figure 1. Caloric restriction (CR) modifies microbiota composition in the cecum. Cecum microbiota was sequenced and the results are shown as a Cladogram representing the Linear discriminant analysis Effect Size (LEfSe) results on the hierarchy induced by the taxa. Only significantly changed taxa names with the corresponding color are shown. The figure presents results with a linear determinant analysis (LDA) score bigger than 2 and a *p*-value smaller than .05. (a). The abundance of Firmicutes (b), Clostridiales (c), Lachnospiraceae (d), Proteobacteria (e), Bacilli (f), and Lactobacillales (g) in the cecum of *ad libitum* and CR mice was presented. Two-tailed Student's *t*-tests were used to compare the experimental groups of the panels B-G.

GSH-aurine conjugates showed a tendency toward increased levels in CR mice; yet, not statistically significantly. The depletion of microbiota minimized the difference between CR and *ad libitum* fed mice in the mucosa of the jejunum (Figure 2l-n) and ileum (Figure 2o-r, Suppl fig S2 F-I) in terms of

GSH-aurine conjugate, other taurine conjugates, and free taurine. Further, the mRNA expression of taurine transporter TauT, which was increased in the ileum of CR mice, was not different between AT and AT CR animals (Figure 3a). In agreement with the expression pattern of TauT and our

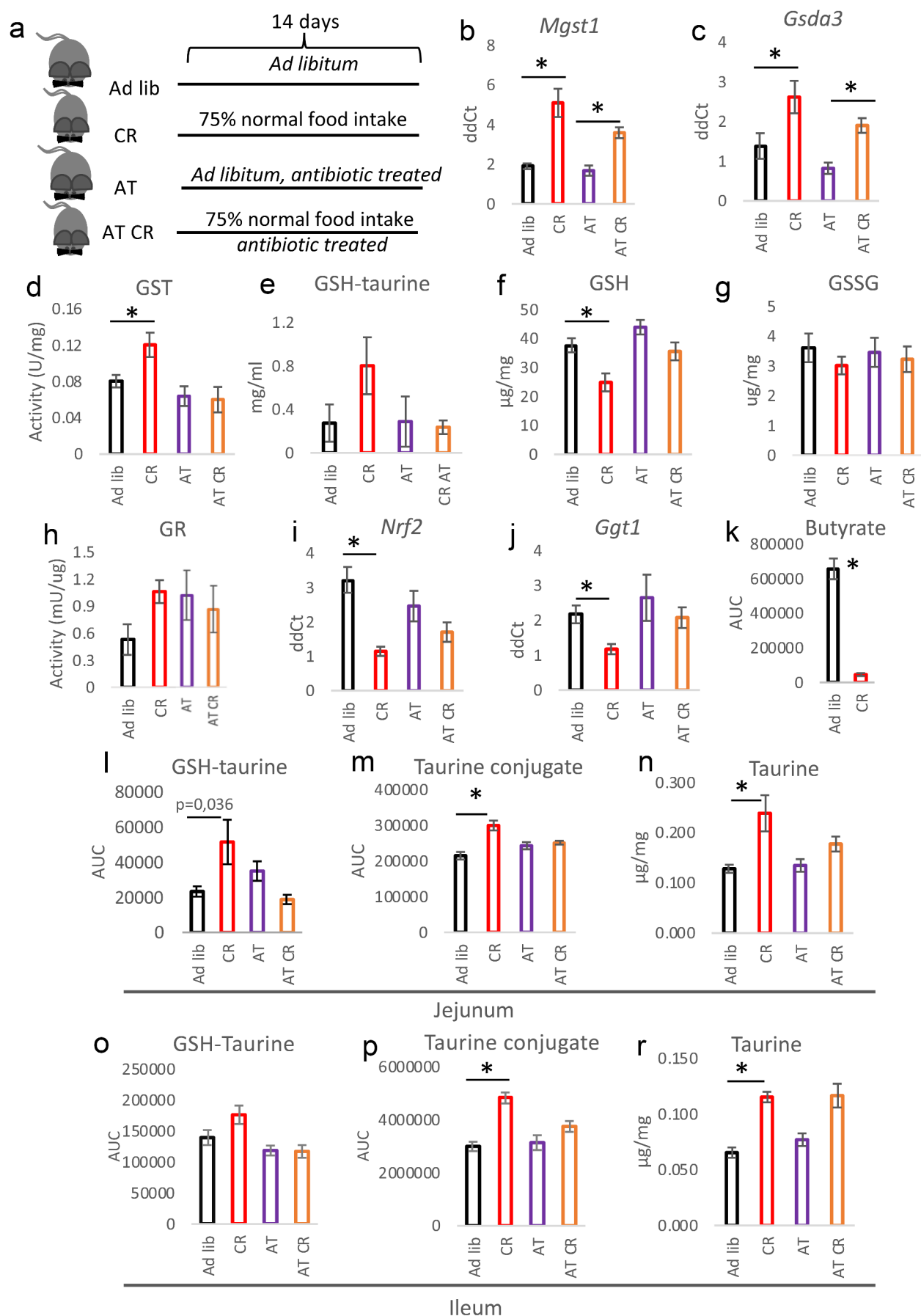


Figure 2. Microbiota depletion neutralizes the CR phenotype in the intestine. The mice were fed *ad libitum* or submitted CR with (AT and AT CR) or without antibiotics treatment (Ad lib and CR) to deplete microbiota (a). Gene expression of the different glutathione-S transferase (GST) subtypes (b-c), and GST activity (d) were measured in the jejunal mucosa. Tissue lysate of jejunum mucosa was

incubated with a solution containing GSH and taurine and occurrence of GSH-taurine conjugate was assessed (e). The levels of reduced glutathione (GSH) (f) and oxidized GSH (GSSG) (g) were measured in the jejunal mucosa. The activity of GSH reductase (GR) (h), as well as expression of nuclear factor erythroid 2-related factor 2 (*Nrf2*; i) and γ -glutamyl transpeptidase (*Ggt1*; j) mRNA, was assessed in the mucosa. Butyrate content was quantified in the feces of CR and *ad libitum* mice (k). The levels of GSH-taurine conjugate (l, o), taurine conjugate *m/z* 249 (m, p), and free taurine (n, r) were measured in the jejunum (l-n) and ileum (o-r). Two-tailed Student's t-tests were used to compare the experimental groups of the panel K. Statistical significance between experimental groups in other panels was evaluated using ANOVA with Bonferroni correction for multiple testing; $n = 6-8$ (panels B-D and F-R), $n = 4$ (panel E); $*p < .05$. Data are presented as the mean \pm SEM.

previous publication,³⁷ CR reduced the levels of taurine and its conjugates in the mice's feces (Suppl fig S2 J-K). In the liver, the expression of genes associated with BA synthesis (*Cyp7a1*) and transport (*Ntcp*) as well as cysteine metabolism

(cysteine sulfonate decarboxylase; *Csd*) was regulated by CR and not by microbiota depletion (Figure 3b-d). Importantly, antibiotics treatment did not impact the expression of any of the measured genes in *ad libitum* fed mice.

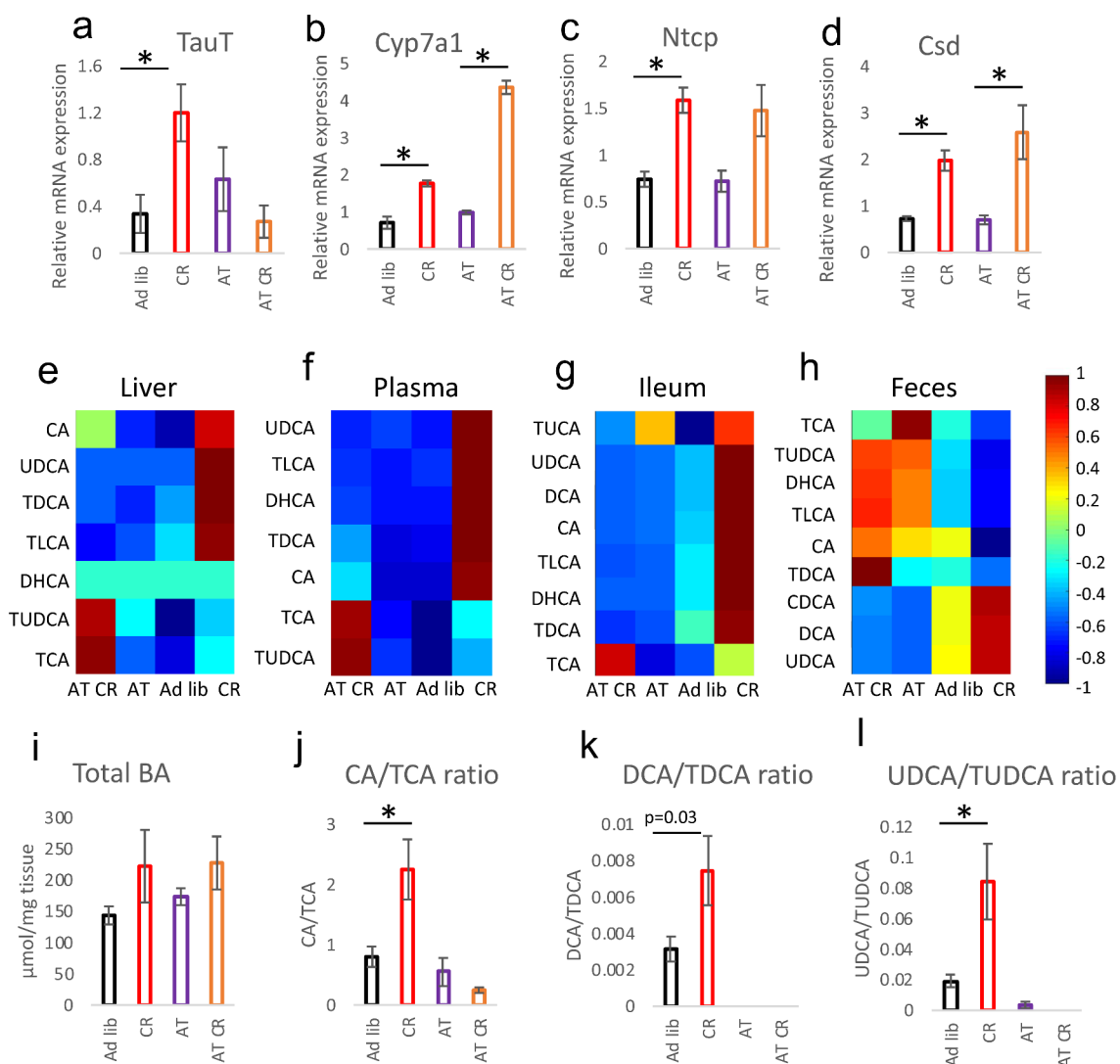


Figure 3. Microbiota and CR jointly regulate the levels of BAs. Gene expression of taurine transporter (TauT) (a), cholesterol 7 α -hydroxylase (Cyp7a1; B), Na^+ /taurocholate cotransporting polypeptide (Ntcp; C), and cysteine sulfonate decarboxylase (Csd; D) was measured in the mucosa of the ileum. The levels of selected bile acids were measured in the liver (e), plasma (f), mucosa of the ileum (g), and feces (h) applying HPLC-MS/MS. Total BAs content was quantified in the mucosa of the ileum using a commercial kit (i). The ratio of CA to TCA (j), DCA to TDCA (k), and UDCA to TUDCA (l) was calculated based on BAs concentration measured in the ileum. Statistical significance between the experimental groups was evaluated using ANOVA with Bonferroni correction for multiple testing; $n = 8$; $*p < .05$. Data are presented as mean \pm SEM. Heatmaps were created by using Z-Scored data, showing the relative deviation from the groups' mean value, and visualized by using the MATLAB extension COVAIN.

Concerning BAs, CR consistently increased levels of the measured BAs in the liver, plasma, and ileum but much less in the feces (Figure 3e-h, Suppl table S1) correspondingly to our previous report.³⁷ However, the differences in the liver, plasma, and ileum were not statistically significant for each BA. Similarly, despite a visible trend, the differences in the concentrations of total BAs in the ileum of *ad libitum* compared to CR mice lacked statistical significance (Figure 3i). In the ileum, antibiotics lowered TDCA, TLCA, and UDCA levels. In the liver, the treatment decreased TDCA and TLCA but increased TUDCA; whereas in plasma it increased the levels of CA, TCA, and TUDCA (Figure 3e-g, Suppl table S1). Antibiotics blunted the CR-related increase in most BAs in all tissues. However, the levels of CA, TCA, and TDCA remained statistically significantly higher in AT CR compared to AT group in the plasma and of TCA in the ileum (figure 3f-g, Suppl table S1). In general, the AT and AT CR treatments resulted in similar patterns of BAs levels changes in the ileum, liver, and plasma (Figure 3e-g, Suppl table S1). Interestingly, a comparison of the ratios of taurine-conjugated (TCA, TDCA, TUDCA) versus their unconjugated counterparts (CA, DCA, UDCA) in the epithelium of jejunum indicated an increased rate of BAs deconjugation in the CR animals (Figure 3j-l). These differences were not present for AT and AT CR animals due to reduction or depletion of the BAs levels. The differences between *ad libitum* and CR taurine-conjugated and unconjugated BAs ratios were much less pronounced in fecal samples (Suppl fig S3A-C).

In order to confirm the role of microbiota, we performed fecal transplants from CR and *ad libitum* fed mice to another group of mice with depleted bacteria and fed *ad libitum* (FT, FT CR) (Figure 4a). Microbiota transplant did not change levels of taurine conjugated BAs in the liver, plasma, or epithelium of ileum (Suppl table S1). The CR transplant triggered a CR-like increase in MGST1 gene expression (Figure 4b) but no statistically significant changes in GSDA3 (Figure 4c) expression, GST activity (Figure 4d), or GSH levels (Figure 4e). Notably, FT CR mice experienced a CR-like increase in GSH-aurine conjugates in the jejunum, whereas no changes in the free taurine and taurine conjugates were measured (Figure 4g-

h). In the ileum mucosa, the levels of GSH-aurine, free taurine as well as taurine conjugates were increased in FT CR compared to FT mice (Figure 4i-k, Suppl fig S3D-I).

Discussion

In the previous study, we showed that CR modulates the level of GSH, taurine, and its conjugates as well as the expression and activity of GSTs.^{14,37} Here we demonstrate that the regulation is microbiota-dependent. Crucially, treatment with antibiotics partly neutralizes or completely removes all of the tested parameters affected by CR. The transplant of the microbiota of CR mice to *ad libitum* fed mice reintroduces the CR phenotype to a certain extend. Therefore, the microbiota is a vital part of the response to CR but it requires other CR-related triggers to fully mimic CR. It has previously been reported that microbiota mediates the effect of CR on weight loss, levels of leptin and insulin,¹⁵ and on metabolic improvements including fat browning, liver health, and better glycemic control.³⁹ Additionally, CR suppresses microbial genes for lipopolysaccharides (LPS) synthesis modulating the immune response.³⁹ Therefore, the here presented data adds a fitting piece to a picture of microbiota-based response to CR.

The microbiota plays a vital role in the metabolism of BAs and bacterial contribution to the observed phenotype is likely connected with the regulation of the conversion of taurine-conjugated BAs.⁴⁰ We propose a model in which upon increased release of BAs to the intestine during CR, microbiota acts to deconjugate BAs from taurine and therefore raises the levels of free taurine and taurine-deconjugated BAs species. The sudden increased appearance of bioactive taurine requires mechanisms to regulate its availability and activity, which may be executed by GSH, leading to the generation of taurine-GSH conjugates. Interestingly, microbiota transplant triggered greater changes in the ileum compared to the jejunum which may be explained by increasing bacterial abundance along the small intestine and greater capacity of the intestine to take up taurine due to high expression of the taurine transporter TauT in the distal intestine.⁴¹ Notably, maintenance of proper taurine levels contributes to increased BA

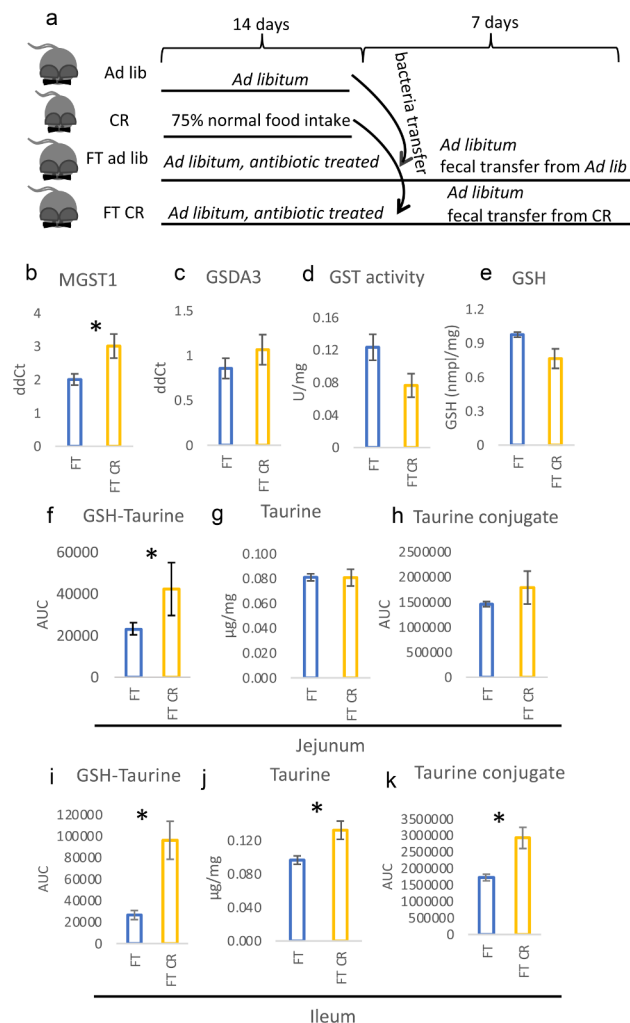


Figure 4. Microbiota can partly induce a CR-like phenotype in the intestine. The mice were fed *ad libitum*, submitted CR, or treated with antibiotics followed by fecal bacteria transfer (FT *ad lib* and FT CR; A). Gene expression of the different GST subtypes (b-c), GST activity (d), as well as levels of GSH (e), were measured in the jejunal mucosa. The levels of GSH-taurine conjugate (f, i), free taurine (g, j), and taurine conjugate *m/z* 249 (h, k) were measured in the jejunum (f-h) and ileum (i-k). Statistical significance between CR and *ad libitum* groups was evaluated using two-tailed Student's t-tests; *n* = 8; **p* < .05. Data are presented as mean ± SEM.

formation and secretion and thereby to the regulation of cholesterol levels.⁴² Furthermore, the enhanced BAs and taurine uptake in the CR intestine previously reported by us¹⁴ likely contributes to diminished or reversed differences for BAs and taurine respectively in the feces compared to the intestine of CR and *ad libitum* fed mice.

The microbiota has been shown to modulate hosts' amino-acid and GSH metabolism.⁴³ Interestingly, the antibiotics treatment of CR mice adjusted (up or down) the levels of GSH-taurine, other taurine conjugates or free taurine, GSH levels, GSTs gene expression and GST enzymatic activity to the levels measured in *ad libitum* fed mice. Importantly, the antibiotics cocktail did not

influence the levels in *ad libitum* fed mice. Therefore, we hypothesize that a CR-specific microbiota is responsible for up- and down-regulation of the levels of the compounds and gene expression. This hypothesis was further confirmed by the results of the fecal transplant approach. Moreover, this regulation seems to be intestine-specific and does not affect gene expression and or BAs production in the liver. As expected,⁴⁴ the antibiotics treatment decreased BAs levels in the intestine of *ad libitum* fed mice. Furthermore, we observed a consistent impact of antibiotics on CR-related changes in BAs composition in the liver, plasma, and mucosa of ileum in antibiotics-treated mice. Antibiotics also strongly

dampened CR-triggered increase in BAs levels; however, the treatment did not neutralize it completely. Furthermore, transplantation of CR-specific microbiota did not affect BAs levels. Therefore, microbiota contributes to the regulation of CR-triggered increase in the levels of BAs but it is not the pivotal factor.

Interestingly, taurine has been reported to reduce the abundance of phylum *Proteobacteria*, class *Bacilli*, and order *Lactobacillales*, while increasing phylum *Firmicutes*, order *Clostridiales*,²⁰ as well as family *Lachnospiraceae*.²¹ In our sequencing results, we found the exact opposite impact of CR on gut microbiota composition. It may seem contradictory considering that the levels of taurine increase in the intestine mucosa during CR. However, due to more efficient uptake during CR³⁷ the level of taurine likely decreases in the intestinal lumen, where microbiota resides. Taurine (together with histamine, and spermine) was suggested to shape the host-microbiota interface through activation of *Nlrp6* inflammasome signaling, resulting in intestinal epithelial cell IL-18 secretion and downstream modulation of anti-microbial peptide transcription,⁴⁵ thereby impacting the microbiome composition and risk of auto-inflammation. Still, more research is required to verify if CR-driven changes in taurine levels affect *Nlrp6*.

Besides GST, also other antioxidative proteins were affected in the intestine during CR in this study. Nonetheless, contrary to GST, the expression of antioxidative proteins is reduced, most likely due to a reduction in oxidative stress accompanying CR.^{46–49} Yet, contradictory data concerning oxidative stress in CR have been reported,⁵⁰ e.g. the expression of SOD and other anti-oxidative enzymes in CR remains controversial.^{50–52} Moderate CR has also been reported to increase the activity of Mn-SOD and GSH concentration in the liver.⁵² Therefore, the impact of CR may be tissue-specific.

In summary, we have shown for the first time that microbiota contributes to the intestinal response to CR by modulating GST activity, levels of GSH, taurine, BAs, and CR-stimulated BAs conjugation. Therefore, gut bacteria may be necessary to profit from the beneficial impact of CR. However, the exact meaning behind the CR-driven increase in taurine and its conjugates in

the intestine is not clear. Moreover, further investigation is required to unveil the mechanisms of microbial activity during CR.

Materials and methods

Animal care and experimental procedures

Male C57Bl/6 mice were purchased from Janvier Labs (Le Genest-Saint-Isle, France) and kept under a 12 h light/12 h dark cycle in standard specific-pathogen-free (SPF) conditions. The mice were given V153x R/M-H auto diet from SSNIFF-Spezialdiäten GmbH (Soest, Germany) and free water access. Mice aged 12 weeks were randomly divided into experimental groups of eight mice, as follows: Ad lib – control *ad libitum* fed; CR – calorie restricted; AT – antibiotics-treated; AT CR – antibiotics-treated and calorie restricted; FT – *ad libitum* fed, antibiotics-treated with fecal microbiota transplant from Ad lib mice; FT CR – *ad libitum* fed, antibiotics-treated with fecal microbiota transplant from CR mice. The groups did not differ significantly in body weight at the beginning of the experimental procedures. The antibiotics treatment and FT were performed and controlled as previously reported.¹⁴ The mice from the CR and AT-CR groups were submitted to 14 days of CR reduced to ~ 75% of daily food intake. To deplete gut flora, mice from the AT, AT-CR, FT, and FT CR groups were repeatedly gavaged with 200 µl of an antibiotic cocktail (vancomycin .5 g/l, neomycin 1 g/l, ampicillin 1 g/l, metronidazole 1 g/l; all from Sigma-Aldrich, Vienna, Austria). The AT and AT-CR groups were gavaged three times within 14 days of the experimental procedure, and the FT group was gavaged twice: 5 and 3 days before microbiota transplant. After gut flora depletion, the mice from the FT groups were gavaged twice at a 2-day interval with freshly extracted fecal microbiota from CR or *ad libitum* mice. To obtain inoculants, fresh feces were mixed with sterile PBS. The mixture was vortexed and centrifuged for 3 min at 1000 ×g, and the isolated supernatant was immediately gavaged into FT mice. FT mice were killed 7 days after the first gavage.

All animal experimentation protocols were approved by the the Bundesministerium für Wissenschaft, Forschung und Wirtschaft, Referat

für Tierversuche und Gentechnik (BMBWF-66.006/0008-V/3b/2018). All experiments were carried out according to animal experimentation Animal Welfare Act guidelines.

Sequencing the 16S rDNA genes and metataxonomic analysis

The samples for sequencing were processed according to the previously published protocol.⁵³ Cecum samples were homogenized in MagNA Pure Bacteria Lysis Buffer from the MagNA Pure LC DNA Isolation Kit III in MagNA Lyser green beads tubes in a MagNA Lyser Instrument (all from Roche, Mannheim, Germany). Next, the samples were mixed with 25 µl lysozyme (100 mg/ml), incubated at 37°C for 30 min, 43.4 µl Proteinase K (20 mg/ml) was added followed by incubation at 65°C overnight. The enzymes were heat-inactivated and 250 µl of supernatant was used for DNA extraction on a MagNA Pure LC 2.0 following the instructions for the MagNA Pure LC DNA Isolation Kit III (all from Roche, Mannheim, Germany). PCRs reactions were run in triplicates using a FastStart High Fidelity PCR system with 5 µl of total DNA, 1x Fast Start High Fidelity Buffer, 1.25 U High Fidelity Enzyme, 200 µM dNTPs, .4 µM primers, and water in 25 µl reaction volume (all reagents from Roche, Mannheim, Germany). The target primers V1-V2: 27 F – AGAGTTTGTATCCTGGCTCAG and 375 R – CTGCTGCCTYCCGTA were applied for the amplification of phylogenetic informative hyper-variable regions using Illumina adapters for an indexing PCR reaction. The PCR reaction products were checked on an agarose gel and their normalization was performed on a SequalPrep Normalization Plate (LifeTechnologies, Carlsbad, CA, USA). Next, 15 µl of the product was used as a template in a single 50 µl indexing PCR reaction for 8 cycles. Finally, 5 µl of PCR products from each sample were pooled and 30 µl of the library was purified using an agarose gel and the QIAquick gel extraction kit (Qiagen, Hilden, Germany). The obtained library was quantified with QuantiFluor ONE dsDNA Dye on Quantus™ Fluorometer (Promega, Walldorf, Germany), its quality was verified using an Agilent BioAnalyzer 2100 (Waldbronn, Germany) and the 6 pM library was

sequenced on a MiSeq desktop sequencer containing 20% PhiX control DNA (Illumina, Eindhoven, Netherlands) with v2 chemistry for 500 cycles.

Raw sequencing data in fastq format was imported in Galaxy web-based platform⁵⁴ and analyzed with the QIIME2 2018.4. The data was pre-processed with DADA2⁵⁵ using default parameters and removing specific primer sequences. The resulting feature representative sequences were classified with the QIIME2 pre-fitted sklearn-based taxonomy classifier against SILVA 16S rRNA database version 132 at 99% identity.⁵⁶

Protein concentration, activity assays, and total bile acids concentration

The levels of total bile acids, GSH and GSSG, as well as the activity of GR (all from BioVision, Milpitas, CA, USA), were assessed using commercial assay kits according to the manufacturer's indications.

Tissue lysate assay

Freshly extracted tissue was lysed in 10x volume (w/v) of lysis buffer (150 mM NaCl, 1% IGEPAL, 50 mM Tris-HCL) by disrupting with syringe and needle. Afterward, 5 µl of the lysate was mixed with 10 µl of 2 M GSH and 2 M taurine and filled up to 200 µl with the lysis buffer. The samples were incubated at 37°C for 20 min.

Electron spin resonance

ESR assay was performed as previously published.³⁷ Shortly, 144 µl of oxygen-free KHB and 6 µl of oxygen-free 10 mM CMH solution were added to 15 µg tissue pieces. The samples were incubated for 60 min in a 37°C shaking incubator, spun down and 100 µl of the solution was used for the measurement. ESR measurements were performed at 150 K in a capillary tube (100 µL) placed into a high sensitivity resonator (Bruker ER 4122SHQE), using an X-band Bruker Elexsys-II E500 EPR spectrometer (Bruker BioSpin GmbH, Rheinstetten, Germany) applying modulation frequency of 100 kHz and a microwave frequency of 9.4 GHz. Spectra were recorded every 20 s, averaging every 10 consecutive spectra. The

sweep width was 450 G, the sweep time 20 s, the modulation amplitude 5 G, the center field 3400 G, the microwave power 20 mW, and the resolution was 1024 points. EPR spectra were simulated and the area under the curve was determined by double integration of the spectrum. A reference-free quantitation of the number of spins was performed, as has been described previously.⁵⁷

Gene expression

Intestine samples were thawed in lysis buffer, disrupted using a syringe and needle. Liver samples were homogenized using Precellys®24 Tissue Homogenizer (Bertin Instruments, Montigny-le-Bretonneux, France). RNA from both types of tissues was isolated using the RNeasy mini kit (Qiagen, Hilden, Germany). For reverse transcription, SuperScript® II Reverse Transcriptase (Invitrogen™, Life Technologies, Carlsbad, CA, USA) was used. Quantitative real-time PCR (qRT-PCR) reactions were performed using the QuantStudio™ 6 Flex Real-Time PCR System with the SYBR Green PCR Master Mix (both from Applied Biosystems, Life Technologies, Carlsbad, CA, USA). The Ct values were normalized to Eef1a1. The results show $\Delta\Delta C_t$ averaged for biological replicates for each experimental group. The sequences of the primers used were published before.³⁷

Detection and identification of GSH and taurine conjugates

The detection protocol was performed as published previously.³⁷ Briefly, 7–10 mg of intestinal mucosa samples were homogenized using syringe and needle and disrupted in five thawing and freezing cycles. Next, nine times the volume of ethanol absolute -20°C was added, vortexed for 30 s and samples were centrifuged for 10 min at 18,000 g at 4°C and the supernatants were analyzed by LCMS in negative modus using an LCMS-8040 Liquid Chromatograph Mass Spectrometer (Shimadzu Corporation, Kyoto, Japan) with an Atlantis T3 3 μm column (2.1x150 mm, Waters, Milford, MA, USA). The column temperature was 40°C . The mobile phases consisted of .1% formic acid in

water (eluent A) and .1% formic acid in acetonitrile (eluent B). The gradient was maintained at an initial 5% B for 2.5 min, to 20% B at 8 min, and was set back to 5% B at 9 min with a hold for one minute.

Identification of conjugates was performed as previously.³⁷ Shortly, standards of GSH and taurine (both from Sigma-Aldrich, St. Louis, MO, USA) were prepared in 70% ethanol. Standards were fragmented in negative modus using an LCMS-8040 Liquid Chromatograph Mass Spectrometer (Shimadzu Corporation, Kyoto, Japan) with an Atlantis T3 3 μm column (2.1x150 mm, Waters, Milford, MA, USA). The mobile phases and the gradient was conforming with the detection protocol. The fragmentation pattern was compared to METLIN's database. Precursor ions in the tested samples were compared to fragmentation patterns of GSH and taurine. The exact mass of the selected precursor ions was measured using an Ultimate 3000 (Thermo Fischer Scientific, Waltham, MA, US) and a microTOF-Q II (Bruker Daltonics, Bremen, Germany) with an Atlantis T3 3 μm column (2.1x150 mm, Waters, Milford, MA, USA) kept at 40°C . The mobile phases and the gradient were set the same as for GSH, taurine, and conjugated detection. The mass and fragmentation pattern of chosen precursors was verified using the METLIN database. The compounds identified as GSH or taurine conjugates were previously published.³⁷

Bile acid analysis

As reported previously,³⁷ bile acids were measured with LCMS. Liver samples were weighted in Precellys homogenizing tubes with 1.4 mm ceramic beads, and nine times the volume of methanol absolute at -20°C was added. Samples were homogenized in the Precellys 24 Tissue Homogenizer (Bertin Instruments, Montigny-le-Bretonneux, France) twice for 15 s at 5000 rpm, vortexed for 30 s, and centrifuged for 10 min at 5000 g at 4°C . The supernatants were transferred to new 1.5 ml Eppendorf tubes, and, to remove the remaining debris, the centrifugation step was repeated this time at 12,000 g. Supernatants were transferred into new Eppendorf tubes and after second centrifugation, supernatants were directly transferred into

HPLC vials. Intestinal samples were processed as described above in the method for GSH and taurine analysis. Plasma samples (50 µl) were extracted with 150 µl MeOH, vortexed for 30 s, and shaken continuously for 10 min with a laboratory rocker. 100 µl of the supernatant was evaporated, re-dissolved in 50 µl methanol, and transferred into an HPLC vial. After the extraction, samples were handled alike. Samples (10 µl) were analyzed by LCMS in positive modus using an LCMS-8040 Liquid Chromatograph Mass Spectrometer (Shimadzu Corporation, Kyoto, Japan) with an Atlantis T3 3 µm column (2.1 × 150 mm, Waters, Milford, MA, USA). The column temperature was 30°C. The mobile phase A consisted of water and eluent B was acetonitrile/methanol (3/1, v/v), both containing .1% formic acid and a concentration of 20 mM ammonium acetate. The gradient was maintained from an initial 30% B for 5 min, to 100% B at 25 min, which was kept constant for 20 min. Afterward, the composition was set back to the initial ratio of 30% B within 2 min, followed by 10 min of re-equilibration.

Acknowledgments

Open access funding provided by the University of Vienna.

Disclosure statement

No potential conflict of interest was reported by the author(s).

Funding

This work was supported by Hochschuljubiläumsstiftung der Stadt Wien under grant H-278677/2020.

ORCID

Kalina Duszka  <http://orcid.org/0000-0002-7455-6090>

Data availability

The microbiota datasets generated during and analyzed during the current study are available in the European Nucleotide Archive [<https://www.ebi.ac.uk/ena/browser/view/PRJEB46415>] repository.

Data availability statement

The authors confirm that the data supporting the findings of this study are available within the article and its supplementary materials.

Statistics

For analysis of statistical differences between four groups, one-way ANOVA with Bonferroni correction for multiple testing was applied using SPSS Statistics 26 (IBM Corp., Armonk, NY, USA). Data sets with two groups of seven to nine biological replicates were compared using a two-sided Student's t-test and a *p*-value lower than .05 was considered statistically significant.

Authors contribution statement

KD designed and performed the experiments, analyzed samples, and wrote the manuscript; AG performed animal experiments, analyzed metabolites, and analyzed the data; MP assisted with the development of the methodology for metabolites detection; ST performed microbiota sequencing analysis; VS contributed expert advice; JK contributed expert advice; All authors corrected and approved the final manuscript.

References

1. Martin R, Makino H, Cetinyurek Yavuz A, Ben-Amor K, Roelofs M, Ishikawa E, Kubota H, Swinkels S, Sakai T, Oishi K, et al. Early-life events, including mode of delivery and type of feeding, siblings and gender, shape the developing gut microbiota. *PloS One*. 2016;11(6): e0158498. doi:10.1371/journal.pone.0158498.
2. Yatsunenkov T, Rey FE, Manary MJ, Trehan I, Dominguez-Bello MG, Contreras M, Magris M, Hidalgo G, Baldassano RN, Anokhin AP, et al. Human gut microbiome viewed across age and geography. *Nature*. 2012;486(7402):222–227. doi:10.1038/nature11053.
3. Ianiro G, Tilg H, Gasbarrini A. Antibiotics as deep modulators of gut microbiota: between good and evil. *Gut*. 2016;65(11):1906–1915. doi:10.1136/gutjnl-2016-312297.
4. Gupta VK, Paul S, Dutta C. Geography, ethnicity or subsistence-specific variations in human microbiome composition and diversity. *Front Microbiol*. 2017;8:1162. doi:10.3389/fmicb.2017.01162.
5. Rothschild D, Weissbrod O, Barkan E, Kurilshikov A, Korem T, Zeevi D, Costea PI, Godneva A, Kalka IN, Bar N, et al. Environment dominates over host genetics in shaping human gut microbiota. *Nature*. 2018;555(7695):210–215. doi:10.1038/nature25973.

6. van Hylckama Vlieg JE, Veiga P, Zhang C, Derrien M, Zhao L. Impact of microbial transformation of food on health - from fermented foods to fermentation in the gastro-intestinal tract. *Curr Opin Biotechnol.* **2011**;22(2):211–219. doi:10.1016/j.copbio.2010.12.004.
7. Zhang C, Zhang M, Wang S, Han R, Cao Y, Hua W, Mao Y, Zhang X, Pang X, Wei C, et al. Interactions between gut microbiota, host genetics and diet relevant to development of metabolic syndromes in mice. *ISME J.* **2010**;4(2):232–241. doi:10.1038/ismej.2009.112.
8. Alvarez Y, Glotfelty LG, Blank N, Dohnalova L, Thaïs CA. The microbiome as a circadian coordinator of metabolism. *Endocrinology.* **2020**;161(6). doi:10.1210/endocr/bqaa059.
9. Santacruz A, Marcos A, Wärnberg J, Martí A, Martín-Matillas M, Campoy C, Moreno LA, Veiga O, Redondo-Figuero C, Garagorri JM, et al. Interplay between weight loss and gut microbiota composition in overweight adolescents. *Obesity (Silver Spring).* **2009**;17(10):1906–1915. doi:10.1038/oby.2009.112.
10. Zhang C, Li S, Yang L, Huang P, Li W, Wang S, Zhao G, Zhang M, Pang X, Yan Z, et al. Structural modulation of gut microbiota in life-long calorie-restricted mice. *Nat Commun.* **2013**;4(1):2163. doi:10.1038/ncomms3163.
11. Zheng X, Wang S, Jia W. Calorie restriction and its impact on gut microbial composition and global metabolism. *Front Med.* **2018**;12(6):634–644. doi:10.1007/s11684-018-0670-8.
12. Ruiz A, Cerdó T, Jáuregui R, Pieper DH, Marcos A, Clemente A, García F, Margolles A, Ferrer M, Campoy C, Suárez A. One-year calorie restriction impacts gut microbial composition but not its metabolic performance in obese adolescents. *Environ Microbiol.* **2017**;19:1536–1551. doi:10.1111/1462-2920.13713.
13. Tanca A, Abbondio M, Palomba A, Fraumene C, Marongiu F, Serra M, Pagnozzi D, Laconi E, Uzzau S. Caloric restriction promotes functional changes involving short-chain fatty acid biosynthesis in the rat gut microbiota. *Sci Rep.* **2018**;8(1):14778. doi:10.1038/s41598-018-33100-y.
14. Duszka K, Ellero-Simatos S, Ow GS, Defernez M, Paramalingam E, Tett A, Ying S, König J, Narbad A, Kuznetsov VA, et al. Complementary intestinal mucosa and microbiota responses to caloric restriction. *Sci Rep.* **2018**;8(1):11338. doi:10.1038/s41598-018-29815-7.
15. Wang S, Huang M, You X, Zhao J, Chen L, Wang L, Luo Y, Chen Y. Gut microbiota mediates the anti-obesity effect of calorie restriction in mice. *Sci Rep.* **2018**;8(1):13037. doi:10.1038/s41598-018-31353-1.
16. Duszka K, Wahli W. Enteric Microbiota–gut–brain axis from the perspective of nuclear receptors. *Int J Mol Sci.* **2018**;19(8):2210. doi:10.3390/ijms19082210.
17. Foley MH, O’Flaherty S, Barrangou R, Theriot CM, Knoll LJ. Bile salt hydrolases: gatekeepers of bile acid metabolism and host-microbiome crosstalk in the gastrointestinal tract. *PLoS Pathog.* **2019**;15(3):e1007581. doi:10.1371/journal.ppat.1007581.
18. Ridlon JM, Kang DJ, Hylemon PB. Bile salt biotransformations by human intestinal bacteria. *J Lipid Res.* **2006**;47(2):241–259. doi:10.1194/jlr.R500013-JLR200.
19. Devkota S, Wang Y, Musch MW, Leone V, Fehlner-Peach H, Nadimpalli A, Antonopoulos DA, Jabri B, Chang EB. Dietary-fat-induced taurocholic acid promotes pathobiont expansion and colitis in Il10^{−/−} mice. *Nature.* **2012**;487(7405):104–108. doi:10.1038/nature11225.
20. Yu H, Guo Z, Shen S, Shan W. Effects of taurine on gut microbiota and metabolism in mice. *Amino Acids.* **2016**;48(7):1601–1617. doi:10.1007/s00726-016-2219-y.
21. Fang H, Meng F, Piao F, Jin B, Li M, Li W. Effect of taurine on intestinal microbiota and immune cells in peyer’s patches of immunosuppressive mice. *Adv Exp Med Biol.* **2019**;1155:13–24. doi:10.1007/978-981-13-8023-5_2.
22. Shimizu M, Zhao Z, Ishimoto Y, Satsu H. Dietary taurine attenuates dextran sulfate sodium (DSS)-induced experimental colitis in mice. *Adv Exp Med Biol.* **2009**;643:265–271. doi:10.1007/978-0-387-75681-3_27.
23. Zhao Z, Satsu H, Fujisawa M, Hori M, Ishimoto Y, Totsuka M, Nambu A, Kakuta S, Ozaki H, Shimizu M, et al. Attenuation by dietary taurine of dextran sulfate sodium-induced colitis in mice and of THP-1-induced damage to intestinal Caco-2 cell monolayers. *Amino Acids.* **2008**;35(1):217–224. doi:10.1007/s00726-007-0562-8.
24. Gondo Y, Satsu H, Ishimoto Y, Iwamoto T, Shimizu M. Effect of taurine on mRNA expression of thioredoxin interacting protein in Caco-2 cells. *Biochem Biophys Res Commun.* **2012**;426(3):433–437. doi:10.1016/j.bbrc.2012.08.116.
25. Kim C, Cha YN. Taurine chloramine produced from taurine under inflammation provides anti-inflammatory and cytoprotective effects. *Amino Acids.* **2014**;46(1):89–100. doi:10.1007/s00726-013-1545-6.
26. Marcinkiewicz J, Mak M, Bobek M, Biedroń R, Bialecka A, Koprowski M, Kontny E, Maśliński W. Is there a role of taurine bromamine in inflammation? Interactive effects with nitrite and hydrogen peroxide. *Inflamm Res.* **2005**;54(1):42–49. doi:10.1007/s00011-004-1322-9.
27. Niu X, Zheng S, Liu H, Li S. Protective effects of taurine against inflammation, apoptosis, and oxidative stress in brain injury. *Mol Med Rep.* **2018**;18:4516–4522. doi:10.3892/mmr.2018.9465.
28. Chupel MU, Minuzzi LG, Furtado G, Santos ML, Hogervorst E, Filaire E, Teixeira AM. Exercise and taurine in inflammation, cognition, and peripheral markers of blood-brain barrier integrity in older women. *Appl Physiol Nutr Metab.* **2018**;43(7):733–741. doi:10.1139/apnm-2017-0775.
29. Silva LA, Silveira PCL, Ronsani MM, Souza PS, Scheffer D, Vieira LC, Benetti M, De Souza CT, Pinho RA. Taurine supplementation decreases

- oxidative stress in skeletal muscle after eccentric exercise. *Cell Biochem Funct.* **2011**;29(1):43–49. doi:[10.1002/cbf.1716](https://doi.org/10.1002/cbf.1716).
30. Thirupathi A, Freitas S, Sorato HR, Pedroso GS, Effting PS, Damiani AP, Andrade VM, Nesi RT, Gupta RC, Muller AP, et al. Modulatory effects of taurine on metabolic and oxidative stress parameters in a mice model of muscle overuse. *Nutrition.* **2018**;54:158–164. doi:[10.1016/j.nut.2018.03.058](https://doi.org/10.1016/j.nut.2018.03.058).
 31. Bucolo C, Fidilio A, Platania CBM, Geraci F, Lazzara F, Drago F. Antioxidant and osmoprotecting activity of taurine in dry eye models. *J Ocul Pharmacol Ther.* **2018**;34(1–2):188–194. doi:[10.1089/jop.2017.0008](https://doi.org/10.1089/jop.2017.0008).
 32. Lee DS, Jo HG, Kim MJ, Lee H, Cheong SH. Antioxidant and anti-stress effects of taurine against electric foot-shock-induced acute stress in rats. *Adv Exp Med Biol.* **2019**;1155:185–196. doi:[10.1007/978-981-13-8023-5_17](https://doi.org/10.1007/978-981-13-8023-5_17).
 33. Trachtman H, Barbour R, Sturman JA, Finberg L. Taurine and osmoregulation: taurine is a cerebral osmoprotective molecule in chronic hypernatremic dehydration. *Pediatr Res.* **1988**;23(1):35–39. doi:[10.1203/00006450-198801000-00008](https://doi.org/10.1203/00006450-198801000-00008).
 34. Kong B, Wang L, Chiang JYL, Zhang Y, Klaassen CD, Guo GL. Mechanism of tissue-specific farnesoid X receptor in suppressing the expression of genes in bile-acid synthesis in mice. *Hepatology.* **2012**;56(3):1034–1043. doi:[10.1002/hep.25740](https://doi.org/10.1002/hep.25740).
 35. Inagaki T, Choi M, Moschetta A, Peng L, Cummins CL, McDonald JG, Luo G, Jones SA, Goodwin B, Richardson JA, et al. Fibroblast growth factor 15 functions as an enterohepatic signal to regulate bile acid homeostasis. *Cell Metab.* **2005**;2(4):217–225. doi:[10.1016/j.cmet.2005.09.001](https://doi.org/10.1016/j.cmet.2005.09.001).
 36. Renga B, Mencarelli A, Cipriani S, D'Amore C, Carino A, Bruno A, Francisci D, Zampella A, Distrutti E, Fiorucci S, et al. The bile acid sensor FXR is required for immune-regulatory activities of TLR-9 in intestinal inflammation. *PLoS One.* **2013**;8(1):e54472. doi:[10.1371/journal.pone.0054472](https://doi.org/10.1371/journal.pone.0054472).
 37. Gregor A, Pignitter M, Fahrngruber C, Bayer S, Somoza V, König J, Duszka K. Caloric restriction increases levels of taurine in the intestine and stimulates taurine uptake by conjugation to glutathione. *J Nutr Biochem.* **2021**;96:108781. doi:[10.1016/j.jnutbio.2021.108781](https://doi.org/10.1016/j.jnutbio.2021.108781).
 38. Ebert MN, Beyer-Sehlmeyer G, Liegibel UM, Kautenburger T, Becker TW, Pool-Zobel BL. Butyrate induces glutathione S-transferase in human colon cells and protects from genetic damage by 4-hydroxy-2-nonenal. *Nutr Cancer.* **2001**;41(1–2):156–164. doi:[10.1080/01635581.2001.9680627](https://doi.org/10.1080/01635581.2001.9680627).
 39. Fabbiano S, Suárez-Zamorano N, Chevalier C, Lazarević V, Kieser S, Rigo D, Leo S, Veyrat-Durebex C, Gaia N, Maresca M, et al. Functional gut microbiota remodeling contributes to the caloric restriction-induced metabolic improvements. *Cell Metab.* **2018**;28(6):907–921 e907. doi:[10.1016/j.cmet.2018.08.005](https://doi.org/10.1016/j.cmet.2018.08.005).
 40. Sayin SI, Wahlström A, Felin J, Jäntti S, Marschall H-U, Bamberg K, Angelin B, Hyötyläinen T, Orešič M, Bäckhed F, et al. Gut microbiota regulates bile acid metabolism by reducing the levels of tauro-beta-muricholic acid, a naturally occurring FXR antagonist. *Cell Metab.* **2013**;17(2):225–235. doi:[10.1016/j.cmet.2013.01.003](https://doi.org/10.1016/j.cmet.2013.01.003).
 41. Anderson CM, Howard A, Walters JR, Ganapathy V, Thwaites DT. Taurine uptake across the human intestinal brush-border membrane is via two transporters: h⁺-coupled PAT1 (SLC36A1) and Na⁺- and Cl[−]-dependent TauT (SLC6A6). *J Physiol.* **2009**;587(4):731–744. doi:[10.1113/jphysiol.2008.164228](https://doi.org/10.1113/jphysiol.2008.164228).
 42. Boyer JL. Bile formation and secretion. *Compr Physiol.* **2013**;3:1035–1078. doi:[10.1002/cphy.c120027](https://doi.org/10.1002/cphy.c120027).
 43. Mardinoglu A, Shoaie S, Bergentall M, Ghaffari P, Zhang C, Larsson E, Bäckhed F, Nielsen J. The gut microbiota modulates host amino acid and glutathione metabolism in mice. *Mol Syst Biol.* **2015**;11(10):834. doi:[10.15252/msb.20156487](https://doi.org/10.15252/msb.20156487).
 44. Theriot CM, Bowman AA, Young VB, Ellermeier CD. Antibiotic-induced alterations of the gut microbiota alter secondary bile acid production and allow for *Clostridium difficile* spore germination and outgrowth in the large intestine. *mSphere.* **2016**;1(1). doi:[10.1128/mSphere.00045-15](https://doi.org/10.1128/mSphere.00045-15).
 45. Levy M, Thaïss C, Zeevi D, Dohnalová L, Zilberman-Schapira G, Mahdi J, David E, Savidor A, Korem T, Herzig Y, et al. Microbiota-modulated metabolites shape the intestinal microenvironment by regulating NLRP6 inflammasome signaling. *Cell.* **2015**;163(6):1428–1443. doi:[10.1016/j.cell.2015.10.048](https://doi.org/10.1016/j.cell.2015.10.048).
 46. Barja G. Aging in vertebrates, and the effect of caloric restriction: a mitochondrial free radical production-DNA damage mechanism? *Biol Rev Camb Philos Soc.* **2004**;79(2):235–251. doi:[10.1017/S1464793103006213](https://doi.org/10.1017/S1464793103006213).
 47. Forster MJ, Sohal BH, Sohal RS. Reversible effects of long-term caloric restriction on protein oxidative damage. *J Gerontol A Biol Sci Med Sci.* **2000**;55(11):B522–B529. doi:[10.1093/gerona/55.11.B522](https://doi.org/10.1093/gerona/55.11.B522).
 48. Lambert AJ, Merry BJ. Lack of effect of caloric restriction on bioenergetics and reactive oxygen species production in intact rat hepatocytes. *J Gerontol A Biol Sci Med Sci.* **2005**;60(2):175–180. doi:[10.1093/gerona/60.2.175](https://doi.org/10.1093/gerona/60.2.175).
 49. Lambert AJ, Portero-Otin M, Pamplona R, Merry BJ. Effect of ageing and caloric restriction on specific markers of protein oxidative damage and membrane peroxidizability in rat liver mitochondria. *Mech Ageing Dev.* **2004**;125(8):529–538. doi:[10.1016/j.mad.2004.06.002](https://doi.org/10.1016/j.mad.2004.06.002).
 50. Agarwal S, Sharma S, Agrawal V, Roy N. Caloric restriction augments ROS defense in *S. cerevisiae*, by a Sir2p independent mechanism. *Free Radic Res.* **2005**;39(1):55–62. doi:[10.1080/10715760400022343](https://doi.org/10.1080/10715760400022343).
 51. Mesquita A, Weinberger M, Silva A, Sampaio-Marques B, Almeida B, Leao C, Costa V, Rodrigues F, Burhans WC, Ludovico P, et al. Caloric restriction or

- catalase inactivation extends yeast chronological life-span by inducing H₂O₂ and superoxide dismutase activity. *Proc Natl Acad Sci U S A*. 2010;107(34):15123–15128. doi:[10.1073/pnas.1004432107](https://doi.org/10.1073/pnas.1004432107).
52. Stankovic M, Mladenovic D, Ninkovic M, Vucevic D, Radosavljevic TT. Effects of caloric restriction on oxidative stress parameters. *Gen Physiol Biophys*. 2013;32(2):277–283. doi:[10.4149/gpb_2013027](https://doi.org/10.4149/gpb_2013027).
53. Klymiuk I, Bilgiler C, Stadlmann A, Thannesberger J, Kastner MT, Högenauer C, Püspök A, Biowski-Frotz S, Schrutka-Kölbl C, Thallinger GG, et al. The human gastric microbiome is predicated upon infection with helicobacter pylori. *Front Microbiol*. 2017;8:2508. doi:[10.3389/fmicb.2017.02508](https://doi.org/10.3389/fmicb.2017.02508).
54. Afgan E, Baker D, Batut B, van den Beek M, Bouvier D, Čech M, Chilton J, Clements D, Coraor N, Grüning BA, et al. The Galaxy platform for accessible, reproducible and collaborative biomedical analyses: 2018 update. *Nucleic Acids Res*. 2018;46(W1):W537–W544. doi:[10.1093/nar/gky379](https://doi.org/10.1093/nar/gky379).
55. Callahan BJ,McMurdie PJ, Rosen MJ, Han AW, Johnson AJ, Holmes SP. DADA2: high-resolution sample inference from illumina amplicon data. *Nat Methods*. 2016;13(7):581–583. doi:[10.1038/nmeth.3869](https://doi.org/10.1038/nmeth.3869).
56. Yilmaz P,Parfrey LW, Yarza P, Gerken J, Pruesse E, Quast C, Schweer T, Peplies J, Ludwig W, Glöckner FO. The SILVA and “All-species Living Tree Project (LTP)” taxonomic frameworks. *Nucleic Acids Res*. 2014;42(D1):D643–648. doi:[10.1093/nar/gkt1209](https://doi.org/10.1093/nar/gkt1209).
57. Zaunschirm M, Pignitter M, Kienesberger J, Hernler N, Riegger C, Eggersdorfer M, Somoza V. Contribution of the ratio of tocopherol homologs to the oxidative stability of commercial vegetable oils. *Molecules*. 2018;23(1):206. doi:[10.3390/molecules23010206](https://doi.org/10.3390/molecules23010206).